Soil surface roughnesss measurements and erosion modelling

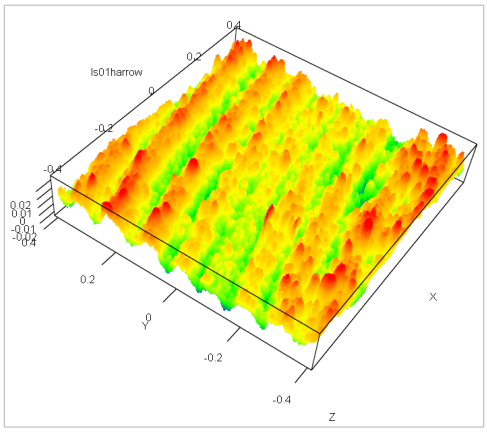

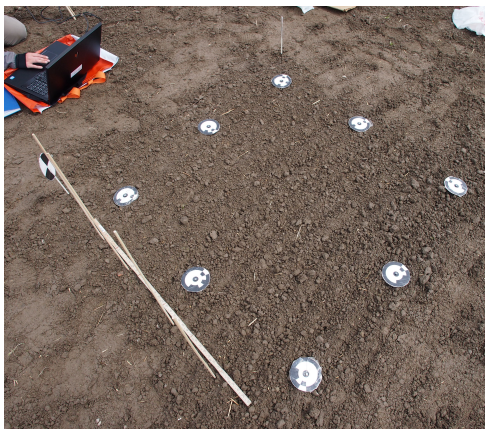

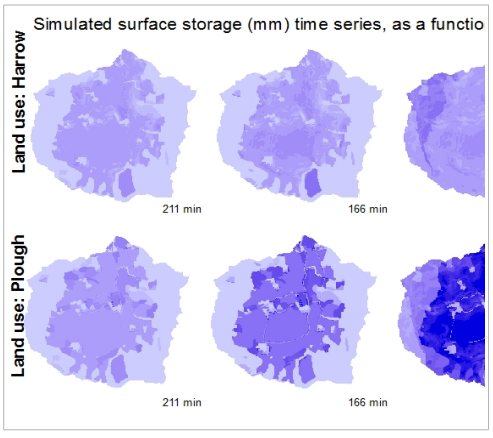

MSc. Thesis by
Line M. Thomsen

Soil Physics and Land Management Group
Wageningen University
The Netherlands

December 2013

Soil surface roughness measurements and erosion modelling

Thesis report submitted to Wageningen University in partial fulfilment of the requirements for the degree of Master of Science (MSc.) in International Land and Water Management, specialisation Land Degradation and Development.

Author: Line M. Thomsen

Supervisor: ir. Jantiene Baartman
Wageningen University, The Netherlands
Environmental Science group
Sub-division Soil physics and Land Management

Local supervisors: Dr. ir. Jannes Stolte – Head of department Land use and Management

MSc Torsten Starkloff – PhD student

Norwegian Institute for Agricultural and Environmental Research
BioForsk Soil and Environment – Ås, Norway
Department Land use and Management

23rd December, 2013, Wageningen, The Netherlands.

Front page: The images show (from upper left corner to lower right corner): 1) Erosion in the Skuterud catchment, Ås, Norway, spring 2013, 2) Pinboard used for soil surface roughness measurement, 3) Roller chain also used for soil surface roughness measurements, 4) An image of a 3D point-cloud also used for soil surface roughness measurement, 5) The photo of the same soil surface as to image 4, 6) Surface run off measurement in the Skuterud catchment, 6) Results from erosion modelling based on data from the Skuterud catchments

Abstract

This study compared five methods for measuring soil surface roughness, two contact methods: pinboard and roller chain, and three non-contact methods: laser scanner, stereophotogrammetry and the “Kinect”. The latter is a 3D depth sensor originally developed for gaming consoles, which recently was proved to be applicable for Earth Sciences (Mankoff and Russo, 2012). Roughness was in this study defined as irregularities in the surface related to soil type and tillage practice. The index random roughness (RR), calculated as the standard deviation of a number of elevation recordings, was used for comparison. The methods were compared in terms of accuracy, precision, resolution, ease of usage, price and land use. Further, the obtained average roughness values were used as input in a physical-based spatially-distributed erosion model, LISEM. This facilitated a one-at-a-time parameter sensitivity analysis. Results showed that the various methods have different pros and cons and since the methods used different principles to obtain roughness data, they are prone to different errors. The “Kinect” proved to be a useful sensor. The erosion model was relatively sensitive to the roughness input data. Interestingly, roughness data obtained with different methods, which in statistical terms were not significantly different from each other (RR 0.81 versus 1.18±0.33) , were still causing a ~50% change in hydrograph peak, indicating that the model sensitivity is not adjusted for the accuracy of measured roughness data. For improved model performance it is suggested to determine the required accuracy and precision as well as the preferred method of measured roughness data when used as input to an erosion model like LISEM.

Key words: soil surface roughnesss, random roughness, erosion modelling, LISEM, the Kinect, data accuracy

Table of Contents

List of abbreviations

2D	two-dimensional, e.g. coordinates that have a x- and y-coordinate
3D	three-dimensional, e.g. coordinates that have a x-, y, and z-coordinate
ANOVA	analysis of variance
DEM	digital elevation model
DN	digital number
GIS	geographical information system
GPS	geographic position system
IR	infrared
LAI	leaf area index
LD	limiting distance
LDD	local drainage direction
LISEM	Limburg soil erosion model
MASL	meter above sea level
MDS	maximum depression storage
RMSE	root mean square error
RR	random roughness
SDS	start depression storage
TLS	terrestrial laser scanner
UTM	universal transverse Mercator

List of appendices

List of tables

List of figures

1 Introduction

Soil erosion is a natural process of sediment removal and settlement forced by climatic factors such as precipitation, overland flow and wind. However, soil erosion rates are accelerated by unsustainable land management practices, often in relation to cultivated agricultural fields (Grimm et al., 2002). Soil erosion is a global problem, causing for instance degraded agricultural land (soil and nutrient loss), damages on roads, algae blooms and even abandonment of land (Morgan, 2005; Øygarden et al., 2006). To introduce sustainable land management practices which may prevent increased soil erosion, processes of soil erosion have been extensively studied, in laboratories as well as in field (Stroosnijder, 2005). But soil erosion monitoring is a challenge because the processes are highly variable spatially as well as temporarily and because erosion often is caused by climatic conditions that fluctuate on an inter-annual time scale (Lal, 1994; Lundekvam and Skøien, 1998; Morgan, 2005). Erosion monitoring is therefore usually laborious and require long-term studies. Since long-term studies are difficult to finance they are rather scarce and much erosion research have relied on modelling. However, soil erosion modelling is in general still not satisfying (de Vente et al., 2013; Takken et al., 1999). The explanation is partly to be found in the lack of accurate input data and the lack of data that capture the spatial heterogeneity of the area of interest (Kværnø, 2011; Sheikh et al., 2010), although also the model structure of existing models have been questioned (Rompaey and Govers, 2002; Wainwright et al., 2008a). At present one way to increase the knowledge of erosion processes is to try to improve the model performance of existing models. This can be done by getting more knowledge on the accuracy and precision of model input data and to test how sensitive the model is to variations in input data. Input data to erosion models covers a wide range of parameters, for instance soil type, soil texture, initial soil moisture level, vegetation cover, land use, slope etc. For many areas this type of data is often only estimated in more or less qualified ways. A parameter which often is needed for soil erosion modelling is soil surface roughness.

Soil roughness are the irregularities in surface which are cause by soil type, grain sizes, rock fragments, vegetation cover and land management. It is usually variation in the surface too small to be captured by conventional topographic map, thus soil roughness is also referred to as the soil micro-topography (Takken, 2000). Soil roughness has a large influence on surface storage, infiltration and overland flow and therefore also on sediment detachment (Amoah et al., 2013). Much research have focused on quantifying the relation between roughness and surface storage and overland flow, while less research have focused on roughness and infiltration (Govers et al., 2000). Soil roughness has been estimated with various methods: pin-profilers, roller-chain, laser scanners and photogrammetric methods. At present there is still a need for improving methods, especially methods that yield a very high spatial resolution, i.e. in grid cell size of millimetres, while at the same time being cost-efficient and allow for mobility in fieldwork. The aforementioned methods differ in obtainable accuracy and resolution. Especially the differences in spatial resolution is interesting as roughness to a certain degree shows scale-dependency, i.e. the roughness of a given surface will depend on the density of elevation measurements. It is unknown how comparable roughness data obtained with various methods are, and it is unknown to what extent a possible difference is problematic when used in an erosion model. To know how the variability of roughness data will influence the output of an erosion model, will in turn help to formulate guidelines for best practices in data collection and will help to improve the model performance.

Only one study were found which compared pin-profilers, roller chain, laser scanner and photogrammetric methods (Jester and Klik, 2005). The study compared the methods in terms of accuracy, resolution and ease of use, but without considering for what purpose the data was needed. In this study we are comparing methods for obtaining roughness data, much along the lines of Jester and Klik (2005) but with the specific purpose of inputting the data to an erosion model which we believe will increase the usability of a method comparison. For improving the model performance it is useful to know how sensitive the model is to roughness data along a realistic range of values. Apart from increasing the knowledge of the model sensitivity to roughness, there is

since 2005 now another reason for executing a method comparison. In 2010 a new depth sensor, the “Kinect”, much like a laser scanner, was developed. Although developed for gaming purpose, this sensor has shown promising results in all sorts of scientific fields where 3D measurements of the surroundings are desired, e.g. in robotics. Mankoff and Russo (2012) showed how the sensor could be used to obtain elevation data in a river bed and on glacier ice, which encouraged us to try to use if for obtaining soil roughness data. The proposed advantages of this sensor is that it is relatively cheap to buy and easy to carry, while the spatial resolution of measurements is on millimetre scale, thus this sensor could be a solution to the lack of a method which yields high spatial resolution, while at the same time is cost-efficient and allow for mobility in the field. This could possibly be a mean to improve the quality of input data for erosion models, which in turn could improve erosion modelling, which ultimately could contribute to an increased understanding of soil erosion causes and effects.

2 Objective and research question

The objective of this study is two-fold: 1) To investigate the applicability of the “Kinect” 3D depth sensor for obtaining soil roughness data as compared to other methods and 2) to test whether this data can improve the performance of a physics-based spatially distributed erosion model.

This leads to the following research questions:

1. What methods have been used to measure soil surface roughness?

2. How can soil surface roughness data be obtained by the “Kinect” 3D depth sensor

3. How can surface roughness data from various methods be compared?

4. Can data obtained from the “Kinect” 3D depth sensors, compared to other methods, improve the LISEM model performance?

To address these research questions a combination of literature review, fieldwork and modelling was executed.

3 Outline of report

The report consists of 8 chapters. Introduction and research objectives have already been presented (chapter 1 and 2), chapter 4 describes the study area, followed by chapter 5 providing a historical overview of micro-topography measurement methods and relevant roughness indicators. This will answer the first research question. Then follows chapter 6, an extensive description of materials and method, which partly answers second research question. Chapter 7 presents the results and discussion, both from fieldwork and modelling. It is divided into two main sections, so that results related to the method comparison first are presented and discussed, followed by results and discussion related to modelling. Finally in chapter 8 will the knowledge gained from the two main section be synthesized and conclusions will be drawn which gives an answer to the second, third and fourth research question.

Terminology
In this report *micro-topography* means the actual soil surface, which is no different than any topography. This term just indicates that the topography is considered with very high spatial resolution, i.e. millimeter or sub-millimeter scale.

Soil surface roughness is a term that covers various roughness components as defined by Takken (2000), i.e. micro-relief variations, random roughness, oriented roughness and higher order roughness, such as field parcel border. *Random roughness* is additionally also the term for an index calculated as the standard deviation of height measurements. In this thesis the index *random roughness* is calculated to quantify the soil surface roughness.

A *3D depth sensor* is any type of sensor that can acquire three-dimensional depth data, i.e. spatial data, which have the form of a x-, y,- and z-coordinate. This includes for instance a laser scanner, a digital photo camera and the “Kinect”

The *“Kinect”* is one of the commercial names for the new type of sensor 3D depth sensors which will be tested in this thesis. However, there is no general term for this type of sensor and in this thesis another commercial product, the “Xtion” was used in stead of the “Kinect”. Consequently, in this report the word *Xtion* is used to name this new 3D depth sensor.

4 Study area

The study area for this thesis is the Skuterud catchment, a relatively small catchment, 450 ha, dominated by cultivated fields with cereal production (figure 4.1). The catchment is located east of Ås, approximately 30 km south of Oslo in Akershus county, Norway. The landscape is undulating with elevations from 150 to 92 masl, with the steepest slopes in the eastern and western part of the catchment (figure 4.2). Annual average temperature is 5.3° C and precipitation is 785 mm (figure 4.3). 60% of the catchment area is cultivated land, while 31% is forest, mainly coniferous or mixed coniferous-deciduous. 7% is urban settlement and roads and 2% is covered by forested peatland located in the southern-most depression in the catchment. Main crops are winter and summer cereals, sometimes in rotation with oil seed and potatoes. Marine deposits cover most of the area. Coarse marine shore deposits dominates on the fringe of the cultivated areas and in the forest. Soil types have only been mapped in the cultivated areas. The predominating soil types in the central part are marine silt loam and silty clay loam soils (Albeluvisols and Stagnosols). In the areas with shore deposits sandy and loamy sand soils dominate (Arenosols, Umbrisols, Podzols, Cambisols and Gleysols). Loamy and sandy loam soils are found in the transition zones between marine and shore deposits.

Monitoring of water and sediment discharge has been carried out since 1993 at the catchment outlet, indicated by a star, figure 4.1. In 2008 monitoring started at one of the sub-catchment, named Gryteland. The monitoring includes detailed measurements of surface runoff (figure 4.4), subsurface drainage discharge, precipitation, and soil-water content and temperature. The sub-catchment covers approximately 27 ha and is dominated by relatively more sandy soils and forest in comparison with the main catchment (Kværnø and Stolte, 2012).

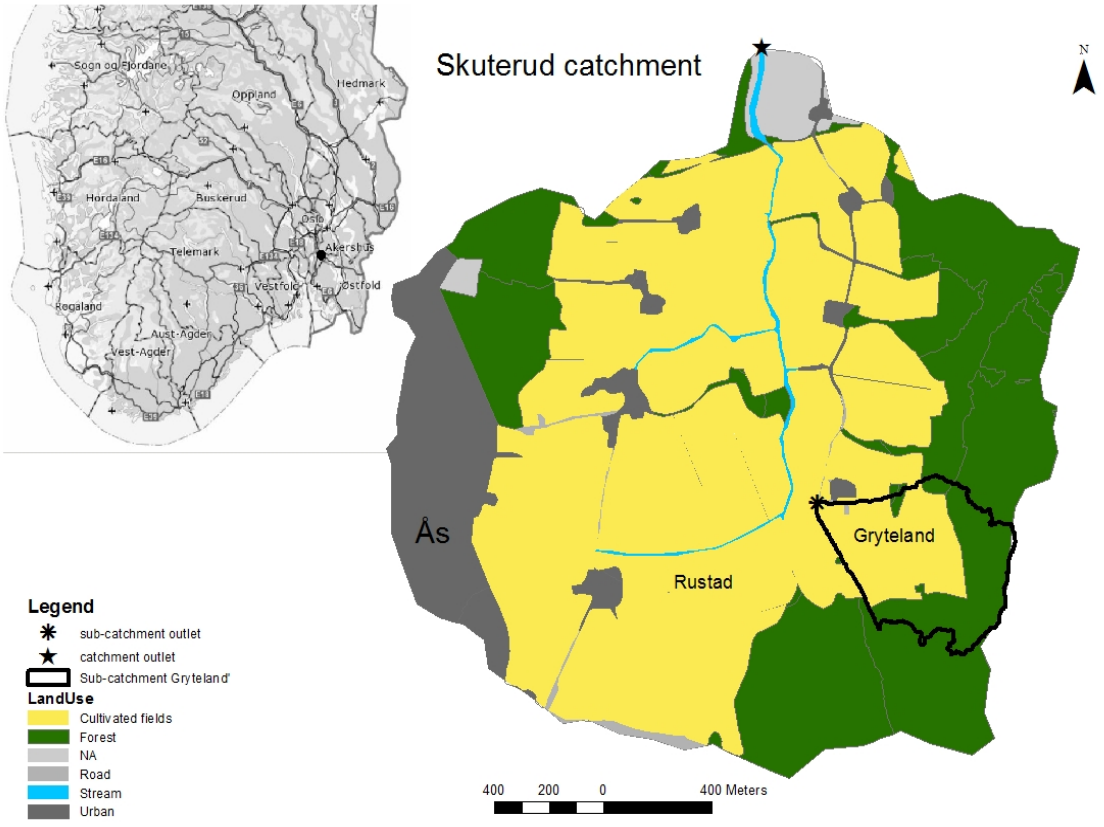

Figure 4.1: Outline and land use of catchment Skuterud, next to Ås. The black dot on the inserted map of southern Norway indicates the location of the catchment. The sub-catchment Gryteland is outlined in black. Land use map obtained from Bioforsk. Norway map obtained from: http://www.skogoglandskap.no/kart/kilden

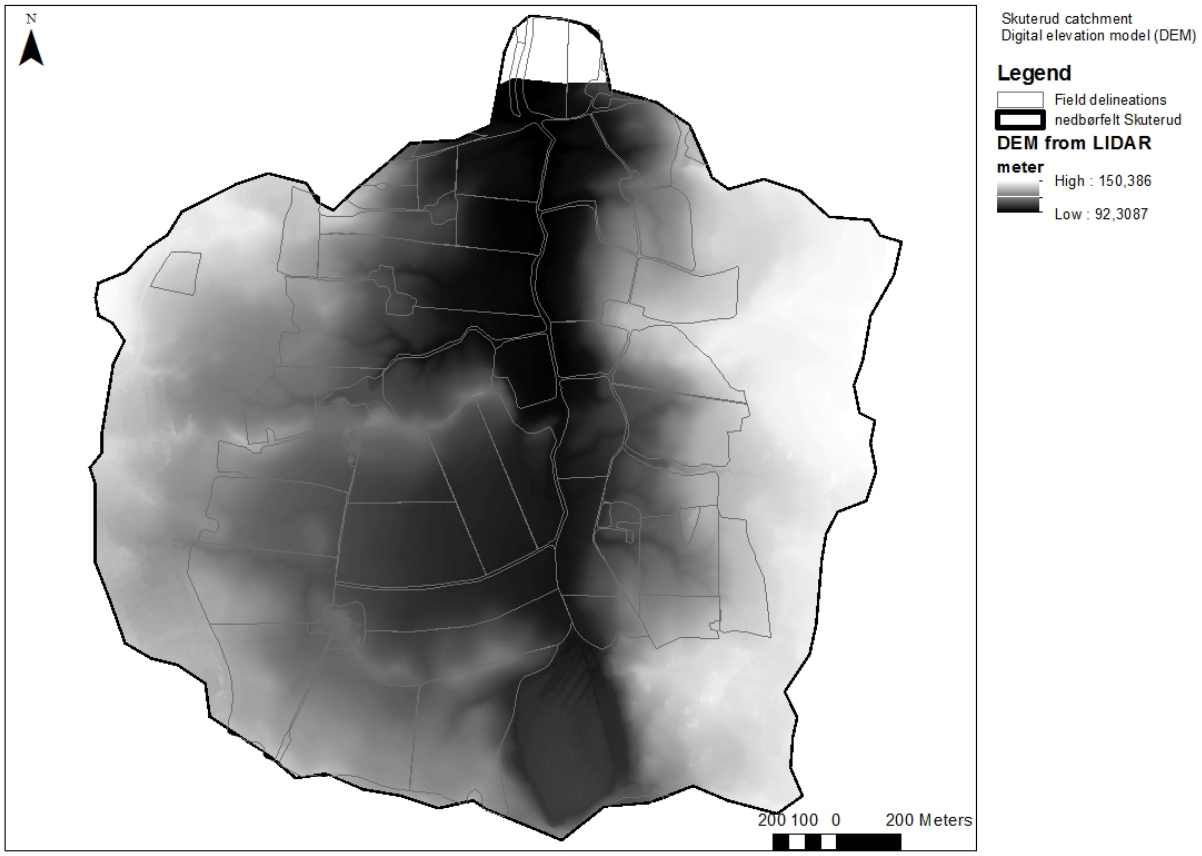

Figure 4.2: Digital elevation model acquired from airborne LIDAR data in 5 m resolution. The upper northern part is not included because the image is based on a slightly different watershed calculation than the outline. Data obtained from Bioforsk.

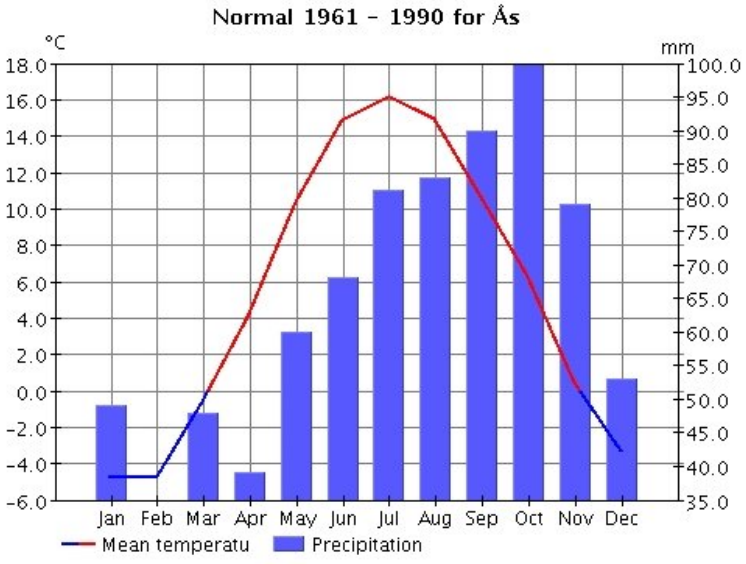

Figure 4.3: Monthly average temperature and precipitation in the period 1961-1990, from climate station in Ås. Obtained from www.eklima.met.no

Figure 4.4: The weir installed at the Gryteland catchment. Picture taken during fieldwork spring 2013. Photo by: Torsten Starkloff.

5 Background

To get an overview of what soil surface roughness is, and how roughness has been studied through the last six decades, the following background chapter is provided.

As mentioned in the introduction, soil surface roughness are the irregularities in the soil surface caused by soil type, grain size rock fragments, vegetation cover and land management practices. Soil roughness has been divided into 4 sub-categories (Takken, 2000): 1) micro-relief variations or grain roughness mainly determined by the soil type, 2) random roughness, which is related to soil aggregates and caused by tillage, 3) oriented roughness describes the systematic variations in topography due to tillage practice 4) higher order roughness represents elevation variations at the field, such as taluds or parcel borders. These categorize are not fundamentally distinguished as they related to the scale with which we consider a soil surface. However, as soil roughness in this thesis mainly is related to surface storage, the most relevant categories are random roughness and oriented roughness. However, oriented roughness, should be considered separate from random roughness as the orientation to a large extent determines the surface storage, e.g. whether the tillage is done parallel or across the contour lines will have a huge influence on the surface storage, whereas the random roughness is assumed to be without an orientation. Thus, in this study only random roughness is considered.

Micro-topography data has been obtained with a variety of methods. Some methods only capture a profile or transect of elevation data, while others covers an area, typical only a few square meters in extent. Five methods are used in the study, which will be described in section 6.2: Roughness measurement methods. Common to all of them is that to quantify roughness from micro-topography data, some type of index has been calculated. Much research has been focused on developing the most informative index, e.g. the index the best correlate with average surface storage or another relevant soil physical parameter.

Various ways to quantify random roughness

Since the late 1950s researchers have tried to quantifying soil surface roughness by various indices. Indices developed have been based on either statistical indicators of surface elevations point measurements or on quantification of the volume or surface areas of voids between soil clods. Most used has been some form of the standard deviation of elevation point data (Doren and Linden, 1986). Allmaras et al. (1966) proposed the so-called random roughness parameter (RR) which was:

$$RR \approx s_x h \qquad \text{Eq. 1}$$

where h is the mean height among 400 height measurements [m] and s_x is the standard deviation of the natural logarithm of the height measurements after having mathematically removed the effect of tillage tools marks and slope (Allmaras et al., 1966). It was not explained how effect of tool marks and slope was removed and consequently no standard method has been proposed for this purpose. Doren & Linden (1986) noted that using an index based on the standard deviation will not reflect the horizontal spacing between elevation peaks or the frequency of peak extremes. Thus, the standard deviation as an index lacks the correlation to important characteristics of the physical-spatial soil surface. However, indices based on the standard deviation are popular because of the simplicity of calculation. An index that incorporates physical-spatial significance is the limiting distance (LD) (Doren & Linden, 1986). This index utilizes the spatial variability between pairs of elevation measurements to quantify the semi-variance, similar to the method used in kriging interpolations. The semi-variance defined as:

$$v_h = \sum_{i=1}^{n} (Z_i - Z_{i+h})^2 / 2n \qquad \text{Eq. 2}$$

where n is the number of elevation pairs that occur in the data set at a certain lag interval, Z_i is the elevation in a given point and Z_{i+h} is another, and h indicate the given lag number. The term mean-absolut-elevation-difference is then defined as:

$$\Delta Z_h = \sum_{i=1}^{n} |Z_i - Z_{i+h}| / n \qquad \text{Eq. 3}$$

where Z_i and Z_{i+h} are similar to the above definition. This analysis is applied to each data set, for each row and column in a grid of elevation measurements. Linear regression analysis is then used to relate the ΔZ_h to the lag distance ΔX_h, giving the following relationship:

$$\Delta Z_h = 1/[(b(1/\Delta X_h)) + a] \qquad \text{Eq. 4}$$

where ΔZ_h is the mean absolute-elevation difference at a horizontal spacing of ΔX_h and a and b are fitted parameters. The term limiting distance (LD) is finally defined as:

$$LD = 1/a \qquad \text{Eq. 5}$$

where a is the fitted parameter from above. The LD is an indicator of the central tendency of the difference in elevation between individual points, while RR is an indicator of the central tendency of the difference between points and the mean elevation (Doren and Linden, 1986). Lehrsch et al. (1988a,b) tested 8 indices for how well they related to physical properties of soil roughness. Their objective was to find the index most sensitive to cultivation method, crop cover and rainfall. Based on their criteria they selected an index based on the micro-relief index (MI) and the frequency (F):

$$MIF\ (mm) = MI \times FREQ \qquad \text{Eq. 6}$$

where MI (mm) is the micro-relief index defined as, for each transect, the area per unit transect length between the surface profile and the regression line through the measured point elevations, and FREQ (mm^{-1}) is the number of elevation maxima per unit transect length. MIF was also correlated to a list of important soil physical properties, but found to be mostly correlated to bulk density, with correlation coefficient of -0.80 and -0.72 between MIF and dry and wet bulk density respectively (Lehrsch et al., 1987). Because of the popularity of the RR index, RR was compared to MIF. It was found that there was a correlation coefficient of 0.78 between MIF and RR and that both indices showed sensitivity to the effect of rainfall, although for RR this effect was not found to be statistically significant (Lehrsch et al., 1988a).

Considerations about the random roughness index

Random roughness (RR) is used in several equations to estimate surface depression storage, the fraction of surface covered with water and amount of rainfall excess needed to start runoff. RR was tested and found to vary significantly with land use, temporal changes and tillage orientation (Cremers et al., 1996). Thus, RR is a relevant index because of the importance as input in physical erosion models and because the index has proved sensitive to physical soil surface characteristics and to changes affected by rainfall and land use. Despite the simplicity of the RR index, there seems to be inconsistency in the way researchers have calculated the index (Zobeck and Onstad, 1987). Allmaras et al. (1966) calculated RR based on 400 height recordings, the upper and lower 10% of recordings were eliminated to avoid erratic data. Further the data was transformed using the natural logarithm, to obtain an approximated normal distribution. Many authors use the RR index but without specifying whether or not the upper and lower 10% of recording are eliminated, whether it is transformed using the natural logarithm and so forth (Zobeck and Onstad, 1987). Further Cremers et al. (1996) compared RR to other roughness indices and conclude that it is not necessary to remove the 10% upper and lower values of a roughness data set, thus reducing the RR-index to the standard deviation (SD) of the dataset, as long as the effect

of slope and oriented roughness have been removed. They compared SD of their roughness data to the limiting distance (LD) index as described above and found the following correlation between LD and SD using 12 transects:

$LD = 1.58 * SD - 0.13$ $r^2=0.98$ Eq. 7

Doren & Linden (1986) found a similar relationship between RR and LD:

$LD = 1.52 * RR + 0.02$ $r^2=0.909$ Eq. 8

Thus, although other indices might show a slightly higher correlation with various soil physical parameters, RR has persisted as the dominating index for soil roughness research.

6 Materials and methods

6.1 Roughness index

Based on the background chapter, in this study the soil roughness was compared using the RR index, calculated as the standard deviation of all elevation recordings, after the effect of slope and oriented roughness have been removed. For the rest of the report calculation of RR follows this description. Slope removal was done by fitting a line (for 2D data) or a plane (for 3D data) through the point-cloud using least root-mean-square error estimates, and calculating the perpendicular distance from a point to the line or plane. To avoid the effect of oriented roughness, only transects along ridges were used to calculate RR for 2D data. For 3D data the RR was calculated using the whole point cloud, assuming that the effect of oriented roughness would be minimal.

6.2 Roughness measurement methods

Five methods were used to obtain micro-relief data from which soil surface roughness was quantified. They can be divided into two groups: 1) contact methods – devices that touch the soil and as such potentially destroy the surface. These are low-tech and cheap methods, while not necessarily faster than group number 2) non-contact methods – devices that use sensors to record micro-topography. These are high-tech methods and usually more expensive but interesting because the accuracy can be extremely high.

6.2.1 Contact methods

6.2.1.a Pinboard

The pinboard or pin-meter was the first method proposed to quantify soil surface roughness, based on work of Kuipers (1957). The device has been developed in many forms and resolutions (Podmore and Huggins, 1981). Allmaras et al. (1966) used a pinboard, see figure 6.1 with 20 pins distributed over a frame of 1 meter with a 5 cm spacing. As is evident from figure 6.1 the board is mounted on a metal frame, creating the possibility to move the board along the frame and get recordings in a grid. Other pinboards have been developed which only acquire data in one transect, for instance the one used by Cremers et al. (1996) which had 57 pins over a 70 cm frame, giving a spacing between each pin of 1.25 cm. In their experiment one transect was recorded by location.

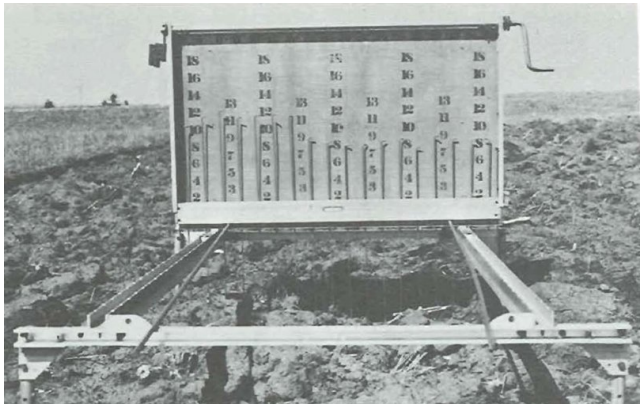

Figure 6.1: Picture showing one of the first documented pinboards. From: Allmaras et al. (1966)

Data acquisition and processing

The pinboard used in this study had 3 mm thick metal pins on a wooden frame of 1 meter (figure 6.2). In total 50 pins was used, having a 2 cm spacing between the pins. The metal pins were lifted up on the frame and at once let loose so they fell to the ground, reproducing the surface elevation in one transect. A white screen was placed behind the row of pins, and a ruler in front and a photo was recorded. Care was taken to ensure that the camera was perpendicular to the board, and as close to the board as possible. The photos was processed in an open-source image-editing program ImageJ[1] (Rasband, 2013), making it possible to establish the scale factor from the ruler in the image. In this way an approximation of the real-world distances was obtained from the image and thus relative elevation measurements could be recorded. The recordings were exported to Excel. With linear regression an approximate slope in the image was found and the distance perpendicular to the slope was calculated. Then the standard deviation of distances were calculated. On each plot one transect were recorded along and across the direction of cultivation. Distortion due to the camera lens was not accounted for, but assumed to be relatively small in comparison with the level of precision for the method.

Figure 6.2: Picture showing the pinboard which was used in the fieldwork for this thesis. Photo by: L.Thomsen

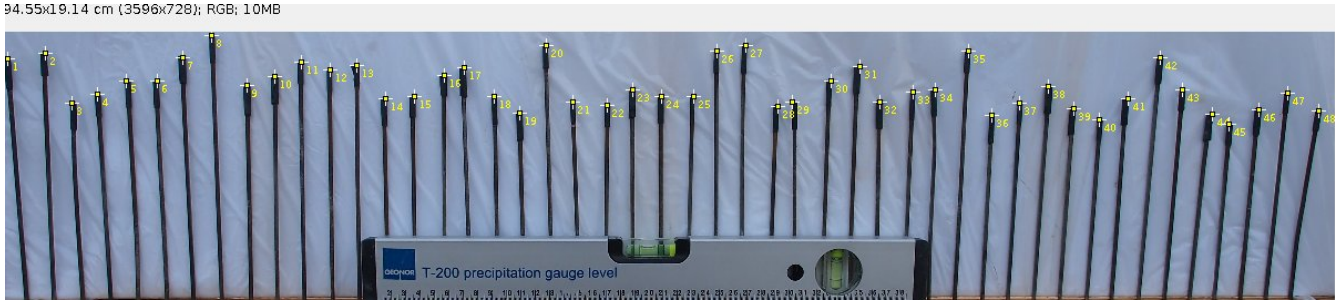

Figure 6.3: Screen-dump from the image processing program. Using the ruler in the image a Cartesian coordinate system covering the picture was created with origin in the upper left corner. Then each tip of pin was digitalized manually and a text file with the coordinates was exported to Excel for further processing.

1 ImageJ v.1.46a, downloaded from http://imagej.nih.gov/ij

6.2.1.b Roller chain

A roller chain is one of the simplest methods to measure soil roughness. The method was first proposed by Saleh (1993) as a fast and practical field method to obtain roughness data. A roller chain is preferred because the joints are fixed and thus approximately only bend in the vertical direction. The ratio between the straight line covered by the chain over the soil profile length covered by the chain is an indication for the roughness (figure 6.4).

Figure 6.4: Picture from measuring soil roughness with a chain. From the fieldwork. Photo by: L. Thomsen

Data acquisition and processing

A one meter long roller chain with joints of 4 mm in diameter and 6 mm between joints was used. The chain was carefully, joint-by-joint, laid out on the surface and the straight length from start to end of the chain was measured using a ruler. For each plot 6 measurements were recorded, 3 replicates along and across the ridges. The ratio between the straight length of the chain and the measured length it covered on the surface was used as a measure for the roughness. The index proposed by Saleh (1993) was used:

$$Cr = (1-L2/L1)*100 \qquad \text{Eq. 9}$$

where L1 is the known length [m] of the chain (the length of the profile) , L2 is the measured horizontal length [m]. Cr was calculated using the average L2 value per plot and related to RR from the pinboard. This was done by first calculating the profile length from pinboard transects and calculate the same Cr index, a regression could then be established between RR from pinboard and Cr from chain. This was necessary on order to compare roughness values from the chain with other methods (Jester and Klik, 2005).

6.2.2 Sensor methods

In the following three different sensor techniques are described. They can all be used to obtain roughness data based on the same principle. From the sensor output data containing a list of x-, y- and z-coordinate data in an arbitrary Cartesian coordinate system are created, also called a 3D point cloud. A 3D point cloud can be used to construct a digital elevation model (DEM) of raster cells of a chosen resolution or the point-cloud can be used directly as elevation data of the soil surface. Since random roughness is defined as the standard deviation of height measurements, roughness can be extracted by calculating univariate statistics on the point cloud or the raster cells in a GIS or statistics software program. In the following the working principle behind each of the methods are briefly explained, with more emphasis of the new 3D depth-sensing system, mentioned in the introduction, because this has not up to now been used in erosion studies.

6.2.2.a Stereophotogrammetry

With stereo photogrammetry two images are used, looking vertically down on the same spot, but separated horizontally so that the scene is viewed from two different angles (Taconet and Ciarletti, 2007). The construction of 3D point data is based on a triangulation process and knowledge on the camera lense. In this thesis, due to time constraints the procedure is not further explained, but detailed information is available in Luhmann et al. (2006). The accuracy of a stereophotogrammetric point-cloud depends on the images available. Shadows in the image will decrease the estimating. The software program used for processing, reported accuracies ranging from 0.02 – 4mm.

Data acquisition and processing
With a digital camera photos of the soil surfaces where taken. On the front page, the fifth image shows as soil surface with black- and white markers. Using these markers the software program PhotoModeler was able to link together two or more images. The data processing was done by T. Starkloff.

6.2.2.b 3D-depth sensing using the "Xtion"

In 2010 a new depth-sensing technology was developed in cooperation between PrimeSense and Microsoft, originally to boost the gaming-console industry with a device, the Kinect, that would enable new no-touch interface between the gamer and the Xbox. Immediately the sensor was hacked and an abundance of open source codes for drivers appeared on the internet ("Kinect - wikipedia," 2013; Kramer et al., 2012). The potential for the use of the sensor has shown to be much greater than first anticipated, for instance the sensor has been used in research in various fields from robotics to surgery to bathymetry and geomorphology studies (Comb et al., 2011; Mankoff and Russo, 2012; Tölgyessy and Hubinský, 2010; Whelan et al., 2012). Although the sensor became known through Microsoft's Kinect, it was PrimeSense that developed the depth-sensing technology, which is why also other similar products exist, for instance Asus' Xtion Pro or Pro Live, and PrimeSense's own Carmine. In this study an Asus Xtion Pro was used (figure 6.5). In the following the terms the *Xtion sensor* and *3D depth sensor* will be used interchangeably, and refers to the PrimeSense 3D depth sensor. The working principle is the same for the sensor in the Kinect and Carmine.

Figure 6.5: The Xtion Pro 3D depth sensor. Source: www.tekwind.co.jp

The 3D depth-sensing technique belongs to a group of 3D reconstruction techniques called structured light imaging. Other types of structured light techniques use so-called gray-coding or sine-waves (Scharstein and Szeliski, 2003; "Structured light imaging," 2011). The Xtion uses light-coding or pattern recognition (PrimeSense, 2013). The Xtion has an infrared (IR) light projector and an infrared camera (figure 6.6). The infrared light projector emits one beam of light that is split by a diffraction grating which emits light in a known speckle pattern. This speckle pattern is reflected when it meets an object and recorded by the infrared camera. This is correlated to the pattern recorded on a reference plane with a known distance to the sensor which is stored in the memory of the sensor. Figure 6.6 illustrates the conceptual device set up ("Method and system for object reconstruction. Patent WO2007043036," 2007).

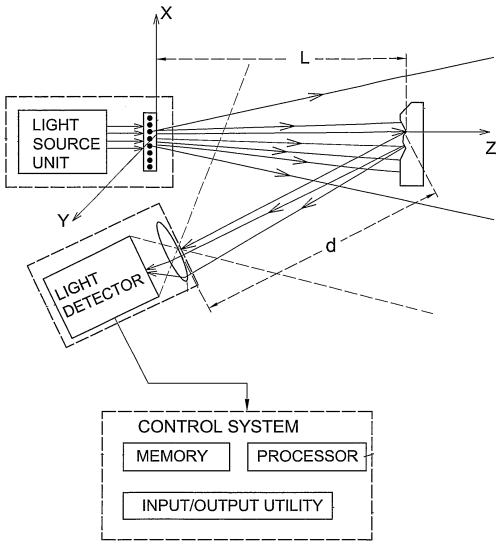

Figure 6.6: A schematic overview of the working principle behind the PrimeSense 3D depth sensing technique. From: "Method and system for object reconstruction. Patent WO2007043036," (2007)

The calculation of the depth to the sensor is based on a triangulation process, using the distortion of the recorded pattern relative to the reference pattern (figure 6.7) (Chow et al., 2012; Khoshelham and Elberink, 2012; "Method and system for object reconstruction. Patent WO2007043036," 2007). For the calculation of depth a coordinate system is defined, so that the origin is at C - the position of the IR camera, see figure 6.7, the Z-coordinates are orthogonal to the object plane and X-coordinates are parallel to the baseline which is the line along the IR camera and projector. The distance, b, is known because the sensors are mounted on the same frame. The focal length in the camera, f, is known, as well as Z_0, which is the reference distance which is stored in the memory of the sensor. When the IR laser projector, here abbreviated with L, emits light, it hits an object

and is reflected and recorded by the ir camera, C. The point in space the light hits is here abbreviated *k*. The object will be closer or further away, than the reference point, point 0, and results in a distorted pattern in the camera, which yield the distance named the disparity, d, in the sensor.

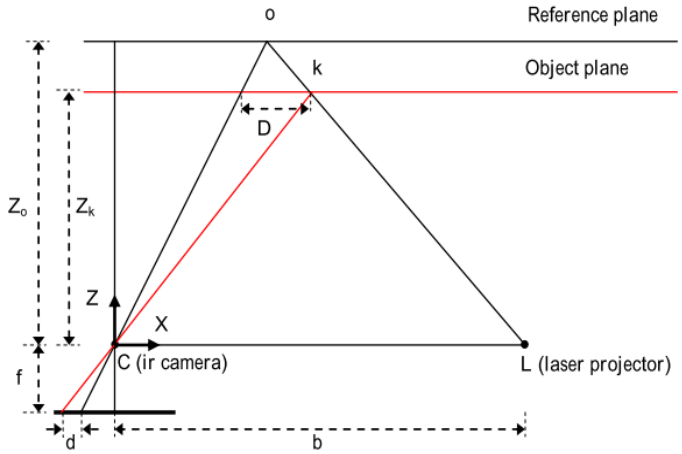

Figure 6.7: Diagram illustrating the triangulation process used in Xtion for depth-calculation. From Khoshelham and Elberink (2012)

Based on triangulation the distance Z_k can be deduced according to this relationship:

$$\frac{D}{b}=\frac{Z_0-Z_k}{Z_0} \qquad \text{eq.10}$$

$$\frac{d}{f}=\frac{D}{Z_k} \qquad \text{eq. 11}$$

substituting D in equation 10 into 9 and isolating Z_k:

$$Z_k=\frac{Z0}{1+\frac{Z0}{fb}d} \qquad \text{eq. 12}$$

Based on this mathematical model Khoshelham & Elberink (2012) executed a manual calibration of the depth measurements from a Kinect device. The PrimseSense algorithms are protected under license, so the formulas above is a best-guess (Konolige & Mihelich 2010). According to the product specifications the Xtion works within a range of 0.8-3.5 m, but without stating the expected accuracy. Several authors have executed test to quantify the accuracy of the Xtion in stable indoor conditions and suggested various calibration routines (Chow et al., 2012; Khoshelham and Elberink, 2012; Mankoff and Russo, 2012). A theoretical random error model for the output of the Xtion, showed that the random error of depth measurement is proportional to the square distance from the sensor to the object, i.e. the further away from an object the higher the probability of error in estimation of the distances:

$$\sigma_Z{}^2=\left(\frac{\partial Z}{\partial d}\right)^2\sigma_{d'}{}^2 \qquad \text{eq. 13}$$

where d is a random variable with a normal distribution, Z is the distance to an object and d is the disparity value, the raw output from the device, as explained above (Khoshelham and Elberink, 2012). The random error model is confirmed by tests where a sensor is scanning a flat wall orthogonal to the sensor at different distances. A plane is fitted to the point-cloud and the root-mean-square-error (RMSE) of each plane fit is plotted against distance from the sensor. Chow et al. (2012) tested an uncalibrated Kinect sensor with this method for distances up to 10m and compared the theoretical random error model with the measured error (figure 6.8). It can be seen that for distances up to 5m the RMSE the theoretical and measured error behaviour are in agreement, whereas beyond this distance, the measured error results in unpredicted errors, confirming the producer's recommendation of using the Xtion only within 5m distances. However, the quality of the Xtion output depends as well on the measurement set up and the surface properties of the object of interest. The Xtion does not work in bright sunlight, because the sensor cannot detect the IR speckles. Bright reflecting surfaces might distort the IR speckle pattern reflection and certain surface will absorb IR light and the speckles will thus not be reflected properly. Large gradients or step changes in distance will also give higher error in the output (Mankoff and Russo, 2012). This can be a problem when assessing soil surfaces, especially over ploughed ridges which can have steep gradients.

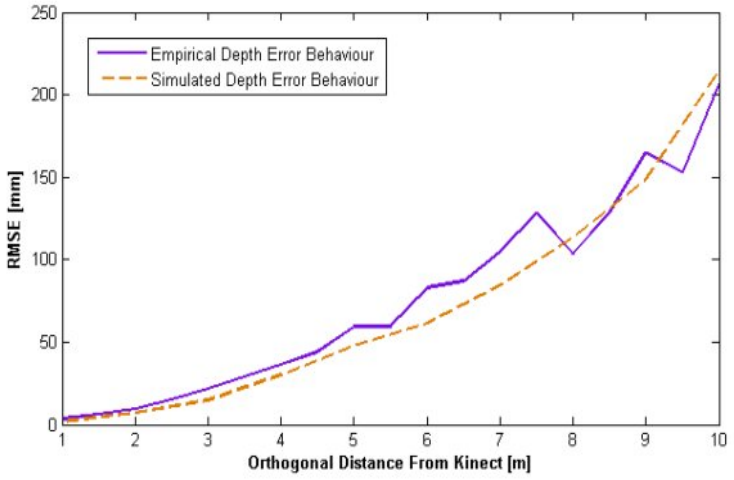

Figure 6.8 Relation between distance to object and error in depth estimation, by a Xtion sensor. Empirical depth error indicates the measured error, while simulated depth error indicates the theoretical error model. From: Chow et al. (2012)

Software interface

After the Kinect-device was hacked, it was possible to develop drivers that could facilitate the interaction between the device and a computer, thus making it possible to extract data from the device. An abundance of software interfaces have been developed for processing Xtion data (for a relevant list see www.openni.org). In this thesis the software Skanect[2] was used. Skanect communicates with the Xtion, grabs the raw data, which is a stream of images of 640 x 480 pixels with depth data quantified as digital numbers (DN) between 0 and 2047. An relationship exists between DN and distance to object (figure 6.9).

2 Skanect Pro v.1.4 (required purchasing a license of 99€ to be able to export the recordings to the xyz-format), obtained from: http://skanect.manctl.com/download/ . Initially we aimed at using the completely opensource code library Libfreenect, https://github.com/OpenKinect/libfreenect and guidance from Kramer et al., (2012), but it proved to be too big a challenge with the level of programming skills we had.

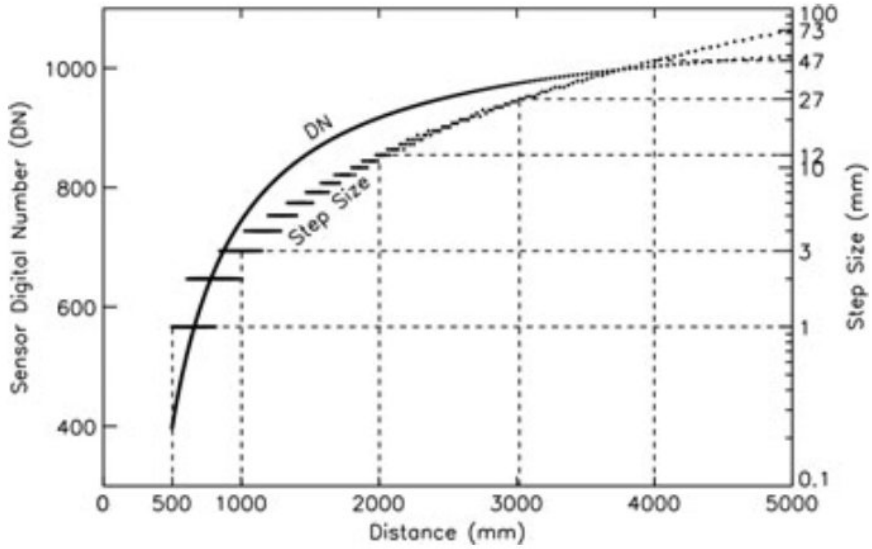

Figure 6.9: Relation between the range of sensor digital number (DN) (primary y-axis) and distance to object. The dashed lines relates to the secondary y-axis, indicating resolution of the depth image at certain distances. This is based on the Libfreenect code-library written for the Kinect. It was not possible to obtain the same information for the Skanect software, but it will be very similar since the sensor hardware is the same. From: Mankoff and Russo (2012)

Data acquisition

Since the Xtion IR camera can have difficulties detecting the IR-light in bright sunshine, the data acquisition was done during the late evenings after sunset. This means that there was delay of 4-5 hours between the data acquisition of the 4 other methods and the Xtion. Only on one occasion did it rain in between the measurements, meaning that the soil moisture was changed, and the surface had experienced splash erosion. However, for far most of the data no changes in surface properties occurred during the delay, thus the data represent the same roughness. For the data acquisition in the forest the trees provided shade enough to get data during the day, simultaneously with the other methods.

For acquisition the Skanect program is initiated, the sensor is plugged to the computer and a recording frame has to be chosen. For this study a cube of $2x2x2m^3$ was set, in order to be sure that the whole plot was covered, while not allowing the program to record too much unused surface. It is necessary to define a cube, rather than a surface since the sensor records 3D data. At the moment recordings are started, the first image is assumed to be at the center of the imaginary cube. Defining this cube ensured a certain accuracy since the Xtion will only record distances within the cube. After activating the program the sensor was swept slowly over the surface in approximately 0.5 m above ground. The sensor was carefully held perpendicular to the soil surface. While recording the Skanect program correlates vertexes from consecutively recorded images, thus creates a surface larger than what is covered in one image frame[3]. The sensor was hand-held, which is a choice that compromises the accuracy of the methods (figure 6.10). However, this approach was chosen because the time constraint did not allow us to construct a framework upon which the sensor could slide to ensure a constant distance to the surface.

3 For further explanations and a very easy video look here: http://skanect.manctl.com/support/ [accessed 2013-12-22]

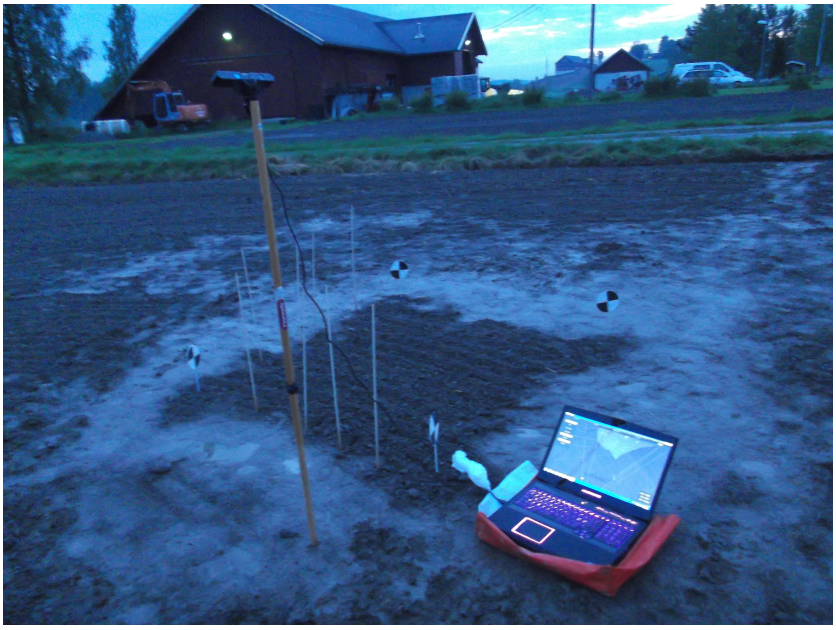

Figure 6.10: Data acquisition with the Xtion during late in the evening. The Xtion is mounted on a wooden stick and is connected to a laptop. Photo by: L. Thomsen

6.2.2.c Terrestrial laser scanner

Laser scanners have been increasingly popular during the last 2 decades for measuring short-range as well as large-range objects with very high precision both in the industry and for surveying as well as in research (Luhmann et al., 2006; Pfeifer and Briese, 2007). Terrestrial laser scanners (TLS) have been used for soil surface studies. While the technique was not very well developed it was only possible to obtain one-dimensional data, whereas the last 20 years have seen increased intensity of TLS to obtain 3D data of micro-topography (Takken 2000; Aguilar et al. 2009; Haubrock et al. 2009; Barneveld et al. 2013).The commercially most popular laser scanner emits pulses of laser light and uses a time-of-flight principle to calculate distance. The laser device emits a laser signal that is reflected when it hits an object and the reflected light is recorded by a receiver on the laser station (Luhmann et al., 2006). The time it takes the laser beam to return to the receiving device is used in the following relationship:

$$d = 0.5tc \qquad \text{Eq. 14}$$

where d is the distance between the object and the scanner, t [sec] is the recorded laser pulse travel time and c [m/sec] is the speed of light. The x-, y- and z-coordinates are calculated using the *d* and the angular measurements of the emitted laser beam with simple trigonometry presented by this equation:

$$\begin{pmatrix} x \\ y \\ z \end{pmatrix} = d \begin{pmatrix} \cos\alpha\cos\beta \\ \sin\alpha\cos\beta \\ \sin\beta \end{pmatrix} \qquad \text{Eq. 15}$$

There are many different types of laser scanners, varying in physical properties, i.e. measuring frequency, accuracy, range of operation, beam diameter etc. (Luhmann et al., 2006). The one used in this study is a time-of-flight laser scanner (Leica ScanStation 2) (figure 6.11), that emits pulses of laser light, using a rotating mirror to

obtain signals in many directions, and further rotates the head of the emitted which is mounted on the scan station, in that way obtains a 360º horizontal and a 270º vertical field-of-view, while acquiring up to 50000 points / sec (Leica-Geosystems, 2007).

According to the manufacturer the instrument accuracy of the laser scanner is 4-6 mm within a range of 50 meter (Leica-Geosystems, 2007). Other important factors that affect the actual accuracy is the measurement setup, distance and view angle to object of interest, as well as ambient conditions, most importantly air temperature gradient, soil moisture and wind (Barneveld et al., 2013) and also surface colour, with for instance a black surface reflecting less energy than a white, causing a range bias (Chow et al., 2012).

Data acquisition and processing

The sensor is mounted on the tripod and connected to a laptop, which runs the required software (Leica Cyclone) for the Leica ScanStation2 to work. A scan of a few square meters of surface takes around 10min. Subsequently, the data is processed and linked together using an algorithm in the software program and outputted as xyz-data (figure 6.12). The data processing was done by R. Barneveld.

Figure 6.11: The Leica ScanStation2 mounted on a tripod. Source:

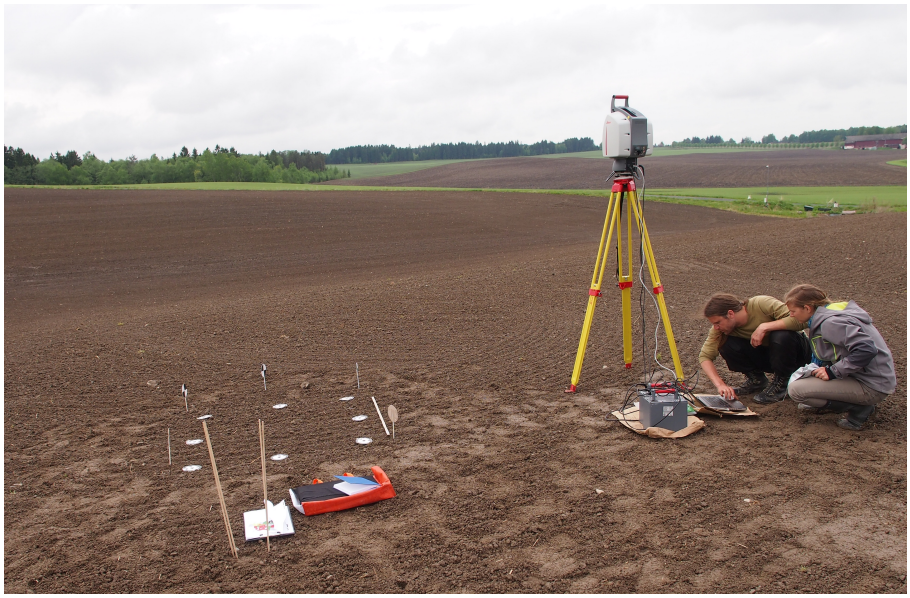

Figure 6.12: Using the TLS to get soil roughness data from the harrowed field in gryteland. Photo from the field work, by T. Starkloff.

6.3 Data sampling strategy

6.3.1 Land units

To compare the different measurement methods it would be useful to create land units based on the soil properties that has the greatest influence on soil roughness. It was initially decided to make land units based on texture class and land management. However, the fieldwork experienced practical and time related restrictions. For instance, while most of the fields were ploughed not all the measurement devices were ready for use and at the time when the equipment was ready most of the fields had been seeded and were inaccessible for us, making it impossible to test for effect of land use and texture class. Instead data collection was based on land use only. Based on observations in Skuterud during June 2013, a land use map was created using the following characteristic surfaces in Skuterud: ploughed, harrowed, direct seeding on stubble and forest For one of the harrowed fields, roughness on 3 plots on two different soil texture types were obtained, showing no significant differences in roughness value based on texture class. As for the ploughed surfaces, since all field in Skuterud were harrowed at the start of the fieldwork and ploughed fields were not found in the study area, instead a mouldboard ploughed field near Leirsund, Lillestrøm (UTM zone 32N, 616634m east, 6653133m west) was included. The soil type here is dominated by heavy clay from fluvial deposits, thus not very comparable to the fields of Skuterud. Later some marginal spots in Gryteland with ploughed ridges were discovered and included in the analysis. The ploughed spots (figure 6.13 and 6.14) were obviously margins which the farmer decided not to harrow and the location were therefore not random or truly representative for the whole field. However, it was expected that the most crucial parameter influencing random roughness was tillage, and therefore it was decided to include these data as well.

Figure 6.13: Margin of field, located in Gryteland, with mouldboard ploughed surface, which was included in the data sampling.

Figure 6.14: Another mouldboardploughed margin, located in Gryteland, which was included in the data sampling

In contrast to the field in Leirsund, the ploughed field margins were located on the most sandy spots in Gryteland, and thus representing a different texture class. Despite the texture difference between the clay and the sandy soils the ploughed fields did also not show significant differences in soil roughness.

6.3.2 Data sampling in practice

In practice the relevant data had to be sampled from the fields that were available and of interest to the research, as the above section illustrates. Thus, the chosen fields of data collection were based on availability rather than random selection. But, within the chosen field geographic coordinates were extracted using a random point generator tool in ArcGIS, ensuring, to a certain extent a randomized data sampling strategy. Table 6.1 gives an overview of the data collection.

Table 6.1: Dates of fieldwork as well as the number (n) of data sampling plots per method and land use

date	Land use	Xtion (n)	Stereo (n)	Pinboard (n)	TLS (n)	Chain (n)
30.05.2013	Harrowed field, Gryteland	1	1	8	1	8
04.06.2013	Harrowed field, Rustad	5	6	12	-	36
07.06.2013	Mouldboard ploughed, Leirsund	-	3	6	-	21
14.06.2013	Forest,	3	3	6	1	18
18.06.2013	Direct seeding on stubble	3	3	6	-	18
19.06.2013	Ploughed, Gryteland	3	3	10	-	21

A land use map of Skuterud from June 2013 was created (figure 6.16, on next page). The map also indicates the locations for data collection. The map was created in ArcGIS 10.1.

Data acquisition routine

On each identified location the five methods were applied. A routine was developed ensuring that the measurements were taken in the same way at all locations. When the random point in the field was found with gps, 5 markers were placed on the surface delineating the field of interest, the markers were placed so that it was parallel to the tillage direction, if there was any. This area was approximately 1x1m^2. The fifth marker was placed randomly on one of the sides, ensuring that when reconstructing the sensor point-clouds it would be possible to recognize the orientation (figure 6.15). At the two occasions where the TLS was available this was the first method to apply. Then 1) Photos were taken for the stereophotogrammetry, 2) the chain was applied, 3) the pinboard was applied and finally 4) the Xtion was applied. The Xtion had to come last because it usually was taken in twilight later in the day, while the other methods were taken during daytime.

Figure 6.15: Field photo from the forest surface, showing the markers used marking the area of intest.

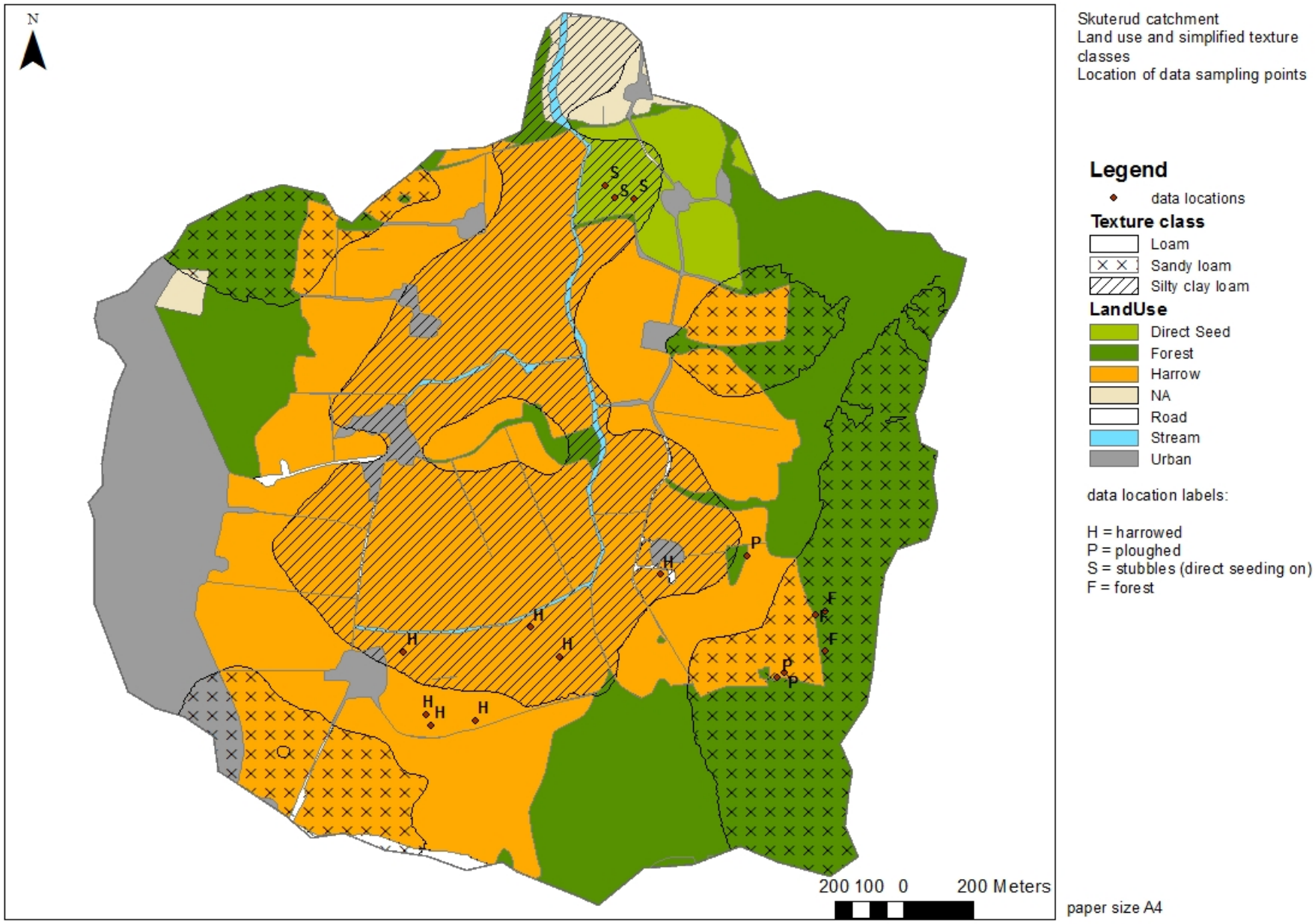

Figure 6.16: Land use map of Skuterud June 2013.

6.4 Point-cloud data processing

All the sensor data was outputted as xyz-data in an arbitrary coordinate system. To remove any effect of slope in the data a plane was fitted to the point cloud using least squares error method with a iterative solver function solving the equation with three unknowns. A plane was defined as:

$$Z = aX + bY + c \quad \text{Eq. 16}$$

with a, b and c being fitted parameters to the data which were estimated based on least root-mean-square error between the points and the plane . After the plane was defined the distance of each point normal to the plane was calculated using:

$$D = \frac{ax_0 + by_0 + cz_0}{\sqrt{a^2 + b^2 + c^2}} \quad \text{Eq. 17}$$

This distance equals the elevation measurement. The calculation was developed in R[4], (Appendix I). For each point cloud a subset of 0.8m x 0.8m around the origin of the coordinate system was considered rather than the full point cloud, this ensured the elimination of the markers as well as surface outside the relevant plot square which was affected by foot steps or tools. With the final elevation data the standard deviation was calculated which corresponds to the random roughness index. The reported values from TLS, Xtion and stereophotos are the RR calculated directly from the 3D point-clouds.

Later the data was loaded into GRASS GIS[5], an open source raster based GIS. When loading the xyz data into GRASS a raster grid file was defined. Depending on the desired resolution of the grid, the number of points that fall within one grid-cell was used to calculate the value of the cell.

6.5 Comparison of measurement techniques

The most interesting aspects of comparing methods to measure roughness are the accuracy, precision and resolution. Accuracy is defined as the degree of conformity of a measured or calculated quantity to the “true” value, while precision is the degree of mutual agreement among a series of measurements of the same value or the reproducibility of a result. Resolution is here defined as the number of measurement points per unit of length, which is along the lines of the work by Jester & Klik (2005). These aspects are all interlinked, but it is important to be able to distinguish them from each other and to be able to quantify all 3 parameters when measuring soil roughness.

6.5.1 Accuracy

In the description of the methods the internal accuracy of the methods was described. But the actual accuracy depended as well on external factors such as measurement set up and the ambient conditions and was therefore difficult to quantify. The absolute accuracy was however not very important for the random roughness index because it was a measure for relative elevation differences within a plot, although, the approximate accuracy of any method of course is interesting to know in the comparison to other techniques. In this study the methods

4 R version 3.0.1 (64bit) downloaded from: http://cran.r-project.org/bin/windows/base/old/3.0.1/, used with the graphical user-interface R Studio 0.97.511, downloaded from: http://www.rstudio.com/ide/download/

5 GRASS version 6.4.3RC3

were only indirectly compared in terms of accuracy. Assuming that TLS provides the closest to “true” roughness value, a value for accuracy can be obtained by calculating the difference between roughness measurements from the other methods and the TLS. Further ANOVA tests were executed to test the degree to which the methods agree about a roughness value, which as such was a measure for the relative accuracy. For the statistical analysis the software SigmaPlot was used.

6.5.2 Precision

The acquired data was compared in terms of precision, with the standard deviation of a group of measurements as a measure for precision. The spatial unit to compare was the land use units, thus, although the measurements were not repeated over the same plot several times, it was assumed that the surfaces within one land unit were spatially uniform and thus represented the same random roughness. Unfortunately not enough replicates were taken to test the assumption of spatially homogeneity within land units. As for the pinboard and chain method the precision was difficult to obtain in any other way since the method was destructive to the soil surface, i.e. the exact same transect will not be present after one measurement.

6.5.3 Resolution

The methods were compared in terms of resolution. The point-clouds were converted to raster files at different resolutions to see the effect of grid resolution on the random roughness index. It was tested if the increased resolution obtained with the TLS compared to the Xtion had an effect on the calculated roughness index.

6.5.4 Other aspects

Other aspects which are interesting to take into account when comparing methods are the ease of obtaining data, the cost related to the method and the possible spatial extent the method can cover. These aspects will briefly be touch upon in the discussion of the methods.

6.6 LISEM – a physically-based erosion model

Another way to compare the roughness data is to see what influence roughness data has in an erosion model. In this thesis the erosion model LISEM was chosen. In the next section the theoretical framework will be discussed briefly, with emphasis on the process of simulating surface storage, as roughness is the main input for these calculations. Further the calibration method is described, together with characteristics of the rain events used to run the model, and a description of how the model results will be used to compare the effect of roughness.

6.6.1 Theoretical framework of LISEM

The Limburg Soil Erosion Model (LISEM) is an event-based physically based model, originally developed to simulate the effect of grass strips on soil loss in the province of Limburg in the Netherlands (De Roo et al., 1994). The model simulates the hydrology and sediment transport during and after a single rain event. The model is raster-based, meaning that a catchment is represented by a grid of equally spaced cells of a chosen size. Preparation of input raster maps is done in the a raster GIS: PCRaster[6] (*PCRaster documentation*, 2013). The model incorporates rainfall, interception, surface storage in micro-depressions, infiltration, vertical movement of water in the soil, overland flow, channel-flow, detachment by rainfall and throughfall, transport capacity and detachment by overland flow. The model is driven by rainfall input data, given as rainfall intensity. The model has been continuously developed during the last 20 years and some of the theoretical framework as well. Two versions are used in this study LISEM version 2.58[7] and the newest version: OpenLISEM version 1.70[8] (Jetten 2013).

A schematic overview of the incorporated physical processes in LISEM is shown in figure 6.17. Each rectangle indicates a physical process, that contributes to an estimated transport capacity for each cell, which in turn is used to estimate flow, detachment and deposition, as well as the water and sediment which is transported to a downslope cell. The thin dotted lines links to the input maps, which have a value for each cell based on land units. Random roughness (RR) is input for calculated surface storage, which together with the local drainage direction (ldd) map, Manning's n and the slope is used to calculate overland flow. In the following only the part of the model simulating surface storage will be described since this is the only process that uses roughness input data (De Roo et al., 1996b; Jetten, 2002).

6 PCRaster version 3.0.1. with Nutshell version 4.5 [10 Mar 2013], a graphical user-interface (instead of a command-line interface). Downloaded via Sourceforge: http://sourceforge.net/projects/pcraster/ and http://sourceforge.net/projects/nutshellqt/

7 Accessed via Jannes Stolte at BioForsk.

8 Accessed via: http://sourceforge.net/projects/lisem/

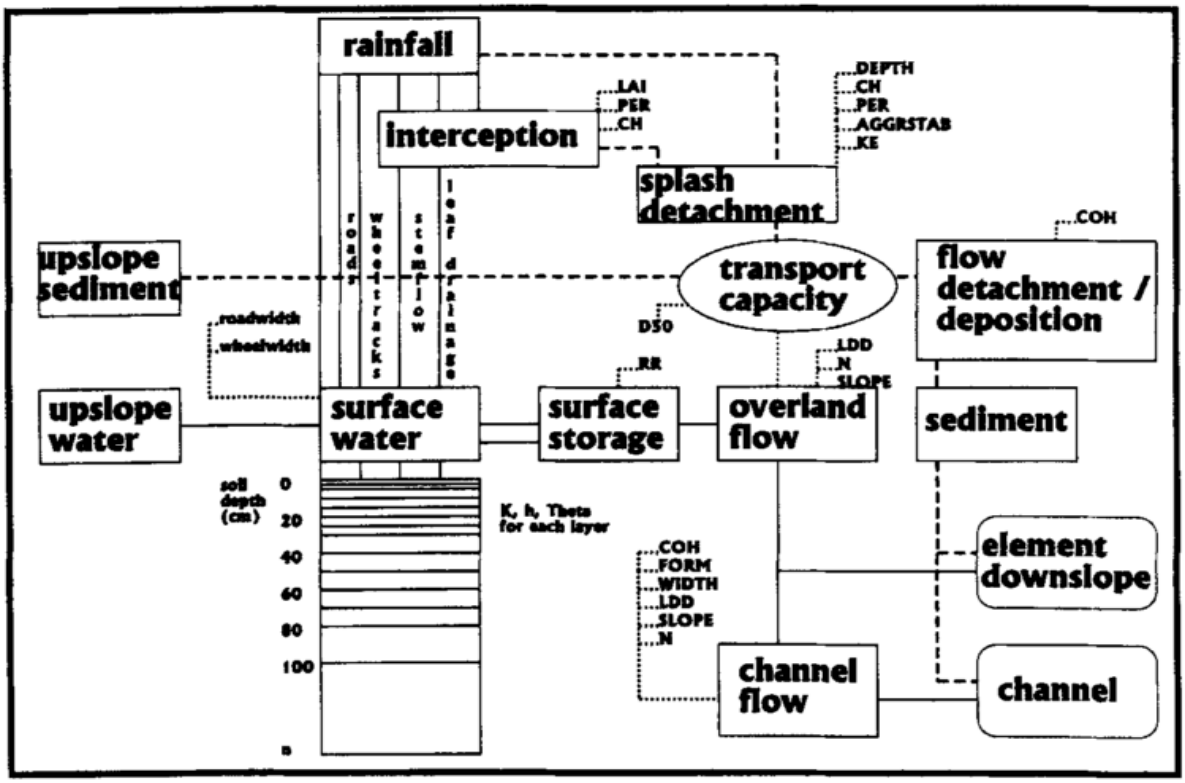

Figure 6.17: flowchart of physical processes incorporated in LISEM, from: De Roo et al. (1996b)

Surface storage and roughness in LISEM

Surface storage relates to micro-depressions in the soil surface in which rain water will pond until they overflow and start overland runoff. The process depends on the infiltration rates, the slope and the soil roughness (Amoah et al., 2013). For a given spatial unit an average surface storage value can be estimated, however it is recognized that surface runoff actually starts before this average value is reached. Runoff is a rather complex spatial process where a network of micro-depressions will fill up and overflow into each other. Thus, in LISEM two concepts are used to simulate surface runoff: the Maximum Depressional Storage (MDS) and the Start Depressional Storage (SDS). MDS is defined as the threshold value for a given area above which the surface micro-depressions will overflow. It means that when this threshold value is reached in any given cell, each additional rain drop will directly create overland runoff out of the cell (Jetten, 2002). In LISEM RR is used to estimated MDS, using the following relationship:

$$MDS = 0.234RR + 0.01RR^2 + 0.012RR*S \quad \text{Eq. 18}$$

where RR is random roughness [cm] and S is terrain slope [%] . This is based on work of Kamphorst et al. (2000) and earlier work of Onstad (1984), who related various roughness indices to MDS, in order to find an easy way to estimate surface storage. It was found that among various indices RR showed the best correlation to MDS ($R^2 = 0.8$). Before threshold MDS is reached some runoff will occur in some part of the cell. In LISEM v2.58[9] it is assumed that when 10% (that is an arbitrarily chosen threshold) of a cell surface is ponded runoff

9 The following explanation follows the LISEM Manual as of 2002 (Jetten 2002). The newest version of LISEM, OpenLISEM v1.7 estimates the fraction of ponded surface slightly different, but since reported results in this report comes from LISEM v. 2.58 this is explained in detail.

starts. The fraction of ponded surface is estimated by:

$f_{ps} = 1 - \exp(- a\ h)$ Eq. 19

where f_{ps} is the cell fraction of ponded surface, h [mm] is the water height at the surface and a [-] is an empirical factor with values between 0.04 and 1.8. It is found that there is a strong linear relationship between factor a and RR ($R^2 = 0.99$):

$a = 1.406 * (RR)^{-0.942}$ Eq. 20

where RR is in mm. When $f_{ps} = 0.1$ runoff will start , this threshold is termed Start Depressional Storage (SDS). For a graphical illustration of the relationship between water height, RR and fraction of ponded surface, see figure 6.18. At threshold SDS: $f_{ps} = 0.1$ and the water height will equal:

$0.1 = 1- \exp(-a\ h) <=> h= \ln(0.9)/ (-a)$ Eq. 21

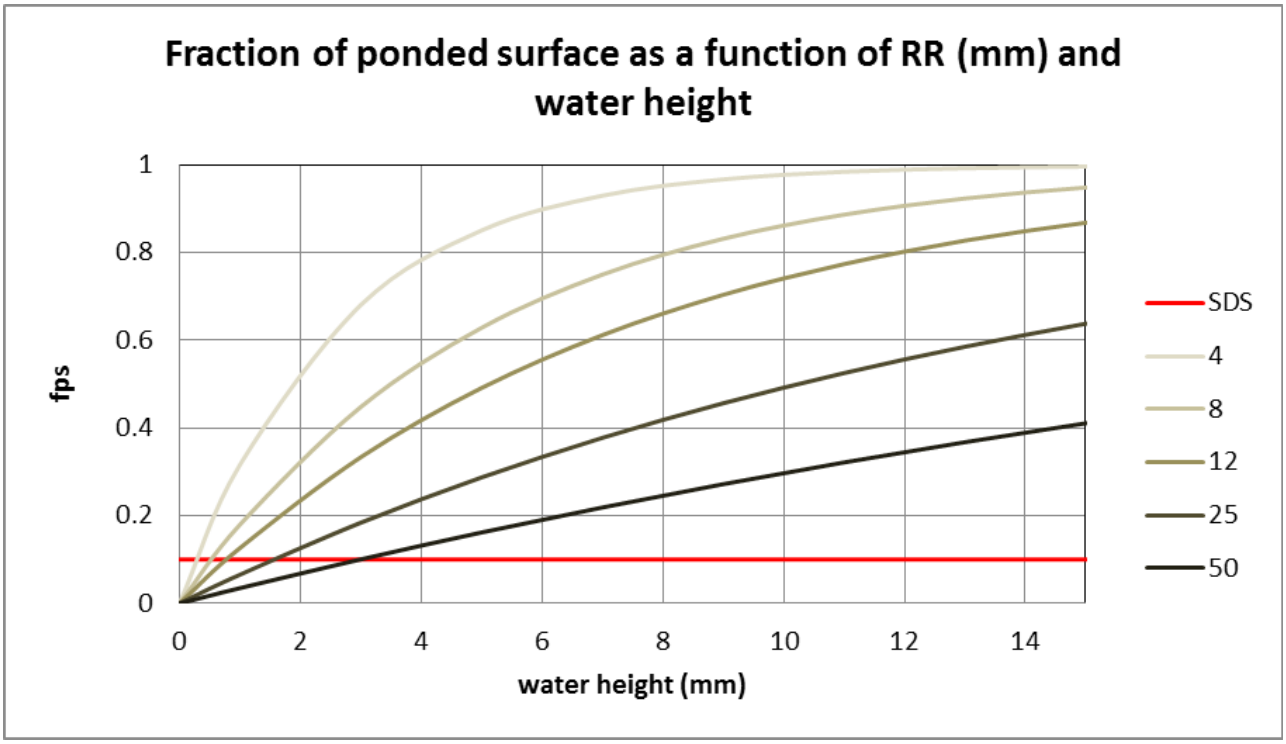

Figure 6.18: Graph showing how the fraction of ponded surface (per cell) will develop as a function of water height, for difference input values of RR (from 4 to 50 mm). The horizontal line (SDS) is the Start Depressional Storage, if fps is above this threshold (0.1) runoff is assumed to start. The graph is made in Excel, for a list of randomly chosen RR values, approximately illustrating the common range of RR values.

Between SDS and MDS the amount (mm) of runoff is modeled in a non-linear way. After MDS is reached runoff increases linearly with the water height in the cell (figure 6.19):

h < SDS: no runoff
h > SDS: runoff = (h – SDS) * (1- exp(-h*(h-SDS)/(MDS-SDS)))
h > MDS: runoff = (h-MDS)

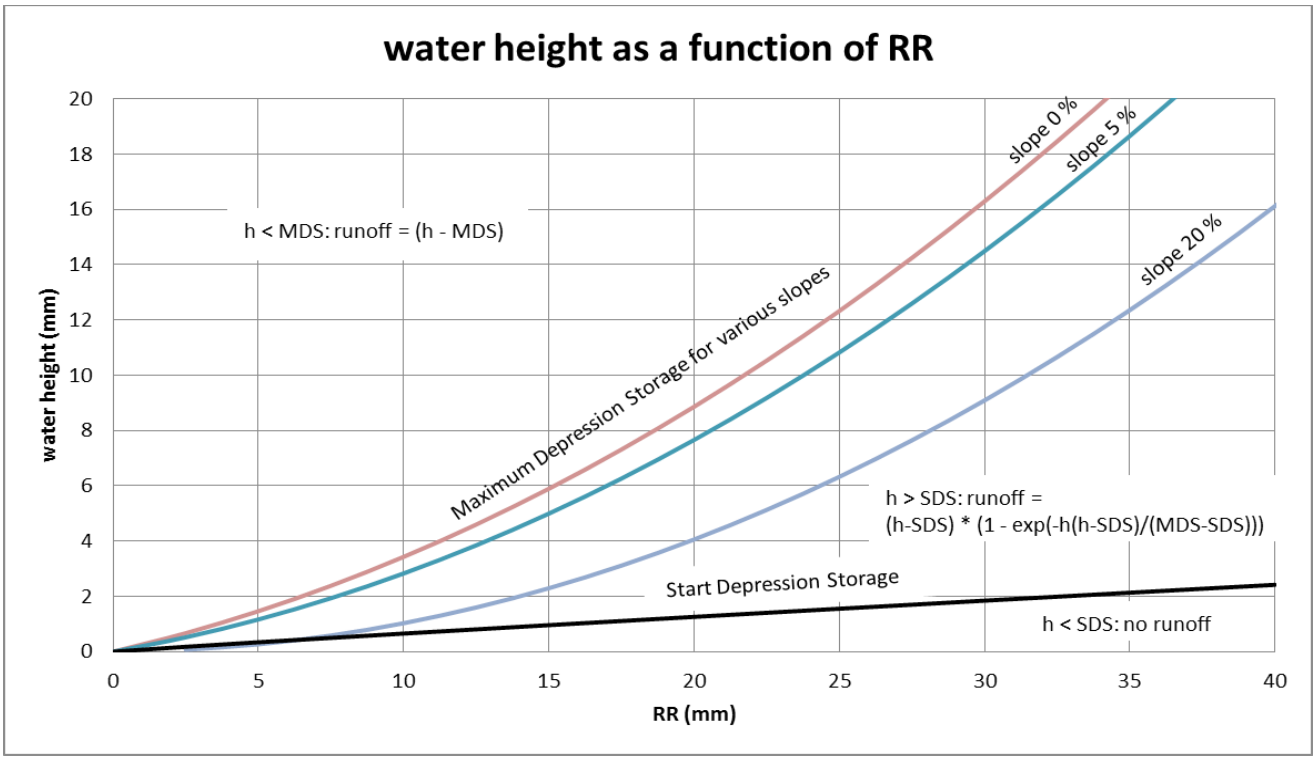

Figure 6.19: Illustrates how runoff is calculated in LISEM depending on the RR, the water height and the slope. Below SDS (the black line) no runoff will occur, this is independent of slope. As soon as the water height has increased to transgress the SDS, the runoff for each cell depends on the slope for the given cell.

The flow width of runoff and the hydraulic radius is assumed linearly related to the fraction of ponded surface, f_{ps},:

$$w = f_{ps} * dx \qquad \text{Eq. 22}$$

where w [m] is the flow width and dx [m] is the cell width. All equations and model descriptions are taken from the LISEM manual (Jetten, 2002).

6.6.2 Model choices

The model was set up for the Skuterud catchment by Kværnø and Stolte (2012) who tested various soil physical data and the influence on model results. This means that unless otherwise mentioned input data choices were based on their work. Also land use units and soil units were based on work of Kværnø and Stolte (2012), see Appendix II. Two rain events were used, one for calibration and another one for modelling. The properties of the two rain events are presented in table 6.2.

Table 6.2 Properties of rain events

	Kværnø and Stolte (2012)	Calibration event	Modelling event
Date	13.08.2010	04.09.2009	19.08. 2008[10]
Duration[11], min	860	1060	1000
Peak intensity, mm/h	24	18	60
Total precipitation, mm	23.7	18.6	49.8
Area	Sub-catchment Gryteland	Sub-catchment Gryteland	Catchment Skuterud
Comment	Event used for calibration by the mentioned authors	Event used for calibration because surface discharge measurements were available, however the event was not big enough to create runoff for catchment Skuteud	Event used for modelling because is was big enough to create runoff, however this event happened prior to the setup of surface discharge measurements and could therefore not be used for calibration

Calibration method

At the outlet of the Skuterud catchment total discharge (combined surface and drainage) and sediment load was measured, however since LISEM only models surface runoff, this data record could not be used for calibration of the model. Instead the sub-catchment Gryteland was considered, because discharge measurements were available (see chapter 4, page 13). It was assumed that upscaling of fitted data input for Gryteland applied directly to Skuterud. Further it was assumed that the calibration factors used with one rain event, applied directly to another event. This was necessary because another (larger) rain event was used for modelling purposes of the whole catchment, since the calibration event was not able to create runoff for the whole catchment. It was thought to be reasonable since it was at the same time of the year and crop status most likely was the same for both events. The larger event could not be used for calibration purpose because this event happen prior to the set up of the measurement station Gryteland. Following Kværnø and Stolte (2012) calibration was done by changing initial K_{sat} values for the clay soil. A K_{sat} multiplication factor was chosen based on the best fit between simulated and measured hydrographs and comparison of total (summed) discharge [m^3] , peak disharge [Q, l/s] and peak timing [min].

10 Event used for model simulation of the Skuterud catchment.

11 Duration indicates here the period of time used for modelling. Thus, for instance the August 29 2011 event is the largest rainfall peak out of 3 consecutively peaks that occurred between the 28th and 30th of August 2011.

6.6.3 Sensitivity analysis

With the acquired roughness data a simple sensitivity analysis was executed to get an initial idea about the model sensitivity to roughness input. This was done by increasing and decreasing input roughness values with 20% and 40% and compare model output results. For these test the assumed most accurate roughness data, from TLS, was used. Further, the average RR value from each of the methods were used as input for a model run and the effect of using different RR input was compared in terms of hydrographs.

6.6.4 Evaluation of land use changes as reflected in RR values

As another way to compare various RR values the model was tested using roughness values obtained from different land uses. This gave some ideas about the effect of land use on surface storage. The model runs were compared in terms of surface storage rather than soil loss because the soil loss rates were very low for the event and because surface storage was directly affected by RR. It was expected that running the model using RR from harrowed fields would yield lower surface storage, while ploughed fields or fields with direct seeding on stubbles would yield relatively higher surface storage. Apart from comparing model runs on hydrographs and output statistics like total runoff, the temporal and spatial patterns were compared by calculating average surface storage as a function of time and elevation classes, as well as visually evaluate surface storage maps from various time steps. For input parameters and land use units for the the model runs, refer to Appendix II.

7 Results and discussions

In this chapter the results of the thesis work are presented followed by discussions. The chapter is divided into two parts:

- Section 7.1: Method comparison. All roughness data collected in the field are compared using statistical tools. Variations in roughness values are discussed, as well as other aspects of the methods such as spatial resolution, ease of acquisition, price, data processing etc.

- Section 7.2: Modelling. Model output from LISEM runs are presented followed by a discussion of the results including various ways to visualise the model output such as hydrographs, discharge numbers, maps of surface storage and spatial correlations between surface storage and various terrain parameters.

7.1 Method comparison for roughness data acquisition

In this section the results from the roughness data collected in the field are presented and compared. The data obtained with the rollerchain was converted to RR values by correlating it to the RR from pinboard. Results showed that the correlation was not very good ($R^2 = 0.55$) and the converted chain data, was mostly a function of the pinboard (Appendix III). The chain method is included in the subsequent statistical tests, but not used further in the model run.

7.1.1 Statistical comparison – precision and accuracy

Data presentation - precision

The field work resulted in a collection of roughness values, summarized in table 7.1. The data is also presented in a bar chart, figure 7.1. Complete overview of the data is presented in Appendix IV.

Table 7.1: Measured random roughness. Table show average random roughness values [cm] for each land use together with standard deviation. For the chain measurements both the RR values as converted is shown, together with the Cr-index. See Appendix III for an explanation of the conversion method.

RR (cm)	TLS	Xtion	Stereo.	Pinboard		Chain (Cr value in italic)
Harrow	0.81 (n=1)	1.18 ±0.33 (n=6)	1.52 ±0.70 (n=7)	1.43 ±0.59 (n=10)		1.63 ±0.31 *(12.55 ±5.07)* (n=10)
Forest	1.05 (n=1)	1.65 ±0.59 (n=3)	0.94 ±0.24 (n=3)	1.38 ±0.51 (n=6)		1.07 ±0.03 *(4.04 ±0.44)* (n=6)
Plough	No data	2.84 ±0.86 (n=3)	2.70 ±0.55 (n=5)	2.71 ±1.09 (n=12)		2.23± 0.42 *(21.63 ±6.42)* (n=10)
Stubble	No data	2.04 ±0.57 (n=3)	0.63 ±0.03 (n=3)	1.10 ±0.37 (n=6)		1.24 ±0.10 *(6.69 ±1.48)* (n=6)

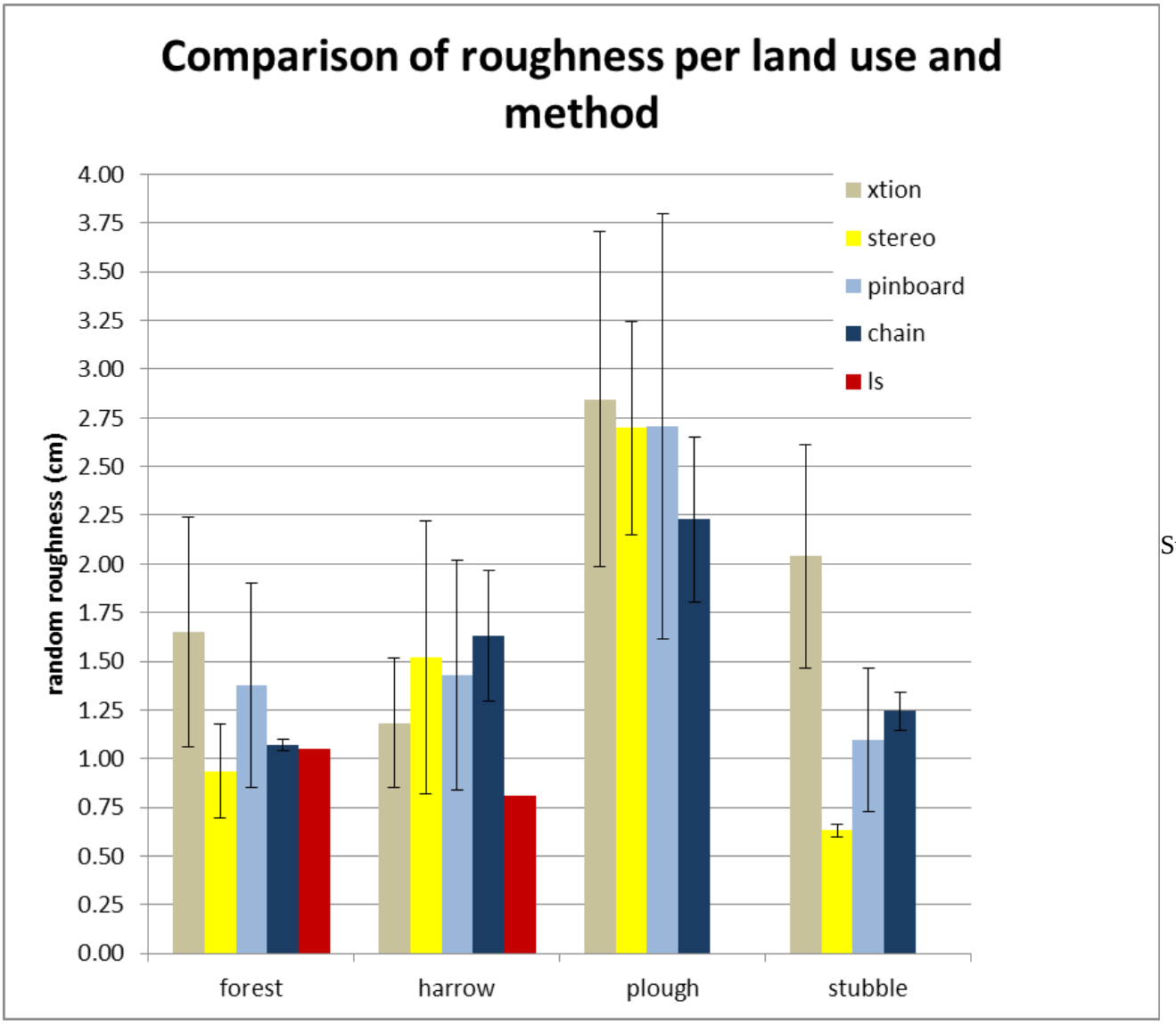

St

Figure 7.1: Bar chart of average random roughness values, acquired on different land use surfaces and using different methods. The error bars indicate one standard deviation. For TLS data (abbreviated ls*) only one plot was acquired, thus no standard deviation could be calculated*

Student's t-test - "absolute" accuracy

For land uses *harrow* and *forest* the "absolute" accuracy of each method was quantified as the difference between TLS and the respective method. The differences were tested with student's t-test for one-samples, where the random roughness from TLS was assumed to be the true mean, and the values to come from a normal distribution (table 7.2). The hypothesis was tested with a 95% confidence level. In addition to the classical hypothesis testing, also the exact probability of making an error by rejecting H_0 while H_0 is true, was calculated. For instance, the P-value associated with the test-statistics of $Xtion_{harrow}$ was 0.64, meaning that there was a 64% chance of making an error if H_0 is rejected. Thus H_0 was not rejected. For the harrowed surface stereo, pinboard and chain are all significant different from TLS, only Xtion was in agreement with TLS. For forest surfaces no significant difference were detected. Prior to the student's t-test data passed the Shapiro-Wilk normality test (Appendix V).

Table 7.2: Results of student's t-test for difference in mean. μ = average TLS RR, while x = Rr_{method}. The null hypothesis, H_0, is that no difference exists, while the alternative hypothesis, H_a, is that a difference exists, P = probability of making a type I error, df=degrees of freedom

One-sample difference of mean t-test H_0: μ-x = 0 H_a: μ-x ≠ 0	x_{Xtion}	x_{Stereo}	$x_{Pinboard}$	x_{Chain}
Harrow (μ=0.81)	No difference H_0 not rejected P=0.64, df=5	**Difference** H_0 rejected. P=0.05, df=6	**Difference** H_0 rejected. P=0.01, df=9	**Difference** H_0 rejected. P<0.01, df=9
Forest (μ=1.05)	No difference H_0 not rejected P=0.30, df=2	No difference H_0 not rejected P=0.66, df=2	No difference H_0 not rejected P=0.22, df=5	No difference H_0 not rejected P=0.22, df=5

ANOVA tests – relative accuracy

An analysis of variance (ANOVA) tests was executed to check for statistical differences in roughness between the methods and between land uses, this is both facilitating the comparison of relative accuracy: *to what extend do the methods agree on a roughness value per land use*, and testing how well each of the methods are able to distinguish different land uses from each other in terms of roughness.

First an ANOVA test was executed to see if there was significant difference between the 4 methods one land use type at a time (table 7.3). For some of the data the normality test failed and an ANOVA test on ranks was done instead. Only for stubbles a significant difference between the various methods was found. To isolate which methods were significant different from each other a multiple pairwise comparison (Dunn's method) was executed for the stubble roughness data. Only Xtion and stereo were significantly different from each other (P<0.05), whereas it could not be confirmed that pinboard and Xtion were different. Because chain had a mean value closer to Xtion than pinboard the chain-Xtion pair was not tested, however they might be significant different because the variance for chain is very small as evident from figure 7.1, for details refer to Appendix V.

Table 7.3: Results of ANOVA tests for comparing methods (95% confidence level). Only the exact level of significance associated with rejecting the H_0 is calculated, when it is not calculated the P-value > 0.05.

ANOVA test for difference between methods	Type of ANOVA test	Result	Level of significance
Forest	Ranks	No difference	P > 0.05
Stubbles	Ranks	**Difference Xtion and Stereo are different.**	P < 0.05 (P=0.013)
Plough	Ranks	No difference	P > 0.05
Harrow	Parametric	No difference	P > 0.05

Secondly, it was tested if there were significant differences between roughness of different land uses. For each method an ANOVA test was executed. For all methods a significant difference was found when comparing the different land uses. To test which land uses were significantly different from each other, again a multiple pairwise comparison was executed, see figure 7.2. All results are significant on 95% level. For details refer to Appendix V. For all four methods only the ploughed surface was significantly different from the other surface. All methods were able to capture the difference between harrowed and ploughed surfaces. Most methods were not able to capture differences between forest, stubble and harrow.

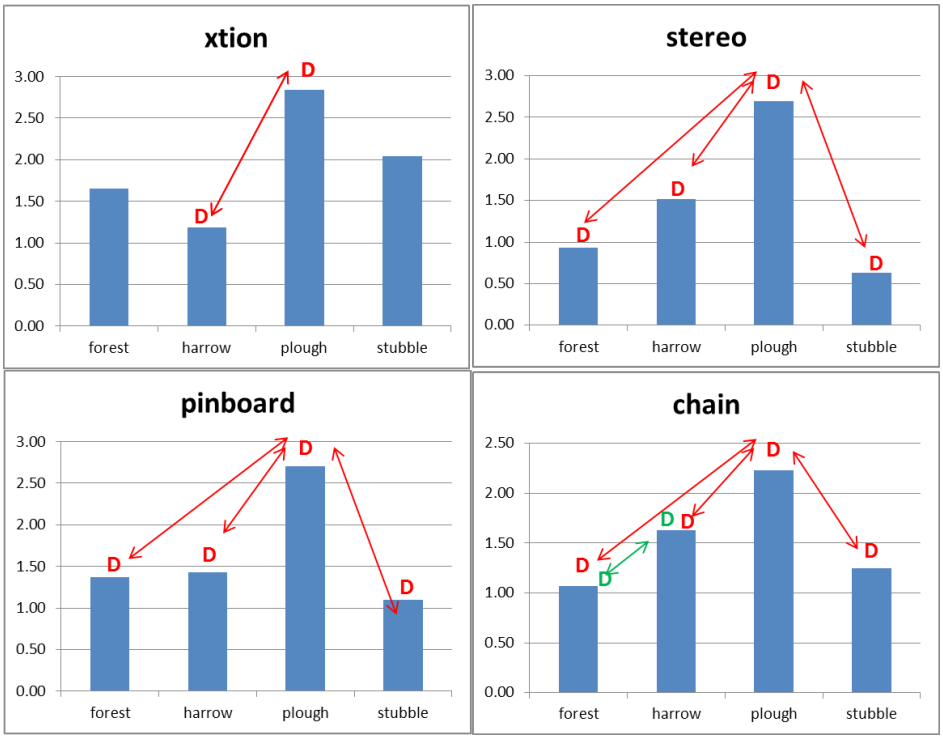

Figure 7.2: Bar charts indicating the average RR values [cm] per method and landuse. Arrows indicates a significant differences between land uses for each of the method. A "D" together with a two-headed arrow indicate significant difference between the two land uses.

To test whether the methods were able to capture the same relative difference between land uses ratios were calculated based on the roughness from *stubble*, since stubble in most cases has the lowest RR value *(*figure 7.3). If the lines followed the same trajory it would indicate that they capture the same relatively difference in roughness that exists between land uses, however, at evident from the lines the methods do not show the same relative differences between land uses. Xtion shows a different pattern compared to stereo, pinboard and chain. Unfortunately, the RR from TLS could not be included because of the lack of measurements on all surfaces.

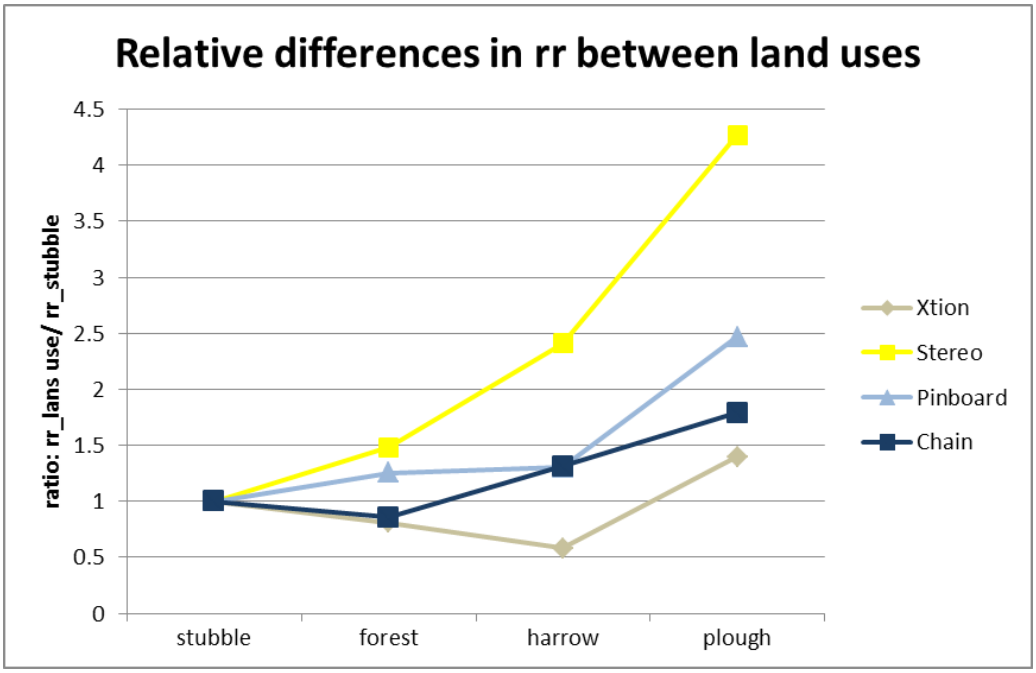

Figure 7.3: Graph showing the relative differences in RR between land uses per method.

7.1.2 Comparison of resolution

Since roughness is scale dependent it is important to compare the methods in terms of the obtainable resolution. Table 7.4 shows the resolution and min. grid cell size of the methods. For chain it was not possible to estimate the resolution. For pinboard the resolution was obtained as height recordings per unit length, but to be able to compare with the sensor methods, the resolution per transect was multiplied with 20, assuming that to cover one m^2 minimum 5 cm was required between consecutive transects because of the metal frame of the pinboard. , which is a relevant parameter because point data usually is converted to raster to use for spatial calculations. The mentioned cell size is based on an subjective evaluation, because even when using a smaller cell size it is possible to create the grid, although the ratio of data to data gap will increase. Not surprisingly are resolution and min. cell size correlated. One important observation is the difference between stereo and Xtion. Xtion has in average 20 000 point more than stereo, while both have a min. grid cell size of 10mm.

Table 7.4: Comparison of resolution of the various roughness methods, expressed both as elevation recordings per unit area (averaged and rounded up to nearest 1000) and maximum raster grid resolution that can be computed from the point cloud

Method	Resolution (points per m^2)	Possible min. grid cell size
TLS	2 705 000	2 mm
Xtion	90 000	10 mm
Stereo	69 000	10 mm
Pinboard	1000	50 mm

The density of the Xtion and stereo point-clouds varied with land use, indicating that the performance of the sensor methods depends on the properties of the surface. As figure 7.4 shows it was not always Xtion that perform best in terms of point density. But the stereo showed the largest variety in point density. On the bare soil surface, harrow and plough, the Xtion had largest point-clouds density, whereas on the plots with vegetation stereo photos had the highest point density.

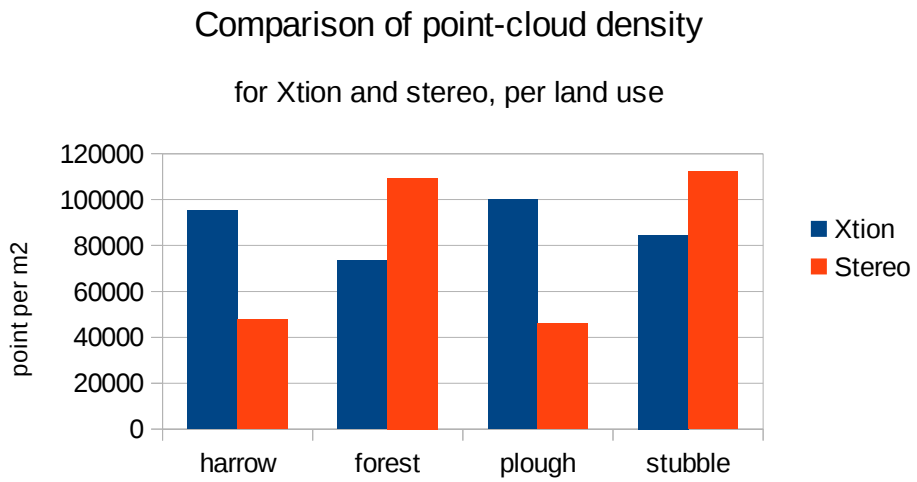

Figure 7.4: Barchart showing the difference in point density for Xtion and Stereo. The point densities are given as points per m2 and is calculated as the average of the number of points for each plot.

The percentages of missing cell values when constructing a 10 mm grid using Xtion and stereophotogrammetry gives an idea about which method had the best coverage (table 7.5). Although it is possible to create a grid with a resolution of 10 mm with both Xtion and stereophotogrammetry there is larger data gap with the stereophotogrammetry. This is especially valid for the ploughed field in Gryteland with an average of 10% missing cell values for rasters based on stereophotogrammetry.

Table 7.5: The average percentage of missing cell values when a 10 mm resolution raster grid is constructed based on the input point-cloud

Land use	**TLS**	**Xtion**	**Stereo**
Harrowed	0.0%	0.7%	4.6%
Ploughed (Gryteland)	-	0.1%	10.6%
Ploughed (Leirsund)	-	-	0.4%
Forest	-	0.0%	0.4%
Direct seeding on stub.	-	0.0%	0.1%

7.1.3 Prices differences

For this study a roller chain was purchased for a value of ~€74. The pinboard was made by R. Barneveld with very cheap materials, ~€20. To apply stereophotogrammetry a high-quality camera is needed. The one we used costed ~€1000, in addition we used the PhotoModeler program, a license for this program can cost €2,145. A TLS costs ~ €60 000. Finally, the Xtion was purchased for ~€100 together with the Skanect program license, €100. Meaning that the Xtion is by far the cheapest sensor method and cost a bit more or the same as the contact methods.

7.1.4 Discussion of results

Having presented the results of the method comparison in terms of precision, accuracy, resolution and price, this section discusses the results and further include practical issues related to the methods.

In terms of absolute accuracy only the surfaces *harrow* and *forest* could be compared. For *harrow* only Xtion was in agreement with TLS. This can possible be explained by the higher point-density of Xtion in comparison with stereo, pinboard and chain. This gives confidence in the Xtion as a new sensor for monitoring roughness. However, for *forest* all methods were in agreement with TLS, which indicates that the methods perform differently depending on the surface properties. This point was also emphasized when observing the bar chart and the graphs with ratios. Based on the ANOVA tests most methods were in agreement about the RR value per land use. Only for the *stubbles* the Xtion showed a significant higher RR value than the other methods. It could indicate that the Xtion point-clouds contain noise. Considering that a filter of 3 times the standard deviation was applied to all point-clouds most outliers are assumed to be removed. For the sensor methods the explanation might as well be differences in the way the data is processed which causes a different surface. Apart from the statistical comparison, a visual comparison gives insight into how much detail of the surface the methods captured. Figure 7.5 shows the point-clouds of *stubble* plot 2 from Xtion and stereo. The z-scale is different so the images cannot be directly compared. However, it is clear that the two methods capture different level of details. In fact the Xtion point-cloud seems very smooth but has a greater range of values, whereas the stereo point-cloud seems more rough but cover a smaller range of values. Since the pinboard and chain are in agreement with stereo it could suggest that the Xtion overestimates the roughness of *stubble*. However, it is difficult to say which method captures the roughness better than the other because the "true" size of soil clods are not measured. To do such evaluations of sensor methods known reference objects are usually used (Luhmann and Wendt, 2000).

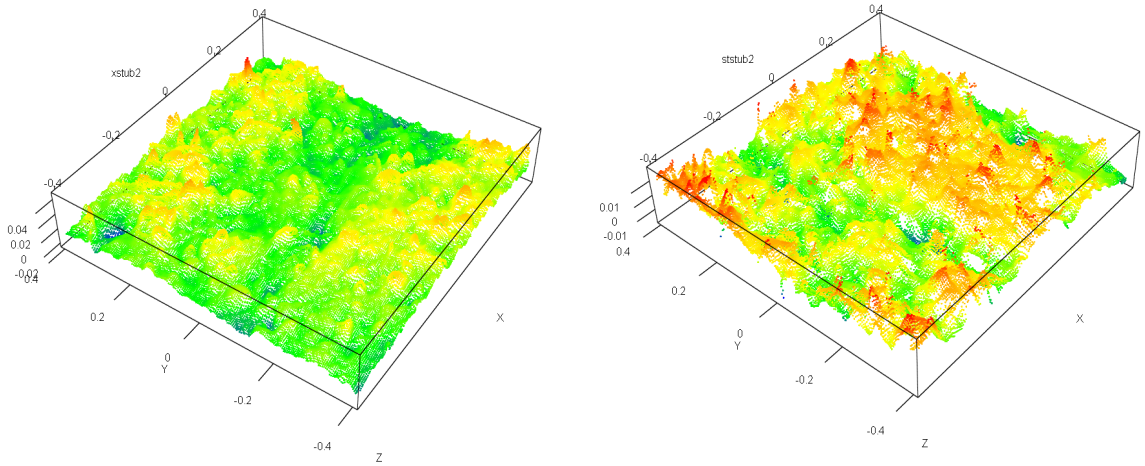

Figure 7.5: Comparison of (from left to right) Xtion (rr = 2.54) and stereo (rr= 0.64). Note that the z-scale is different, for Xtion the z-scale is from -0.02 to 0.04m, whereas for stereo the z-scale is from -0.01 to 0.01m. The scale difference makes it difficult to visually compare the images, but it can be seen that the Xtion elevations stretch over a large range of values than the stereo. Note also that the images are not viewed from the same angle. The stereo is rotated 90 degrees clockwise compared to the xtion.

Like with *stubble*, the Xtion seems to over-estimate the roughness for *forest* in comparison with the other methods (see barchart, figure 7.1), although there is no significant difference between any methods. Figure 7.6 shows point-clouds from TLS, Xtion and stereo from *forest*, here the z-scale is the same for all three images. It is surprising that the stereo has a very similar RR value to the TLS value when considering the visual differences, both in point-density and smoothness of surfaces. In contrast to the Xtion it is observed that the TLS manages to captured more detail, whereas Xtion seems to smooth out the surface. A possible explanation could be the

algorithm the Skanect software uses for stitching together the recordings. Another explanation could be that the speckles correlation technique upon which the Xtion sensor relies is more sensitive to irregularities like grass straws, and not able to capture very thin or fine features because the sensor technique depends on the correlation of the whole speckle pattern. In another study it was also observed that the Xtion could not capture very fine structures (Mankoff and Russo, 2012). However, it is important to remember that only one plot is recorded with TLS, whereas the Xtion and stereo is represented by the average of three plots. The discrepancy that is observed when using sensor methods on vegetated surfaces indicates that sensor methods are best used on bare surfaces. In general it is problematic to get roughness values from vegetated plot, because it is the roughness of the soil that is targeted. Removing the vegetation also seems problematic because it is difficult to remove vegetation without disturbing the soil surface.

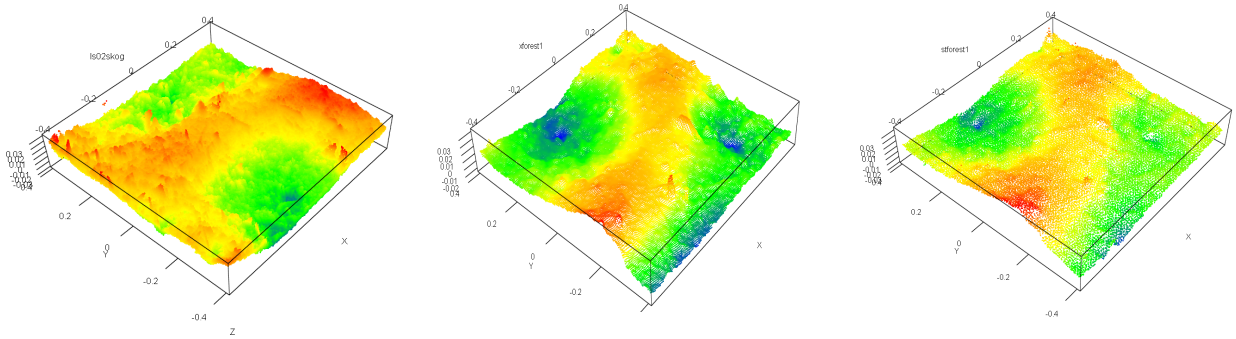

Figure 7.6: Comparison of the point-clouds of forest plot 1. From left to right is: TLS (RR =1.05), Xtion (RR =1.30) and stereo (RR=1.13). Please note that the TLS cloud with regard to viewing angle (by coincidence) is turned 180 degrees compared to the two other clouds.

Looking at the RR values for the *harrowed* surfaces, the TLS value is much lower than the other methods. Especially the difference between the stereo and the TLS is remarkable. This is different than what would be expected, usually increasing resolution would lead to increased roughness, similar to the so-called coastline problem, i.e. on a map showing a coast-line, the measured length of the coast line will depend on the scale (or the resolution) of the map. The smaller the scale of the map the longer will the measured coast line appear (Barneveld et al., 2013) A possible explanation could be that TLS data was only captured on the Gryteland field (see table 6.1, page 29), while the other methods were applied on field Rustad as well. It is clear that the Rustad field had larger soil aggregates than the Gryteland field, see figure 7.7, which probably is reflected in the higher roughness values. An explanation for the differences in aggregate size could be differences in tillage practices and machinery. Both fields were seeded just prior to the measurement, but it is likely that the Gryteland field in addition was prepared with a seedbed preparation machine, e.g. PTO-driven harrow, while seeding (T. Starkloff, pers. Comm.). Another explanation could be that the two fields were tilled at different soil moisture levels, causing a difference in soil aggregate size (Arvidsson & Bölenius, 2006). Yet another explanation could be that the moisture level at the time of data acquisition was different. For the contact methods, pinboard and chain, this meant that the hard soil surface was easier to follow causing an image of a rougher surface, whereas the more moist soil surface was very easier to penetrate consequently causing a more smooth surface. In contrast to the harrowed surfaces the RR values from *ploughed* surface were in much better agreement with each other, despite the fact that the values were partly acquired from Leirsund on heavy clay soil, partly from Gryteland on very sandy soils. This reconfirms our assumption that tillage practice are of greater importance than texture composition with regards to roughness. On the other hand the variation of values were very large, thus no strong conclusion can be drawn based on this data, in particularly also because the number of replicates was limited.

The performance of each individual method with regard to distinction of land uses from each other, showed somehow disappointing results, because mostly only *ploughed* surfaces could be distinguished from the other surfaces, whereas *harrow, forest* and *stubble* not were significantly different from each other. This could both be because the surfaces are not different in terms of roughness or because the few numbers of replicates do not

allow to detect differences. As the graph of ratios suggests, the methods do not agree on the relative roughness of each land use. This would be interesting to underpin with a larger number of replicates.

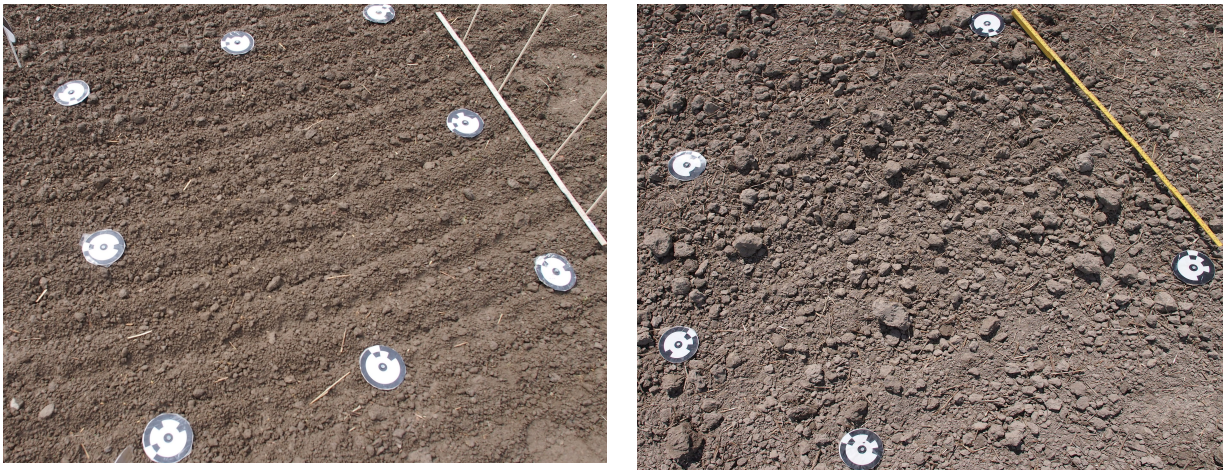

Figure 7.7: Comparison of harrowed field from Gryteland – left (more soil moisture, smaller roughness value) and Rustad – right (drier, higher roughness value)

Regarding the precision of the methods, there are no clear trends when comparing the methods. For *ploughed* surfaces the precision seems in general to be lower than with the other methods. Intuitively, it seems reasonable because the *ploughe*d surface have some larger scale roughness patterns. The lower precision is also reflected in the table of missing cell values (table 7.5). There seems to be larger data gaps in the *ploughed* surfaces than the other surfaces. This is mainly valid for stereo. The stereo technique has problems reconstructing the surface if there are larger areas in shade. The decrease in precision for rougher surfaces was confirmed by other studies that focused on the influence of tillage on roughness (Álvarez-Mozos et al., 2011; Govers et al., 2000).

As already shown in comparison above, most of the RR estimates from the methods were statistically not different from each other. This is interesting considering that the resolution of the methods are different and that roughness which is scale dependent would be expected to change with resolution. The scale-dependency of roughness and surface storage has received quite some attention as a research topic, however it is mainly with focus on surface storage. One of the few studies that actually compared roughness and the effect of resolution from TLS, stereo, pinboard and chain is by Jester & Klik (2005). They compared effect of rain on soil roughness in laboratory settings on two different plots instead of land uses and field conditions as this study is concerned with. In accordance with our findings they observed that the laser scanner provides greater detail of the surface. They did not relate RR from pinboard and chain with the sensor methods. Their study showed that the calculated surface storage and surface inclinations were underestimated using stereo compared to TLS. This is somehow in contrast with our findings since the estimated RR values are lower for TLS than for stereo and thus the MDS value will be lower as well. Martin et al. (2008) tested both the scale-dependency of RR and MDS and reported a 20mm increase in RR as grid cell size increased from 7.5 mm to 1m. This, they stated, is a relatively small change and thus concluded that the RR index was robust along this resolution range.

Another aspect of the scale-dependency and resolution is the considered length of surface for calculating the roughness index. Taconet & Ciarletti (2007) used stereophotogrammetry to obtain DEM of micro-topography and tested the scale-dependency of a roughness index. They observed that the roughness index increased when the considered length of DEM increased from 0.5m to approximately 3 m. However the index first increased abruptly and later oscillated around an asymptotic value, indicating that after a certain length the scale-

dependency has no influence. They concluded that the minimum length of the DEM for a 7.5% accuracy was 0.841m. This somehow confirms the findings in this study that the roughness value do not change significantly across our resolutions, since we extracted roughness values on plots with a length of 0.8m minimum. An interesting observation is that most studies compared changes in resolution from the same method, i.e. a TLS is used to create a high-resolution DEM and a comparison is facilitated by increasing the sampling interval from the raster grid (for instance Álvarez-Mozos et al. (2011)), whereas this study compares different methods which have varying resolution. This might create differences in the results and would be interesting to study further. It is also interesting to observe that the studies which are concerned with soil roughness and comparison of resolution among themselves choose to focus on very different scale ranges and parameters to compare the methods, something that makes it difficult to actually compare different studies of soil roughness.

Following the last observation that studies are focusing on different scales for comparison, it is logic to critically discuss the way we decided to compare roughness among methods, especially for the point-clouds. In the literature review no other studies were found that calculated the RR on the raw point data. Most studies concerned with soil roughness construct raster grids which in a way reduces the detail of the data, because an average value will be assigned to each cell in the raster grid. In this study it was thought to be an advantage to calculate RR on point data, partly because also the pinboard data is point data and partly because it was assumed that the oriented roughness would be removed when all data in the plot was used to calculate the RR value. The last assumption might be a misinterpretation, for further studies this should be tested, for instance by constructing raster grids of all the point-clouds and then compare the RR of the full point-cloud with RR from transects along and across tillage direction. Alternative ways to compare point clouds are for instance presented by Khoshelham & Elberink (2012) who worked with a 3D depth sensor. They compared point-clouds of TLS and the 3D depth sensor by referencing marks and selected 1000 point-pairs randomly and measured the discrepancy. This method is probably better suited for indoor environments, where more parameters can be held constant. Other ways to compare point-clouds could be to construct DEM and subtract them from each other, however to facilitate that we would need clear distinguishable features in each plot so that the point-clouds could be recognized to each other. For further research it is recommended to use reference markers to enable referencing of point-clouds. An interesting approach was used by Aguilar et al. (2009) and Planchon et al. (2001). Both studies used laser scanner and stereophotogrammetry and created raster grids of 1 mm out of the point-clouds. Using the formula proposed by Planchon et al.(2001) the RR of the raster grid was calculated as:

$$RR = \sqrt{\frac{\sum_{ji} \left(z_{ij} - z_{i.} - z_{.j} + z_{..} \right)^2}{n-1}} \qquad \text{Eq. 23}$$

Where j and i indicates the row and column index, z_{ij} is the value of a given cell, $z_{i.}$ is the mean of row i, $z_{.j}$ is the mean of column j, and $z_{..}$ is the mean of all cells, n is number of cells in the grid. This method to calculate RR is advantageous because it removes effect of slope and tillage-marks simultaneously according to the authors. As the point-density of our stereo and Xtion point-clouds could only support $1cm^2$ grids, this method was thought to be too imprecise for our study. It would be interesting to also calculate this index and compare with our current results.

The price of the various devices was presented in the material and methods chapter. Moreover, price should be considered together with time of data acquisition. In this fieldwork the stereo was the fastest method considering time spend in the field. Also considering mobility in the field stereo was attractive because very little equipment was needed – the camera and five carton paper markers. However, many hours went afterwards into data processing. Similarly, with the Xtion data acquisition was very fast. But several drawbacks have to be considered here: i) the data has to be acquired during late evening/night or cloudy weather for the technique to work, ii) it has to be connected to a laptop which has enough battery power for the whole fieldwork time period. The data

collection is easiest with two persons. The data processing is very easy, thanks to the Skanect program which automatically link together the recordings, however, it is not known how exact the algorithm which is applied during the Skanect processing is. The TLS we used is stationary, it was very heavy to carry the equipment, which apart from the sensor also include the tripod and big batteries to make it run. The data processing is relatively easy as well, since a software program is linked to the sensor. The pinboard was the absolute most time-consuming method and it was very unhandy to carry around, further the data processing was long and tedious, because each picture had 50 pintips which had to be digitized. A roller chain is easy to carry, but it is not very fast to acquire data, since great care has to be taken when placing the chain. Thus, the chain method was after the pinboard the most time-consuming field method.

Considering the obtainable (low) resolution both for pinboard and chain compared to the relatively uneasy way of acquiring data and the price, the contact methods are only useful when there is not access to electricity supply or if no laptops are available. Comparing the three sensor methods the best choice of method depends on the budget available and whether mobility or accuracy is of greatest importance. For mobility both the stereophotogrammey and Xtion is worthy while the accuracy of the TLS is best. However, in order to use the stereophotogrammetry a lot of money and time has to be invested in the necessary software, whereas for the Xtion this is not necessary. For further studies the new generation of Microsofts's Kinect incorporates time of flight sensor technology, similar to a TLS[12], which might as well create opportunities for improved and cheap measurements for soil surface roughness. Experiments with drones and 3D depth sensors for indoor scanning proves that there od potential for this method (Huang et al., 2011), although many issues have to be addressed for outdoor use, for instance the effect of climatic conditions (wind, rain, sunlight) on the accuracy, precision of the GPS in the drone and availability of reference markers on the field (B. Veldhuisen, Pers. Comm.). Laser scanners are also in fast development and it is possible to find both cheaper and lighter versions than the one we used here.

12 http://www.brekel.com/kinect-2-details/ accessed 3 Nov 2013

7.2 Random roughness as input to LISEM

In this section results from various model runs are presented. After a small notice on LISEM model versions, the presentation of results will follow this order 1) the results of the calibration process, 2) model responses to variation in roughness input, 3) the temporal development and spatial patterns of surface storage based on different RR input data. Subsequently, the results are discussed.

Model version differences

Inconsistencies in model outputs between the older LISEM v.2.58 and the new openLISEM were discovered which indicates a potential bug in the openLISEM version, since model results evidently show behaviour that is in disagreement with the process theory behind the model (Appendix VI). Executing a sensitivity analysis using openLISEM yielded increased peak discharge when RR was increased and vice versa. This is according to the theory expected to be opposite. At the moment there is no good explanation for this model behaviour, contact has been made with the developer (Victor Jetten). Because the (older) LISEM v2.58 showed expected response according to the model theory, this model version was used for the rest of the study. In the following whenever "LISEM" is mentioned it is referring to LISEM v2.58.

7.2.1 Calibration

Before testing the influence of RR on LISEM output, the model was calibrated for the Gryteland subcatchment, using the rain event of 04 September 2009 (section 6.6.2, page 36). Based on best fit of hydrographs, peak discharge [l/s] and total discharge [m^{3}] the adjustment factors are chosen. Finally a K_{sat} multiplication factor of 3 and a Manning's N for the fields of 0.45 (instead of initially 0.6) were chosen (figure 7.8 and 7.9). This is along the lines of the work of Kværnø & Stolte (2012) who adjusted K_{sat} with a factor 4.51 for a similar rain event (13 August 2010). The pedo-transfer function used for estimating K_{sat}, (the Mualem-van Genuchten equation) does not take macropore flow into account, while the Albeluvisols in Gryteland can be highly macroporous, which makes it reasonable to increase K_{sat} (Kværnø and Stolte, 2012). For an overview of input parameters, refer to Appendix II.

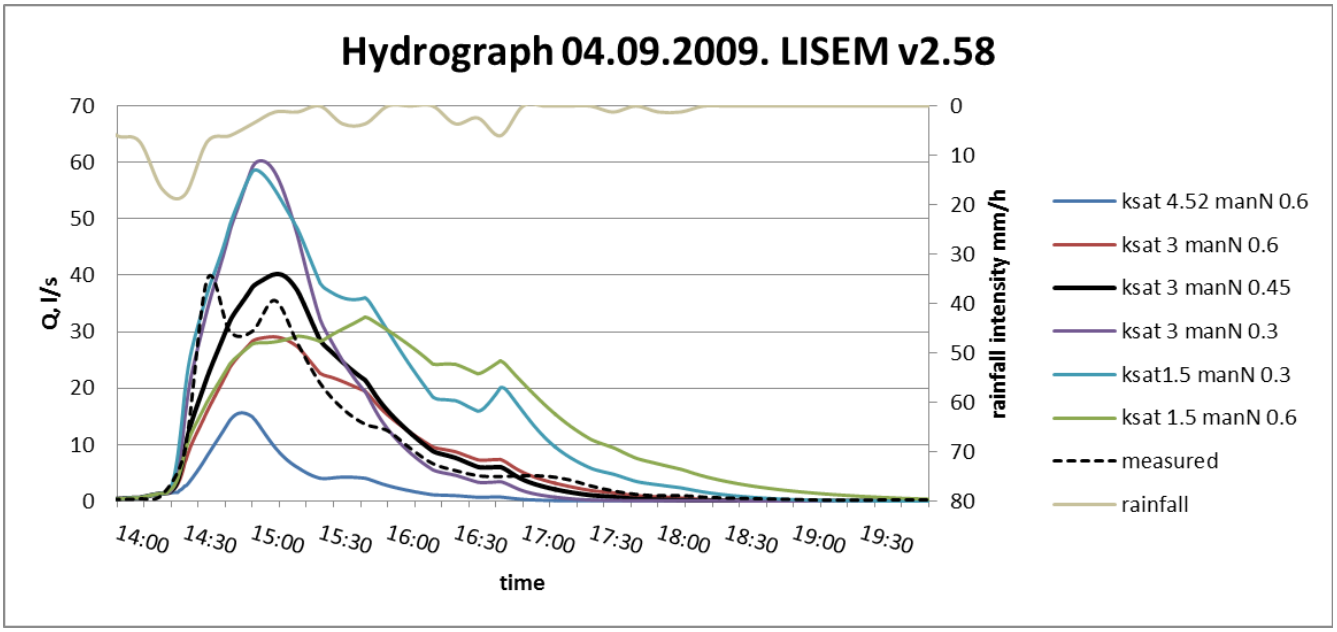

Figure 7.8: Comparison of simulated hydrographs and measured hydrograph from Gryteland watershed outlet point. The different colored lines indicate model runs with different Ksat multiplication factors and the value of Manning's n for the cultivated fields.

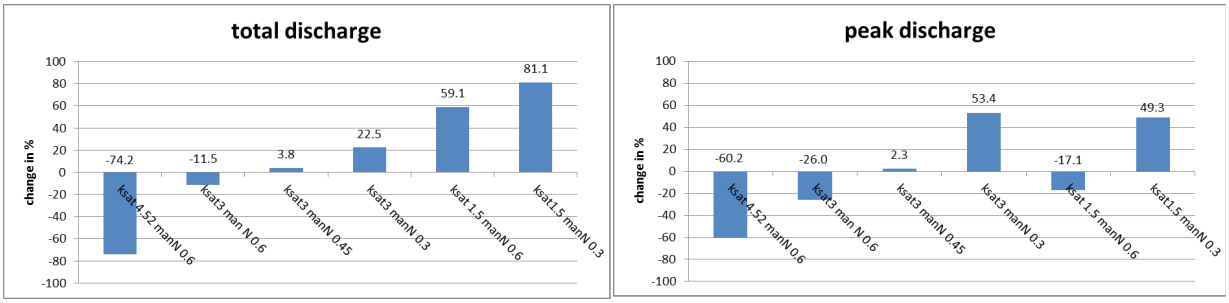

Figure 7.9: Calculated differences between measured and simulated total discharge and peak discharge using different calibration factors.

7.2.2 Sensitivity analysis

7.2.2.a Simple 20-40% sensitivity analysis

A simple RR input sensitivity analysis was executed using the 04 September 2009 event and the sub-catchment, suing RR values from TLS (table 7.6). Peak discharge increased when RR was decreased and vice versa (figure 7.10). Apart from peak discharge, also timing of the rising limb was affected although this effect was mainly visible when RR is increased by 40%. A delay in the rising limb is an expected consequence of increasing the roughness, because on a very rough surface it will take longer time before the micro-depressions are filled up with water. The differences in total discharge and peak discharge are summarized in figure 7.11. The influence of increasing and decreasing RR is similar, although increasing RR seems to have a relatively greater impact on both total and peak discharge compared to decreasing RR. This is in agreement with another study that tested the sensitivity of several of the input parameters, using the LISEM v1.0 (De Roo et al., 1996a).

Table 7.6: Random roughness input values used for the sensitivity analysis.

RR (cm)	Forest	Urban	Harrowed
TLS	1.05	1	0.81
TLS + 20%	1.26	1.2	0.972
TLS + 40%	1.47	1.4	1.134
TLS -20%	0.84	0.8	0.648
TLS -40%	0.63	0.6	0.486

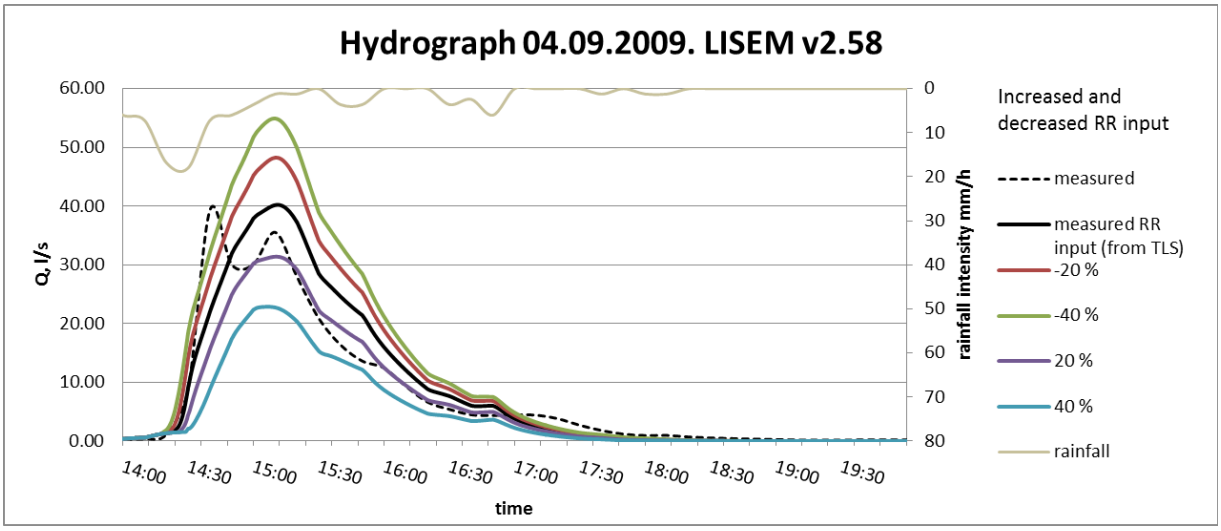

Figure 7.10. Hydrographs from the sensitivity analysis. The black-coloured hydrograph indicates the model run using the original measured RR data from terrestrial laser scanner. The coloured hydrographs are model runs with RR input increased and decrease the the given percentage.

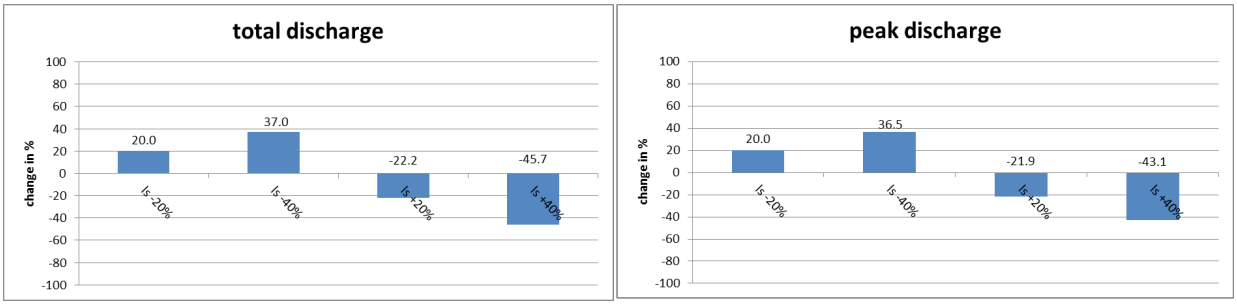

Figure 7.11. Calculated differences in percentage between the model run using measured roughness data and roughness data that was increased or decreased with 20% and 40%. «ls» indicate that the data is from laser scanner (ls).

7.2.2.b Model response to roughness data from various methods

The LISEM model was tested with the roughness estimates from the different methods to illustrate the impact the data acquisition method has on the model output (figure 7.12 and figure 7.13). This is similar to the sensitivity analysis just presented, but with certain differences. One difference is that the roughness value is not uniformly changed with a percentage, but changed according to the measured value for each land use, another difference is that the RR values are not arbitrarily increased or decreased but the result of different acquisition methods, which proved to be at much higher percentages than 20-40% as were the case for the sensitivity analysis. Table 7.7 shows together with the mean roughness value per methods, the difference in percentage between the TLS value and the value from the relevant method. The differences are not consistent, thus for the harrowed surfaces the roughness increases from TLS, through Xtion and stereo, to pinboard, but the same is not true for the forest surface. Based on the sensitivity analysis it is not surprising that the RR input values from the pinboard has such a big influence on the output. However, it is remarkable that the difference in RR acquired with different methods can be this large.

Table 7.7: Random roughness input values for various land uses, used in LISEM. The numbers in parenthesis is the change in percentage from the TLS-value to the given measured value.

RR in cm	Forest	Urban	Arable		
			Ploughed	Harrowed	Direct seeding
Terrestrial laser scanner[13]	1.05	1	-	0.81	-
Xtion 3D depth sensing	1.65 (+57%)	1	2.84	1.18 (+46%)	2.04
Stereophotogrammetry	0.94 (-10%)	1	-	1.52 (+88%)	-
Pinboard	1.38 (+31%)	1	-	1.43 (+77%)	-
Values used by Kværnø & Stolte (2012)	3.2 (+205%)	0.80	-	0.88 (+ 9%)	-

13 Used for calibration

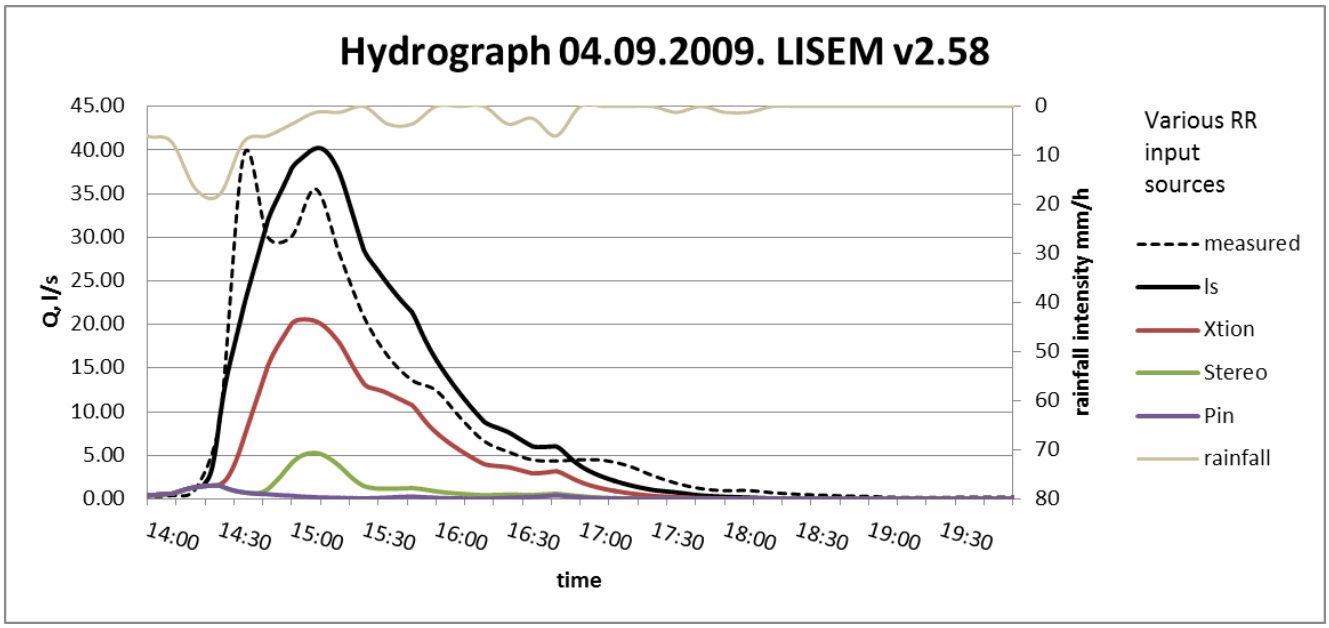

Figure 7.12. Hydrographs as a function of RR input data.

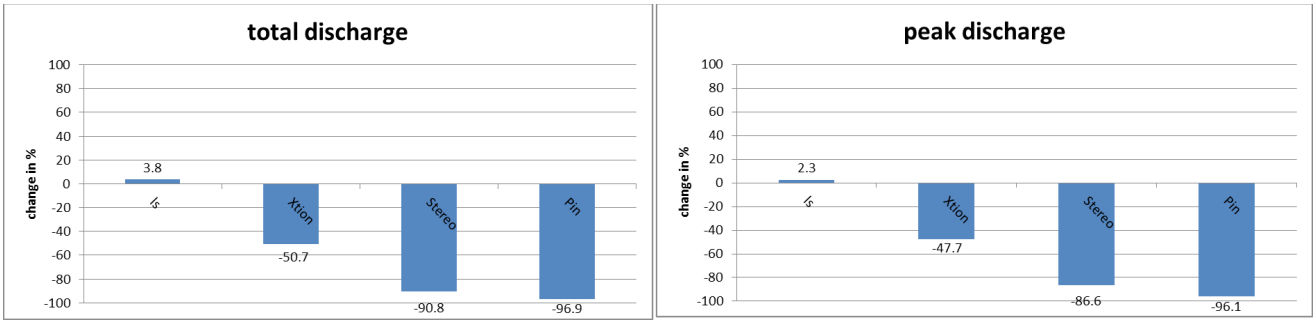

Figure 7.13. Bar chart indicating the calculated differences in percentage between the measured discharge and the simulated. The names per bar indicate the method used for acquiring the RR data which was used as input.

7.2.3 Spatial and temporal differences in model output

To test how the land use differences, as reflected in different RR values affected the model output the LISEM model was set up for the larger catchment Skuterud. Model properties other than RR input and leaf area index (LAI) were held constant (Appendix II). When the cultivated areas were assumed to be ploughed or harrowed instead of direct seeding on stubbles, the LAI was set to zero. For these model runs the roughness data from Xtion was used, because only with Xtion did we acquire roughness data for all types of land use (figure 7.14). In agreement with the sensitivity analysis and method comparison, the hydrograph peak decreases in accordance with increased roughness. The black hydrograph based on the TLS roughness are included to show that there is agreement between the model run using RR from TLS (harrowed) and Xtion (harrowed). Model run with direct seeding on stubbles ("stubbles") has a LAI of 2.5, yields more runoff than on the ploughed fields, probably because the model is more sensitive to RR input than LAI input.

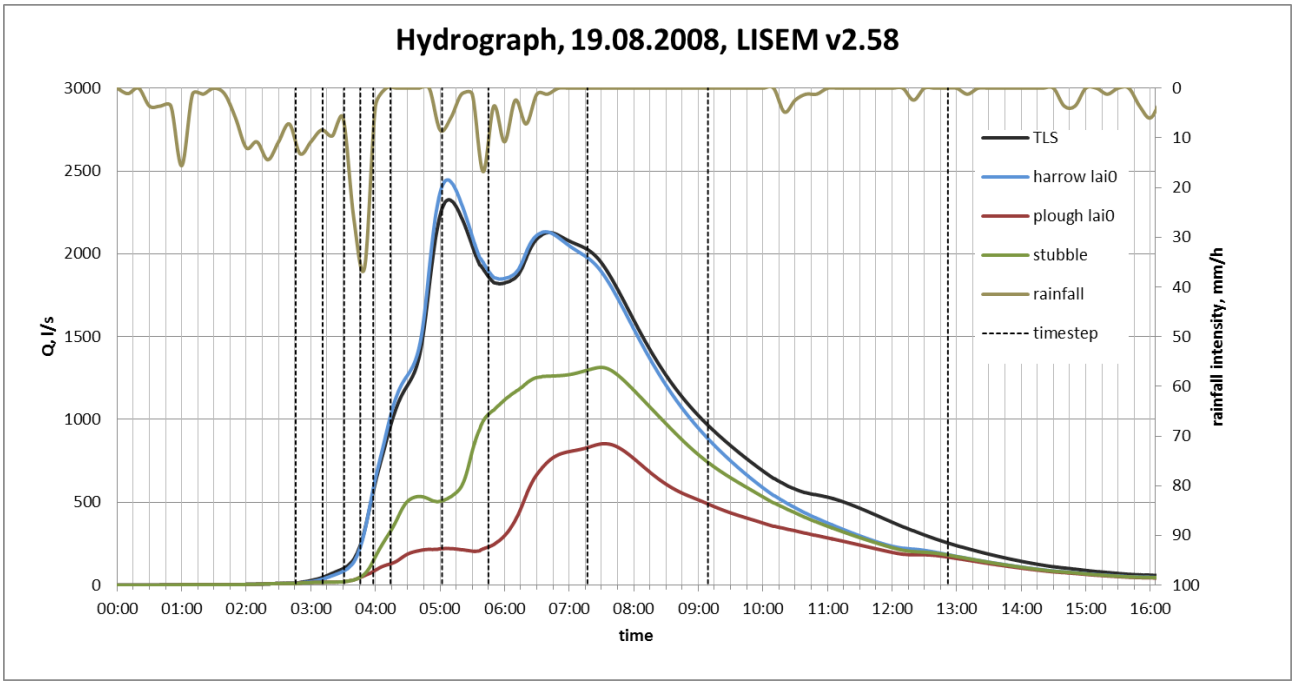

Figure 7.14: Simulated hydrographs from Skuterud catchment, using various RR input. The hydrograph TLS indicates the model result based on RR from TLS, this is included to show that the RR from Xtion are in good agreement with the TLS. Apart from the RR input also the LAI (leaf area index) was set to zero for the cultivated fields, for land use to reflect a realistic situation. The dashed vertical lines indicates time transect which are used later on.

Apart from the comparison of hydrographs a temporal analysis of surface storage was executed (figure 7.15). The graph is based on simulated average surface storage values for given points in time. The points in time were chosen based on the hydrograph, indicated as transects on figure 7.14. From start to time 02:45 the surface storage develops similarly among the different land uses (figure 7.15), because the rain intensity is low enough compared to the infiltration and maximum storage capacity and so surface storage build up with all 3 land uses. From 02:45 onwards an increasing rainfall intensity causes the 3 surfaces to fill up unequally. At 03:45 the peak rain intensity occurs which causes the stubble field and the harrowed surface to reach the maximum storage capacity. This is evident because the surface storage does not build up after this point, although another rain intensity peak occurs around 05.30. In contrast the surface storage for the ploughed fields increases (slightly) again from 05:00 to 05.30 until the maximum storage capacity is reached. After 07.00 it stops raining and the water runs off, thus decreasing the amount of water stored on the surface due to runoff and infiltration.

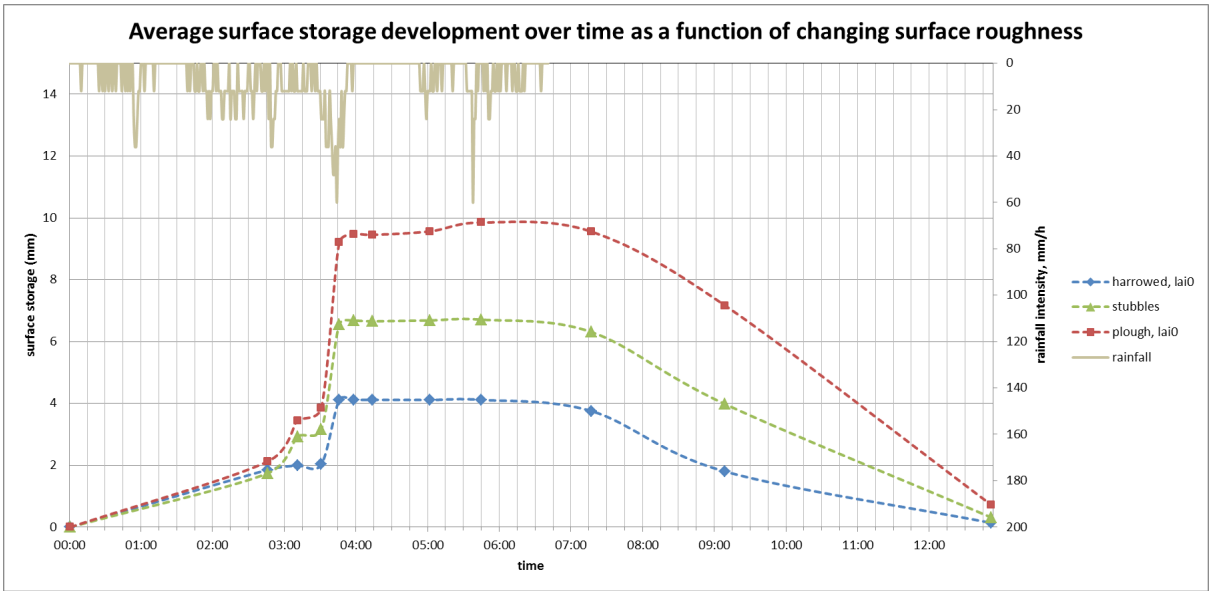

Figure 7.15: Surface storage development over time calculated for each time step as the average over the whole Skuterud catchment. The secondary y-axis shows rainfall intensity in mm/h. The surface storage is generally following the expected trend based on the roughness input. Around time 03:15 and time 05:45 there are interesting differences between the graphs.

To get an overview of the spatial patterns, maps of surface storage over time are compared. Figure 7.16 shows maps of surface storage over the Skuterud catchment at five time steps for the three different land uses. It is clear that with ploughed surfaces the surface storage capacity is higher than when the surface is harrowed or with stubbles. This is especially clear from min. 238 onwards (around time 04.00), because there the proportion of water storage at the cultivated area compared to the surrounding forest seems to be higher for the ploughed fields, whereas for the harrow surface the surface storage remain less on the cultivated areas compared to the forest. On the last map, min 549 (around time 09:00) the surface storage seems to be concentrated on the flattest areas and especially in the depressions in the landscape, which intuitively could be expected.

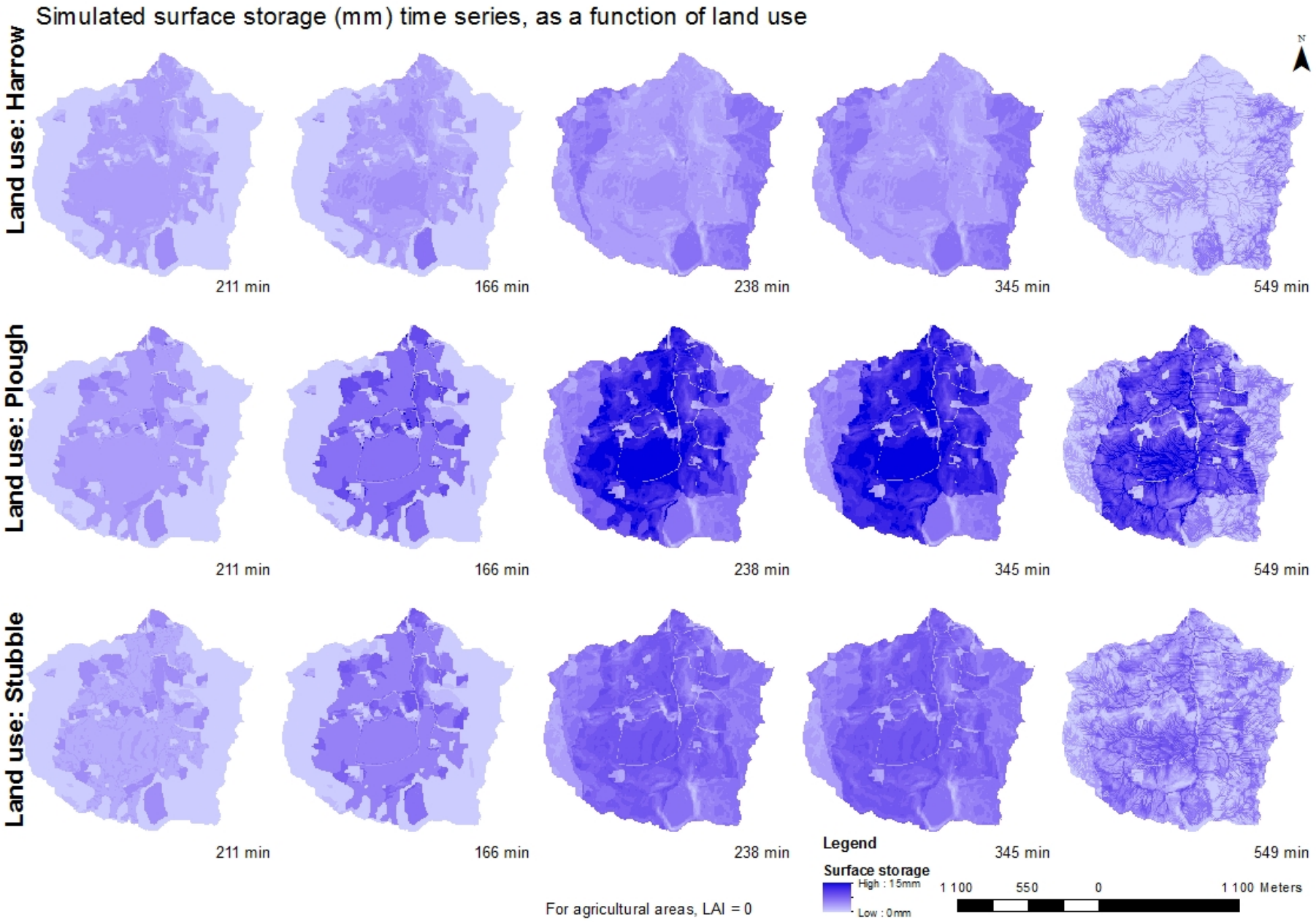

Figure 7.16: surface storage over time as a function of land use

To see if a relation between elevation and surface storage within the catchment existed, the DEM was classified into 50 equally sized classes. For each elevation class the number of cells was extracted. For each group of cells the average surface storage value was calculated. When surface storage was plotted against elevation class, it gave an indication about where in the catchment the surface storage was located, in relative terms, e.g. highest elevation classes are on the periphery of the catchment, lowest in the centre and downstream (figure 7.17, 7.18 and 7.19). It is useful to compare with the DEM of the catchment presented in chapter 4. The columns show the frequency distribution of cells per elevation class. The lines indicate per time step the average surface storage. Comparing the level of the lines in each plot gives an impression of the temporal development of surface storage as a function of elevation and land use. Note that the highest elevation classes have a constant development in surface storage when the 3 land uses are compared, this is because the highest locations in the catchment in general are covered with forest or urban area, and thus the RR has not been changed. It is interesting to see that the ploughed surface has an increasing amount of surface storage the lower the elevation, meaning that the lower part of the catchment is filling up relatively more than with the other land uses, thus acts as a buffer. It can be explained by the fact that the maximum storage capacity is higher for ploughed surfaces and when run off starts relatively more water is stored within the center, downstream parts of the catchment whereas this is flowing out of the catchment much earlier with the other surfaces.

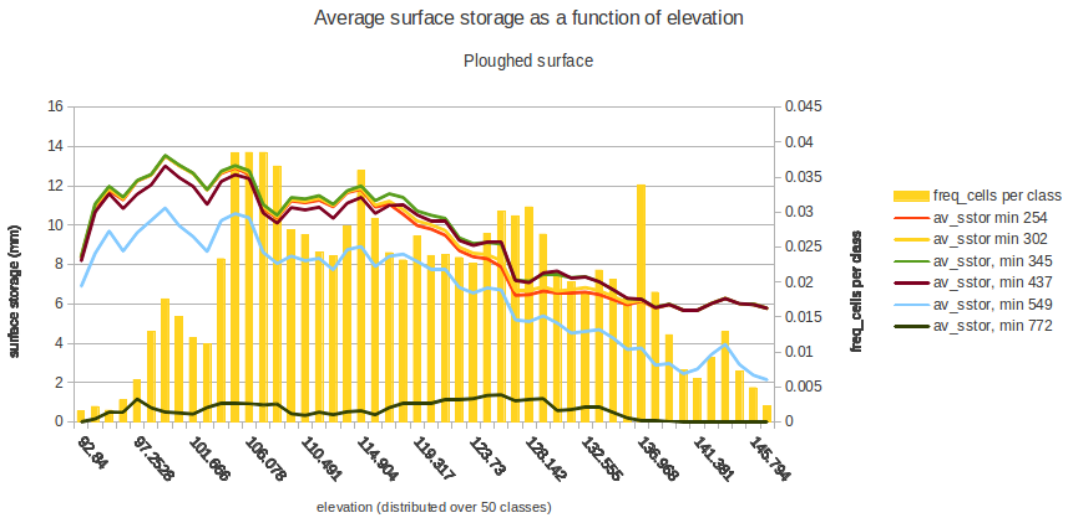

Figure 7.17: Surface storage [mm] for ploughed surfaces at different points in time (lines) (primary y-axis) as a function of elevation classified into 50 equal classes (x-axis). The frequency of cell count per elevation class is shown on the secondary y-axis.

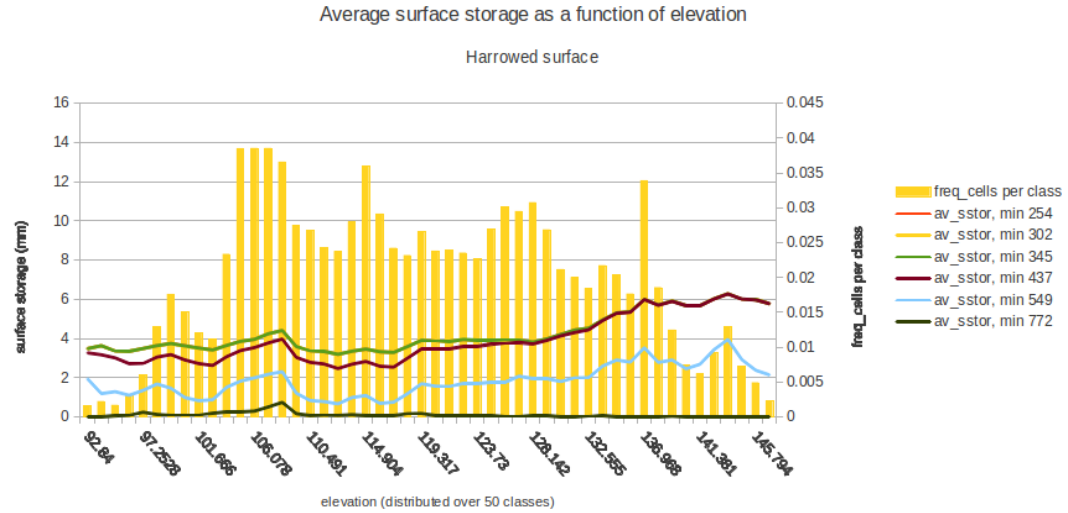

Figure 7.18: Surface storage [mm] for harrowed surfaces at different points in time (lines) (primary y-axis) as a function of elevation classified into 50 equal classes (x-axis). The frequency of cell count per elevation class is shown on the secondary y-axis.

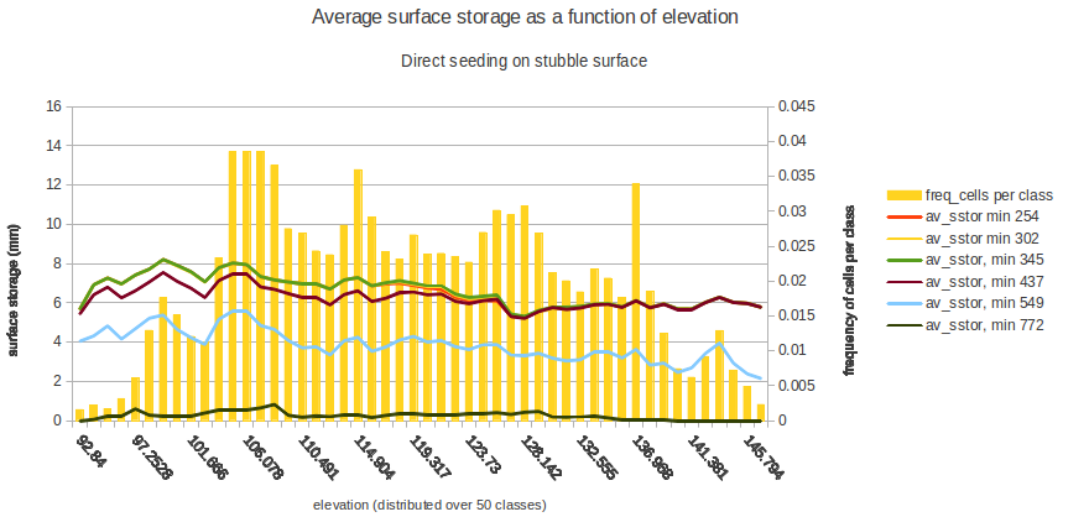

Figure 7.19: Surface storage [mm] for direct seeding on stubbles surfaces at different points in time (lines) (primary y-axis) as a function of elevation classified into 50 equal classes (x-axis). The frequency of cell count per elevation class is shown on the secondary y-axis.

7.2.4 Discussion of results

In this section the results of the model runs will be discussed.

As the 20-40% sensitivity analysis showed LISEM is relatively sensitive to changes in RR value. So it is not surprising that the hydrographs from the model run with RR from different methods show such a large difference in hydrograph peak. What is more surprising is that the values indeed are this different. Although both the one-sample difference of mean and the ANOVA test did not find any significant difference between RR_{harrow} from TLS and Xtion, the Xtion RR was still 46% greater than the TLS RR in absolute terms. In other words the sensitivity of LISEM is not adjusted for the inaccuracy there exists between various ways to obtain soil roughness data. The temporal and spatial analysis show patterns which is in agreement with the process theory behind the model, however, it remains unknown how well the model captures the actual spatial and temporal patterns, as there is a lack of field observations.

As the spatial and temporal analysis of land use changes showed the surface storage build up differently both spatially and temporally in accordance with the roughness of the soil. The ploughed surfaces which had the largest RR values could store more water than both direct seeding on stubble and harrowed surfaces could. Interestingly, the modelling showed that even after six hours of rain surface storage still built up on the ploughed surfaces, whereas the maximum storage capacity was reached after four hours for both harrowed and direct seeded surfaces. It indicates that for rain events shorter than six hours and with the given rain intensities, a ploughed surface in Skuterud will on average store more surface water and thus create less runoff than a surface with direct seeding. This is an interesting observation because one of the prevailing recommendation to Norwegian farmers is to use direct seeding as an erosion prevention measure (Grønsten et al., 2007). The model results provided here could suggest that whether direct seeding on stubbles or autumn ploughing is best might be a function of the assumed rainfall intensity and length, however more runoff does not necessarily mean higher erosion risk, this depends as well on the vegetation cover and the runoff speed. It would be interesting to do further research into this topic, especially to evaluate pros and cons for both land management techniques against the predicted frequency of large rain events.

In LISEM, MDS is calculated based on a study executed by Kamphorst et al. (2000). In their work both a pinboard with 30 mm spacing and a TLS providing 2 mm spacing were used. From the pinboard with consecutive transects and TLS, raster based DEM were calculated, the first one with 30mm resolution, the latter one with 2mm resolution. Initially MDS was calculated using an algorithm that identified all depressions in the plot and virtually filled them up with water. Effect of changing resolution on the average MDS value was tested, showing that as long as the DEM resolution was between 10-30 mm the MDS value was stable. This would imply that also RR values should be obtained from the same resolution range to correlate to the MDS. Kamphorst et al. (2000) did not test this, and they extracted their RR values from all the DEM regardless of whether the elevation data was from a 2mm TLS or a 30 mm pinboard. It might very well be that RR which in LISEM is used to determine MDS is performing best when RR is obtained with methods that yield a DEM resolution of 10-30 mm. This would be a topic for further research. However, with the increase in computational power and better availability of very-high resolution DEM it might in the future be more feasible and accurate to estimate MDS directly from DEMs instead of calculating the RR index. It is already possible to scan areas of up to $100m^2$ today with TLS (Barneveld et al., 2013). With the ongoing fast development of drones it might in the near future be possible to acquire high-resolution micro-topography data with a 3D depth sensor mounted on a drone. At the moment when a whole hillslope or even catchment can be scanned with high-resolution sensors it might be possible to bridge the gap between the surface storage processes and modelling input, e.g. high-resolution DEM can be used directly as input for simulating surface storage when modelling a rain event using LISEM.

There are several other critical parameters that are important for better modelling results, which could not be taken into account in the thesis because of time constraints or lack of available data. LISEM is a data input heavy model (Kværnø, 2011) and although great effort has gone into acquiring input data many parameters are still assumed and potentially inaccurate, for instance soil data from forest areas (33% of the Skuterud catchment) which is extracted from the national soil survey rather than field studies (Wang, 2013). Another weakness in the model set up is the lack of discharge measurements at the Skuterud outlet station. Having this data available would allow the model to be calibrated on the whole catchment, instead of using the sub-catchment. Applying the calibration factors from the sub-catchment to the whole catchment introduces uncertainties, especially because the soils are relatively more sandy in Gryteland compared to the whole catchment (Kværnø and Stolte, 2012). Further, the results of the calibration are applied directly on another rain event. Several studies indicate that calibration results are depending on the magnitude of rain event and therefore LISEM should be calibrated individually for rain events of different magnitude (Baartman et al., 2012; Hessel, 2002). Arbitrary choices were made regarding cell size (10m) and time step (30 sec) again following the example of (Kværnø and Stolte, 2012). Tests show that predicted discharge and soil loss vary considerably with cell size and time step, with a increase in cell size and time step resulting in a decrease in predicted discharge most likely due to a decrease in slope by increasing cell size (Hessel, 2005).

In LISEM RR is only used for estimating surface storage, but roughness also affects the overland flow by exerting a resistance to runoff . This is expressed through Manning's formula and Manning's n. In LISEM we used assumed values of Manning's n. Some authors have suggested a relationship between surface roughness and Manning's n (Mwendera & Feyen 1992). It would be interesting to test the effect of estimating Manning's n from RR, also since LISEM sensitivity tests have indicated that the model is responsive to changes in Manning's n with an order of magnitude similar to RR, see figure 7.12.

A factor which has not received much attention in this study is the effect of slope gradient on roughness. The effect of slope is indeed removed when calculating the RR index, but this does not change the fact that roughness is altered with slope gradient which is also altering the surface storage as well as overland flow (Álvarez-Mozos et al., 2011; Hessel, 2002). A way to overcome this could be to apply a correction factor depending on slope in the preparation of input maps for LISEM.

The oriented roughness, which is the systematic pattern on cultivated fields caused by tillage has not been given much attention in this thesis, mainly because the topic has been restricted to random roughness. However oriented roughness has a great impact on both surface storage and overland flow. For instance, if the tillage direction follow the slope the ridges will act as channels that concentrate and increase the surface runoff, whereas ridges along the contour lines will retain water. In other words, on agricultural soils the oriented roughness is often more important than the random roughness for surface storage and overland flow (Takken, 2000; Takken et al., 2000). Until now most DEMs cannot capture micro-topography, and consequently tillage direction have to be implemented indirectly in the model. Several studies have focused on tillage direction for improving runoff models (Takken et al. 2005; Takken et al. 2001; Hyväluoma et al. 2013). An algorithm for taking tillage direction into account in the flow-routing was developed and implemented to LISEM by Takken et al. (2001)[14]. Due to time constraints it was not possible to test this flow-routing algorithm in combination with the roughness data in this thesis, but would be an interesting topic to research further. It is recognized that erosion on agricultural fields in Norway is clearly affected by tillage practices (Lundekvam and Skøien, 1998; Lundekvam et al., 2003).

14 which is available on the internet: http://geo.kuleuven.be/geography/modelling/erosion/tcrp/download/index.htm [accessed 2013-11-07]

Finally, it is, due to the lack of erosion observations, not possible to conclude how well LISEM performs for simulating erosion and runoff patterns. It seems even hard to conclude whether one type of roughness input data is yielding a better performance than another due to the numerous other unknown or arbitrarily chosen parameters, some of the most important ones being calibration procedure and K_{sat} values, different rain events and model cell size. To increase the knowledge of the performance of LISEM in the Skuterud catchment erosion observation is needed. Work is ongoing to facilitate erosion monitoring using an unmanned aerial vehicle to observe and locate erosion features or even quantify soil loss using a digital camera or even a 3D depth sensor (T. Starkloff, per. comm.). Experiments have shown promising results, for instance Marzolff & Poesen (2009) successfully used various unmanned aerial vehicles to monitor gully development in Spain.

The lack of erosion observations is a regrettably general trend among erosion model studies as several authors have pointed out (Jetten et al., 2003; Takken et al., 1999) . In most erosion studies calibration and validation is done only on outlet data, while the most interesting feature of the model is the spatial prediction of erosion patterns. Thus, models happen to be calibrated and validated for the wrong reason, e.g. simulating well discharge timing and peak, but failing to identify erosion features (Jetten et al., 2003). Most spatially distributed erosion model simulate sediment transport using the sediment transport capacity approach (Nord and Esteves, 2010; Sander et al., 2007). Alternatives to this approach is the transport distance approach suggested by (Wainwright et al., 2008a) or the continuous deposition approach suggested by (Hairsine and Rose, 1992). As Nord & Esteves (2010) note in their introduction and which is evident from numerous comments that were published following the critics of the transport capacity approach initially posted by Wainwright et al. (2008) the discussion of the approach to erosion modelling is still not closed, just as there are still many unknown factors that make erosion modelling and erosion mitigation a challenge today and for future research (Rompaey and Govers, 2002; Wainwright et al., 2010, 2009a, 2009b, 2008b).

As this discussion has emphasized the evaluation of the performance of LISEM is hampered by the numerous parameters which simultaneously can be adjusted. However, in the literature several authors have drawn attention to the disappointing performance of erosion models, not only regarding LISEM but also similar spatially-distributed physically based models such as WEPP, KINEROS2 and EUROSEM (Jetten et al., 2003; Takken et al., 1999). A recent review tried to compare the model performance of 14 erosion models, including LISEM (de Vente et al., 2013). Their main conclusions are that most models still provide insufficient performance for identification of sediment sources and dominant erosion process, performance seems to be more difficult for smaller catchment and that spatially distributed models generally provide lower accuracy than spatially lumped models. The latter point echoing an interesting observation by Rompaey & Govers (2002) that more complex models not necessarily result in better accuracy. This is interesting when considering LISEM which indeed can be impractical to work with because of the need for very detailed field campaign to suffice the data input requirements (de Vente et al. 2013). A striking point is that while the physics-based models (including LISEM) have the greatest potential to simulate land use or climatic changes they are often optimized for one small catchment with specific environmental conditions and produce poor validation results when applied in other catchments or with other rain events, which ironically is the contrary of the intention. It would be interesting to test the performance of LISEM towards a less complex model to evaluate whether there indeed are any benefit of using LISEM in a catchment like Skuterud over another more simple model.

8 Conclusions

The objective of this thesis was two-fold: 1) To investigate the applicability of the 3D depth sensor for obtaining soil roughness data as compared to other methods and 2) to test whether this data can improve the performance of a physical-based spatially-distributed erosion model. Based on the results presented and discussed in the last chapter conclusions are here drawn with regard to these two objectives.

The applicability of the 3D depth sensor was investigated by comparing it to four other roughness measurement methods on a variety of parameters: Accuracy, precision, resolution, price, easy of data acquisition. Further land use was used as a covariate. From the method comparison some general conclusion about the methods can be made. The agreement between the methods differed with land use, meaning that not all land surfaces are equally easy to monitor, for instance, the rougher the surface the more replicates are needed to obtain a realistic roughness estimate. Interestingly, the methods did not agree on the order of ratios, which indicates that the methods did not capture the same relative roughness between land uses. This might partly be explained by the fact that it is complicated to compare contact methods with the sensor methods, as the methods uses different principles to obtain the micro-topography data, and therefore are sensitive to different surface features, e.g. it seemed like the sensor methods had difficulties quantifying roughness when the plot was vegetated, while the contact methods were affected by varying soil moisture content. The contact method are, based on experiences in this thesis, only recommended to use when no electricity is accessible, since the (un)ease of acquiring data and data-processing together with obtainable (low) resolution and accuracy make them very unattractive to work with. While these general considerations relates to interesting questions such as what influences the soil roughness, the applicability of the 3D depth sensor is already proven, since the method did not show deviating results and proved to be as useful as both TLS and stereophotogrammetry. All sensor methods have their pros and cons and whether one method is preferable over another depends on the purpose of acquiring the data. i.e. are resolution and accuracy of greatest importance the TLS might be the best choice, but if also the price and mobility in the field are important parameters the 3D depth sensor or the stereophotogrammetry might be better options.

For this study the purpose of acquiring the roughness data was to use it as input for the LISEM model, with the goal of improving the model performance. A first step to evaluate the performance of the model was to see how sensitive the model was to RR input data. As the results showed the model was very sensitive to the RR input, so sensitive that the variations between average values from the various methods caused unrealistic hydrograph peak reductions. For instance, the RR_{TLS} was 0.81, while RR_{Xtion} was 1.18 (±0.33), which was not statistically different from each other, however using RR_{Xtion} resulted in a ~50% reduction of both peak discharge and total discharge compared to measured values, while RR_{TLS} yielded only ~3% increase in peak discharge and total discharge compared to measured values. It can then be concluded that the accuracy and precision of RR when used for LISEM are extremely important, as the model sensitivity is very high. Yet, considering the possible range of RR values for the same land use, which was investigated in the first part of the thesis, this suggests that the model sensitivity to RR not only is extremely high, but maybe even is too high, as the RR_{TLS} and RR_{Xtion} statistically were indifferent. This would imply that either the data or the model needs to be adjusted. As the model is now, it would improve the performance if a required precision (in terms of standard deviation) of the RR input and a preferred method of acquiring RR data could be determined and stated in the LISEM manual. But, another option is to try to adjust the LISEM model sensitivity to a “realistic” obtainable accuracy and precision. To come back to the second research objective, it can be concluded that the model performance evaluated on hydrographs only, was not improved by using the 3D depth sensor (if improvements are defined as how well the hydrographs fit to measured data), on the other hand, based on our data we can not conclude that the 3D depth sensor decreased the performance of the model. In fact, it is more informative to conclude that the model was too complex to evaluate the performance properly. For further studies it might be useful to test a less complex model against LISEM.

Acknowledgement

I would like to thank BioForsk Soil and Environment in Ås, Norway, for partly financing my stay during 8 month in Ås while working on my thesis. Thanks to Jannes Stolte and Jantiene Baartman for supervision of the thesis. Thanks to Torsten Starkloff, Robert Barneveld and Christophe Moni for great help and support, both in the field and behind the computer, during my time at BioForsk without which the thesis would not have been completed.

Bibliography

Aguilar, M.A., Aguilar, F.J., Negreiros, J., 2009. Off-the-shelf laser scanning and close-range digital photogrammetry for measuring agricultural soils microrelief. Biosyst. Eng. 103, 504–517.

Allmaras, R.R., Burwell, R.E., Larson, W.E., Holt, R.F., 1966. Total porosity and random roughness of the interrow zone as influenced by tillage.

Álvarez-Mozos, J., Campo, M.Á., Giménez, R., Casalí, J., Leibar, U., 2011. Implications of scale, slope, tillage operation and direction in the estimation of surface depression storage. Soil Tillage Res. 111, 142–153.

Amoah, J.K.O., Amatya, D.M., Nnaji, S., 2013. Quantifying watershed surface depression storage: determination and application in a hydrologic model. Hydrol. Process. 27, 2401–2413.

Arvidsson, J., Bölenius, E., 2006. Effects of soil water content during primary tillage – laser measurements of soil surface changes. Soil Tillage Res. 90, 222–229.

Baartman, J.E.M., Jetten, V.G., Ritsema, C.J., Vente, J., 2012. Exploring effects of rainfall intensity and duration on soil erosion at the catchment scale using openLISEM: Prado catchment, SE Spain. Hydrol. Process. 26, 1034–1049.

Barneveld, R.J., Seeger, M., Maalen-Johansen, I., 2013. Assessment of terrestrial laser scanning technology for obtaining high-resolution DEMs of soils. Earth Surf. Process. Landforms 38, 90–94.

Chow, J.C.K., Ang, K.D., Lichti, D.D., Teskey, W.F., 2012. Performance analysis of a low-cost triangulation-based 3D camera: Microsoft Kinect system. Int. Arch. Photogramm. Remote Sens. Spat. Inf. Sci. XXII ISPRS Congr.

Comb, B., Guibert, A., Memin, E., Heitz, D., Combès, B., 2011. Free-surface flows from Kinect : Feasibility and limits. Vol. Reconstr. Tech. 3D fluid solid Mech. 2–5.

Cremers, N.H.D.T., Van Dijk, P.M., De Roo, A.P.J., Verzandvoort, M.A., 1996. Spatial and temporal variability of soil surface roughness and the application in hydrological and soil erosion modelling. Hydrol. Process. 10, 1035–1047.

De Roo, A.P.J., Offermans, R.J.E., Cremers, N.H.D.T., 1996a. LISEM: A single-event, physically based hydrological and soil erosion model for drainage basins. II: Sensitivity analysis, validation and application. Hydrol. Process. 10, 1119–1126.

De Roo, A.P.J., Wesseling, C.G., Cremers, N.H.D.T., Offermans, R.J.E., Ritsema, C.J., Van Oostindie, K., 1994. LISEM: a new physical-based hydrological and soil erosion model in a GIS-environment, theory and implementation, in: Variability in Stream Erosion and Sediment Transport, Proc. Symposium, Canberra, 1994. pp. 439–448.

De Roo, A.P.J., Wesseling, C.G., Ritsema, C.J., 1996b. Lisem: A single-event physically based hydrological and soil erosion model for drainage basins. I: Theory, input and output. Hydrol. Process. 10, 1107–1117.

De Vente, J., Poesen, J., Govers, G., Boix-Fayos, C., 2009. The implications of data selection for regional erosion and sediment yield modelling. Earth Surf. Process. Landforms 34, 1994–2007.

De Vente, J., Poesen, J., Verstraeten, G., Govers, G., Vanmaercke, M., Van Rompaey, A., Arabkhedri, M., Boix-Fayos, C., 2013. Predicting soil erosion and sediment yield at regional scales: Where do we stand? Earth-Science Rev. 127, 16–29.

Doren, D.R., Linden, D.M. Van, 1986. Parameters for Characterizing Tillage-induced Soil Surface Roughness. Soil Sci. Soc. Am. J. 50, 1–6.

Govers, G., Takken, I., Helming, K., 2000. Soil roughness and overland flow. Agronomie 20, 131–146.

Grimm, M., Jones, R., Montanarella, L., 2002. Soil Erosion Risk in Europe.

Grønsten, H.A., Øygarden, L., Skjevdal, R.M., 2007. Høstkorn - redusert jordarbeiding gir mindre tap av jord og næringsstoffer. Bioforsk Tema 2, 1–4.

Hairsine, P.B., Rose, C.W., 1992. Modeling Water Erosion Due to Overland Flow Using Physical Principles. 1. Sheet flow. Water Resour. Res. 28, 237–243.

Haubrock, S.-N., Kuhnert, M., Chabrillat, S., Güntner, A., Kaufmann, H., 2009. Spatiotemporal variations of soil surface roughness from in-situ laser scanning. Catena 79, 128–139.

Hessel, R., 2002. Modelling soil erosion in a small catchment on the Chinese Loess Plateau. Utrecht University.

Hessel, R., 2005. Effects of grid cell size and time step length on simulation results of the Limburg soil erosion model (LISEM). Hydrol. Process. 19, 3037–3049.

Huang, A.S., Bachrach, A., Henry, P., Krainin, M., Fox, D., Roy, N., 2011. Visual Odometry and Mapping for Autonomous Flight Using an RGB-D Camera, in: International Symposium on Robotics Research. Flagstaff, Arizona, USA, pp. 1–16.

Hyväluoma, J., Lilja, H., Turtola, E., 2013. An anisotropic flow-routing algorithm for digital elevation models. Comput. Geosci. 60, 81–87.

Jester, W., Klik, A., 2005. Soil surface roughness measurement—methods, applicability, and surface representation. Catena 64, 174–192.

Jetten, V., 2002. LISEM manual.

Jetten, V., 2013. OpenLISEM - a spatial model for runoff , floods and erosion [WWW Document]. URL http://blogs.itc.nl/lisem/ (accessed 10.15.13).

Jetten, V., Govers, G., Hessel, R., 2003. Erosion models: Quality of spatial predictions. Hydrol. Process. 17, 887–900.

Kamphorst, E.C., Jetten, V., Guérif, J., Pitkänen, J., Iversen, B. V, Douglas, J.T., Paz, A., 2000. Predicting Depressional Storage from Soil Surface Roughness. Soil Sci. Soc. Am. J. 64, 1749–1758.

Khoshelham, K., Elberink, S.O., 2012. Accuracy and resolution of Kinect depth data for indoor mapping applications. Sensors (Basel). 12, 1437–54.

Kinect - wikipedia [WWW Document], 2013. URL http://en.wikipedia.org/wiki/Kinect (accessed 8.7.13).

Konolige, K., Mihelich, P., 2010. Kinect Calibration: Technical. [WWW Document]. URL http://www.ros.org/wiki/kinect_calibration/technical (accessed 8.7.13).

Kramer, J., Burrus, N., Echtler, F., Herrera, D., Parker, M., 2012. Hacking the Kinect. Apress.

Kværnø, S.H., 2011. Variability and uncertainty in soil physical properties: Effects of data source on functional criteria. Norwegian University of Life Science.

Kværnø, S.H., Stolte, J., 2012. Effects of soil physical data sources on discharge and soil loss simulated by the LISEM model. Catena 97, 137–149.

Lal, R., 1994. Soil erosion research methods, Soil erosion research methods, (2nd eds.). Soil and Water Conservation Society [etc.], Ankeny [etc.].

Lehrsch, G.A., Whisler, F.D., Römkens, M.J.M., 1987. Soil surface roughness as influenced by selected soil physical properties. Soil Tillage Res. 10, 197–212.

Lehrsch, G.A., Whisler, F.D., Römkens, M.J.M., 1988a. Selection of a Parameter Describing Soil Surface Roughness. Soil Sci. Soc. Am. J. 52, 1439–1445.

Lehrsch, G.A., Whisler, F.D., Römkens, M.J.M., 1988b. Spatial Variation of Parameters Describing Soil Surface Roughness. Soil Sci. Soc. Am. J. 52, 311–319.

Leica-Geosystems, 2007. Leica ScanStation 2 Product Specifications [WWW Document]. URL http://hds.leica-geosystems.com/downloads123/hds/hds/ScanStation/brochures-datasheet/Leica_ScanStation 2_datasheet_us.pdf (accessed 9.8.13).

Luhmann, T., Robson, S., Kyle, S., Harley, I., 2006. Close range photogrammetry - Principles, Methods and Applications, 1st ed. Whittles Publishing, Caithness, Scotland, UK.

Luhmann, T., Wendt, K., 2000. RECOMMENDATIONS FOR AN ACCEPTANCE AND VERIFICATION TEST OF OPTICAL 3-D MEASUREMENT SYSTEMS XXXIII, 493–500.

Lundekvam, H., Skøien, S., 1998. Soil erosion in Norway. An overview of measurements from soil loss plots. Soil Use Manag. 14, 84–89.

Lundekvam, H.E., Romstad, E., Øygarden, L., 2003. Agricultural policies in Norway and effects on soil erosion. Environ. Sci. Policy 6, 57–67.

Mankoff, K.D., Russo, T.A., 2012. The Kinect: A low-cost, high-resolution, short-range 3D camera. Earth Surf. Process. Landforms.

Martin, Y., Valeo, C., Tait, M., 2008. Centimetre-scale digital representations of terrain and impacts on depression storage and runoff. Catena 75, 223–233.

Marzolff, I., Poesen, J., 2009. The potential of 3D gully monitoring with GIS using high-resolution aerial photography and a digital photogrammetry system. Geomorphology 111, 48–60.

Method and system for object reconstruction. Patent WO2007043036 [WWW Document], 2007. URL http://patentscope.wipo.int/search/en/WO2007043036

Morgan, R.P.C., 2005. Soil erosion and conservation. Blackwell, Malden, MA [etc.].

Mwendera, E.J., Feyen, J., 1992. Estimation of depression storage and Manning's resistance coefficient from random roughness measurements. Geoderma 52, 235–250.

Nord, G., Esteves, M., 2010. The effect of soil type, meteorological forcing and slope gradient on the simulation of internal erosion processes at the local scale. Hydrol. Process. 24, 1766–1780.

Øygarden, L., Lundekvam, H., Arnoldussen, A.H., Børresen, T., 2006. 1.1 Norway, in: Boardman, J., Poesen, J. (Eds.), Soil Erosion in Europe. John Wiley & Sons, Ltd., pp. 3–15.

PCRaster documentation, 2013.

Pfeifer, N., Briese, C., 2007. Laser scanning - principles and applications. Vienna, Austria.

Pignatelli, C., Piscitelli, A., Damato, B., Mastronuzzi, G., 2010. Estimation of the value of Manning's coefficient using Terristrial Laser Scanner techniques for assessment of flooding by extreme waves. Zeitschrift für Geomorphol. Suppl. 54,, 317–336.

Planchon, O., Esteves, M., Silvera, N., 2001. Microrelief induced by tillage : measurement and modelling of Surface Storage Capacity. Catena 46, 141–157.

Podmore, T.H., Huggins, L.F., 1981. An Automated Profile Meter for Surface Roughness Measurements. Trans. ASABE 663–666.

PrimeSense, 2013. PrimeSense technology [WWW Document]. URL

http://www.primesense.com/solutions/technology/ (accessed 8.7.13).

Rasband, W., 2013. ImageJ - documentation [WWW Document]. URL http://rsbweb.nih.gov/ij/docs/index.html (accessed 9.2.13).

Rompaey, A.J.J. Van, Govers, G., 2002. Data quality and model complexity for regional scale soil erosion prediction. Int. J. Geogr. Inf. Sci. 16, 663–680.

Saleh, A., 1993. Soil roughness measurement : Chain method. J. Soil Water Conserv. 48, 527–529.

Sander, G.C., Parlange, J.-Y., Barry, D. a., Parlange, M.B., Hogarth, W.L., 2007. Limitation of the transport capacity approach in sediment transport modeling. Water Resour. Res. 43, n/a–n/a.

Scharstein, D., Szeliski, R., 2003. High-accuracy stereo depth maps using structured light. 2003 IEEE Comput. Soc. Conf. Comput. Vis. Pattern Recognition, 2003. Proceedings. I–195–I–202.

Sheikh, V., van Loon, E., Hessel, R., Jetten, V., 2010. Sensitivity of LISEM predicted catchment discharge to initial soil moisture content of soil profile. J. Hydrol. 393, 174–185.

Skidmore, E.L., 1994. Comment on Chain Method for Measuring Soil Roughness. Soil Sci. Soc. Am. J. 61, 0–1.

Stroosnijder, L., 2005. Measurement of erosion: Is it possible? Catena 64, 162–173.

Structured light imaging [WWW Document], 2011. URL http://www.metrilus.de/range-imaging/structured-light/

Taconet, O., Ciarletti, V., 2007. Estimating soil roughness indices on a ridge-and-furrow surface using stereo photogrammetry. Soil Tillage Res. 93, 64–76.

Takken, I., 2000. Effects of roughness on overland flow and erosion. Geografie-geologie. Katholieke Universiteit Leuven, Leuven, Belgium.

Takken, I., Beuselinck, L., Nachtergaele, J., Govers, G., Poesen, J., Degraer, G., 1999. Spatial evaluation of a physically-based distributed erosion model (LISEM). Catena 37, 431–447.

Takken, I., Govers, G., Jetten, V., Nachtergaele, J., Steegen, A., Poesen, J., 2005. The influence of both process descriptions and runoff patterns on predictions from a spatially distributed soil erosion model. Earth Surf. Process. Landforms 30, 213–229.

Takken, I., Govers, G., Sinzumusi, A., 2000. The effect of oriented roughness on the hydraulics of interrill overland flow. Unpubl. Work.

Takken, I., Jetten, V., Govers, G., Nachtergaele, J., Steegen, A., 2001. The effect of tillage-induced roughness on runoff and erosion patterns. Geomorphology 37, 1–14.

Tölgyessy, M., Hubinský, P., 2010. The Kinect Sensor in Robotics Education 1–4.

Wainwright, J., Parsons, A.J., Müller, E.N., Brazier, R.E., Powell, D.M., 2009a. Letters to ESEX Response to Hairsine ’ s and Sander ’ s “ Comment on ‘ A transport-distance based approach to scaling erosionrates ’: Parts 1 , 2 and 3 by Wainwright et al .” Earth Surf. Process. Landforms 890, 886–890.

Wainwright, J., Parsons, A.J., Müller, E.N., Brazier, R.E., Powell, D.M., 2009b. Response to Kinnell ’ s “ Comment on ‘ A transport- distance approach to scaling erosion rates : III . Evaluating scaling characteristics of M AHLERAN ’ ” Earth Surf. Process. Landforms 1321, 1320–1321.

Wainwright, J., Parsons, A.J., Müller, E.N., Brazier, R.E., Powell, D.M., 2010. Standing proud: a response to “Soil-erosion models: where do we really stand?” by Smith et al. Earth Surf. Process. Landforms 35, 1349–1356.

Wainwright, J., Parsons, A.J., Müller, E.N., Brazier, R.E., Powell, D.M., Fenti, B., 2008a. A transport-distance approach to scaling erosion rates : 1 . Background and model development. Earth Surf. Process. Landforms

826, 813–826.

Wainwright, J., Parsons, A.J., Müller, E.N., Brazier, R.E., Powell, D.M., Fenti, B., 2008b. A Transport-Distance Approach to Scaling Erosion Rates : 2 . Sensitivity and Evaluation of M AHLERAN. Earth Surf. Process. Landforms 984, 962–984.

Wang, T.C., 2013. Modeling grass zones as a land use measure in the Skuterud catchment using the Limburg Soil Erosion Model. Norwegian University of Life Science.

Whelan, T., Mcdonald, J., Kaess, M., Fallon, M., Johannsson, H., Leonard, J.J., 2012. Kintinuous : Spatially Extended KinectFusion, in: RSS Workshop on RGB-D: Advanced Reasoning with Depth Cameras. Sydney, Australia.

Zobeck, T.M., Onstad, C.A., 1987. Tillage and rainfall effects on random roughness: A review. Soil Tillage Res. 9, 1–20.

Appendices

Appendix I R-code for processing point-cloud data

The following is the raw code that was developed to process the 3D point-clouds in R.

```
Name<-
c("ls01harrow","ls02skog","st5mmGrytelandharrowed","stforest1","stforest2","stforest3","stharrowplot1","stharrowplot2","stharrowplot3","st
harrowplot4","stharrowplot5","stharrowplot6",
"stplleir1","stplleir2","stplleir3","stplsku1","stplsku2","ststub1","ststub2","ststub3","xforest1","xforest2","xforest3","xharrow1","xharr
ow2","xharrow3","xharrow5","xharrow6","xharrowGryt","xplsku1","xplsku2","xplsku3","xstub1","xstub2","xstub3")
Data<-vector("list", length(Name))
Data[[1]]<-read.table("C:/users/JORTTH/Desktop/line.data/ls01harrow.xyz",header=FALSE,sep = "",dec = ".",col.names=c("x","y","z"))
Data[[2]]<-read.table("C:/users/JORTTH/Desktop/line.data/ls02skog.xyz",header=FALSE,sep = "",dec = ".",col.names=c("x","y","z"))
…#full list of read data are not shown
Data[[34]]<-read.table("C:/users/JORTTH/Desktop/line.data/xstub2.xyz",header=FALSE,sep = "",dec = ".",col.names=c("x","y","z"))
Data[[35]]<-read.table("C:/users/JORTTH/Desktop/line.data/xstub3.xyz",header=FALSE,sep = "",dec = ".",col.names=c("x","y","z"))
pin<-read.table("C:/users/JORTTH/Desktop/line.data/pin_r.csv",header=FALSE,sep = "",dec = ".")
#Data[[1]]
#k<-1
##### laser scaning recentering
for (k in 1:2){   # always 1:2
length(abs(Data[[k]][,2])<0.4)
Data[[k]][1:100,]

max(Data[[k]][,1])
min(Data[[k]][,1])
max(Data[[k]][,2])
min(Data[[k]][,2])

xmax<-max(Data[[k]][,1])
xmin<-min(Data[[k]][,1])
ymax<-max(Data[[k]][,2])
ymin<-min(Data[[k]][,2])

Data[[k]][,1]<-Data[[k]][,1]-mean(c(max(Data[[k]][,1]),min(Data[[k]][,1])))
Data[[k]][,2]<-Data[[k]][,2]-mean(c(max(Data[[k]][,2]),min(Data[[k]][,2])))
}
#######
#Data2<-vector("list", length(Name))
Coo<-matrix(0,11,length(Name))
dimnames(Coo)[[1]]<-
c("a","b","c","R2","mean.raw.subset","Sd.raw.subset","mean.corr.subset","Sd.Corr.subset","n.raw","n.subset","n.subset.corr")
dimnames(Coo)[[2]]<-Name
Elevation<-vector("list", length(Name))   #      Elevation compared to the best fit regression plan
Datat<-vector("list", length(Name))       #      xyz file after horizontal transformation
Datat_r<-vector("list", length(Name))     #      XYZ file after horizontal transformation and out-
                                                    lier elimination
for (k in 1:35){
  Coo[9,k]<-dim(Data[[k]])[1]
  #  k<-23
           if(max(abs(Data[[k]]))>4){Data[[k]]<-Data[[k]]/100}                        # test if the matrix is in cm and convert it in m
                                                                                      if necessary
# take a subset of 0.8mx0.8m to exclude the markers
  Data[[k]]<-Data[[k]][which(abs(Data[[k]][,1])<0.4 & abs(Data[[k]][,2])<0.4),]

  }
#i<-30              #defining the plane based least square error estimation
for (i in 1:35){

X<-Data[[i]]$x
Y<-Data[[i]]$y
Z<-Data[[i]]$z

Plane<-nls(Z ~ a*X + b*Y + c , start=list(a=1, b=1, c=1), trace=T)
(RSS.p2 <- sum(residuals(Plane)^2))
(TSS2 <- sum((Z - mean(Z))^2))
R2.2<-1 - (RSS.p2/TSS2)
Coo[1,i]<-summary(Plane)$coefficients[1,1]
Coo[2,i]<-summary(Plane)$coefficients[2,1]
Coo[3,i]<-summary(Plane)$coefficients[3,1]
Coo[4,i]<-round(R2.2,4)
Coo[5,i]<-mean(Z)
Coo[6,i]<-sd(Z)
Plane<-NULL

#calculating the point-to-plane from each z coordinate. Per point-cloud calculating the mean and standard deviation, i.e. the random
roughness
Elevation[[i]]<- -(Coo[1,i]*X+Coo[2,i]*Y-Z+Coo[3,i])/(Coo[1,i]**2+Coo[2,i]**2+1)**0.5
Coo[7,i]<-mean(Elevation[[i]])
Coo[8,i]<-sd(Elevation[[i]])

i<-30              #filtering out data outside a defined confidence interval
confidence<-3
Datat[[i]]<-cbind(X,Y,Elevation[[i]])
#Datat_r[[i]]<-Datat[[i]][-which(abs(Datat[[i]][,3]-Coo[7,i])>abs(confidence*Coo[8,i])),]
```

```
Datat_r[[i]]<-Datat[[i]][which(abs(Datat[[i]][,3]-Coo[7,i])<abs(confidence*Coo[8,i])),]

Coo[10,i]<-length(Elevation[[i]])
Coo[11,i]<-dim(Datat_r[[i]])[1]
}
##################################################
### 3D scatterplot. Visualizing data
library(rgl)
myColorRamp <- function(colors, values) {
  v <- (values - min(values))/diff(range(values))
  x <- colorRamp(colors)(v)
  rgb(x[,1], x[,2], x[,3], maxColorValue = 255)
}
i<-30

X<-Data[[i]]$x
Y<-Data[[i]]$y
Z<-Data[[i]]$z

cols <- myColorRamp(c("blue", "green","yellow","orange","red"), Z)
plot3d(X,Y,Z, col=cols, size=3,aspect=c(1,1,0.2),main=Name[i])

cols <- myColorRamp(c("blue", "green","yellow","orange","red"), Datat_r[[i]][,3])
plot3d(Datat_r[[i]][,1],Datat_r[[i]][,2],Datat_r[[i]][,3], col=cols, size=3,aspect=c(1,1,0.2), xlab="X", ylab="Y", zlab="Z",main=Name[i])


#### write data to table

write.table(Coo, file = "foo3.csv", sep = ",", col.names = NA)
i<-30
#for (i in 1:35){
  write.table(Datat_r[[i]], file = paste("F",Name[i]), sep = ",", col.names = NA)
}
```

Appendix II Model input parameters

Model input parameters for the subcatchment Gryteland (table 8.1). The soil units indicate which areas that were assigned a calibration factor (only clay) (figure 8.1) and the land use units indicate which area that were assigned a different RR value. The model input parameter for the whole catchment are almost identical (table 8.2). For Skuterud only the land use units are shown (figure 8.3), each land use units equal a different RR value.

Table 8.1: Model input parameters for sub-catchment Gryteland

Constant model parameters (abbreviation, unit)	Forest (5)[15]	Urban (1)	Arable (12)	Gully
Saturated hydraulic conductivity (K_s, cm d^{-1})	86.1 (sand) 17.55 (clay)	86.1	86.1 (sand) 17.55 (clay)	-
Chosen adjustment factor for K_s (only clay soil map unit, figure 8.1)			3	-
Porosity (Θ_s, m^3 m^{-3})?????? INPUT?	0.4	0.4	??	-
Depth topsoil (-, cm)	25	25	25	-
Initial matric potential (inithead, cm)	-50	-50	-50	-
Manning's n	1,2	2,4	0.45[16]	-
Soil fraction covered by vegetation (per, -)	0.9	0.9	1	-
Vegetation height, (ch, m)	7	-	0.7	-
Leaf area index (lai, -)	6	-	2.5	-
d50 value of the soil (d50, µm)	50	50	50	-
Cohesion of bare soil (coh, kPa)	500	500	25	-
Additional cohesion by roots (cohadd, kPa)	10	5	1	-
Aggregate stability (aggr, -)	200	200	200	-
Channel cohesion (chancoh, kPa)				15000
Channel Manning's n (chanman, -)				0.01
Channel width (chanwidt, m)				1
Slope of channel sides (chanside, -)				45

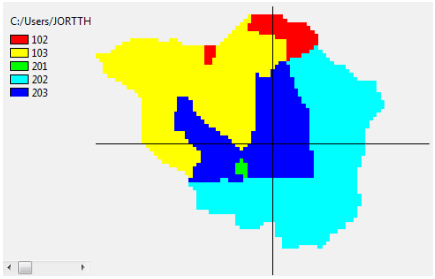

Figure 8.1: LISEM soil units. Key: 102 = forest on clay, 103 = agriculture on clay, 201 = urban on sand, 202 = forest on sand, 203 = agriculture on sand.

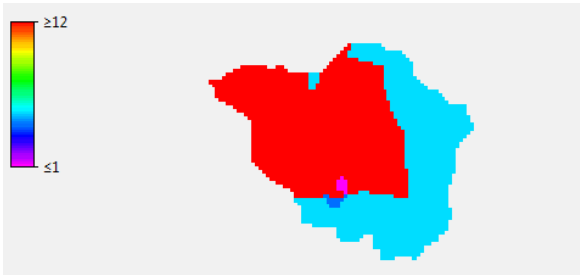

Figure 8.2: LISEM land units. Key: forest (turquoise), agriculture (red), urban (purple) and deciduous forest (blue).

15 A very small area is covered with deciduous trees which for some of the parameters has different values. They are not included in the table. For ch (m) = 0.2, lai (-) = 1.46

16 Adjusted for calibrating the hydrograph. Originally Manning's n was 0.6 for cultivated fields.

Table 8.2: Model input parameters for catchment Skuterud

Constant model parameters (abbreviation, unit)	Forest (5, 4)[17]	Urban (1)	Arable (12)	Peat (16)	Stream
Saturated hydraulic conductivity (K_s, cm d^{-1})					
Chosen adjustment factor for K_s (only clay soil map unit)	1.3		1.3		
Porosity (Θ_s, m^3 m^{-3})					
Depth topsoil (-, cm)	25	25	25		
Initial matric potential (inithead, cm)	-300	-300	-300	-300	
Manning's n	1.2	2.4	0.6	1.2	
Soil fraction covered by vegetation (per, -)	0.9	0.9	1	0.9	
Vegetation height, (ch, m)	7	0.2	0.7	7	
Leaf area index (lai, -)	6	1.46	2.5	4	
d50 value of the soil (d50, µm)	50	50	50	50	
Cohesion of bare soil (coh, kPa) diff bw article/pcr maps	20	30	variable	50	
Additional cohesion by roots (cohadd, kPa)	10	5	1	0.01	
Aggregate stability (aggr, -)	150	170	25-120	190	
Channel cohesion (chancoh, kPa)					15000
Channel Manning's n (chanman, -)					0.04
Channel width (chanwidt, m)					5
Slope of channel sides (chanside, -)					45

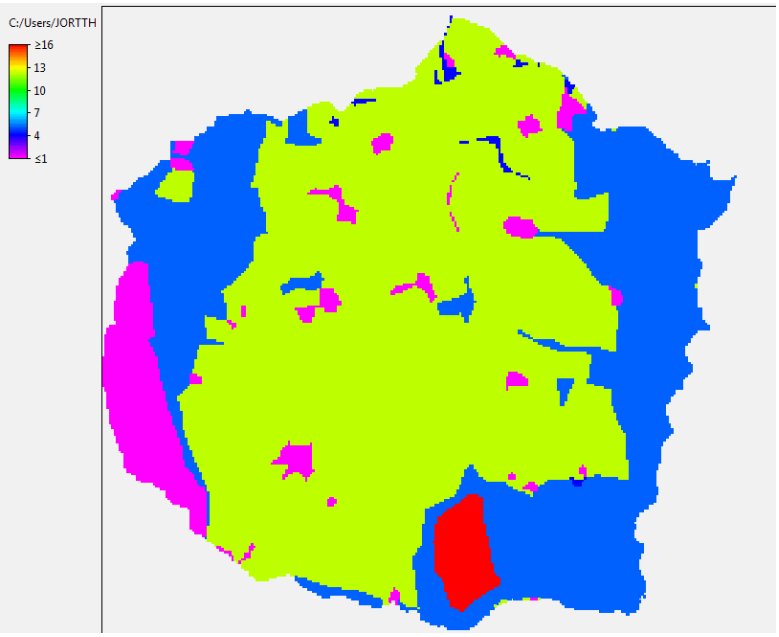

Figure 8.3: Land unit map of the whole Skuterud catchment, each cell is 10m x 10 m. Unfortunately, the colour key is not equivalent to the one in figure 8.2, since the colouring is randomly generated. Here: Forest (blue), deciduous forest (dark blue), green (agriculture), urban (purple) and peat (red). Please note that the two maps do not have the same scale, thus Gryteland are magnified in figure 8.2 compared to here.

17 Same as footnote 16

Roughness input

It is assumed that the RR of the cultivated fields on 04 September 2009 were similar to measured RR from harrowed fields. This is based on two arguments: 1) after harvest it is common not to plough the fields but leave them idle with stubbles, confirmed by a google earth image from the 05. September 2012 showing stubbles in Gryteland (figure 8.4), so there is a high probability that the fields also had stubbles on the same date three years earlier. 2) It is then further assumed that the roughness of a post-cultivated crop field (with stubbles) has a similar roughness as a recently harrowed field. It is recognized that the roughness changes over the growing season (Cremers et al., 1996), but several counteracting factors are in play. The growth of crop will increase the roughness when the seedlings break through the soil, but rain will simultaneously decrease the roughness. Based on this it is assumed to be reasonable to apply the roughness for a harrowed surface on a September field. A roughness value of 0.81 cm is also in agreement with values from a similar study, reporting roughness values from July at harvest of 0.99cm (sugar beet), 1.14 cm (corn) and 0.94cm (winter wheat) (Cremers et al., 1996). It is important to emphasize that the land use which in most graphs are named "stubbles" are indicating *direct seeding on stubbles*, and is as such different from stubbles because the seeding machines have made rills in the soil and it has been lightly tilled..

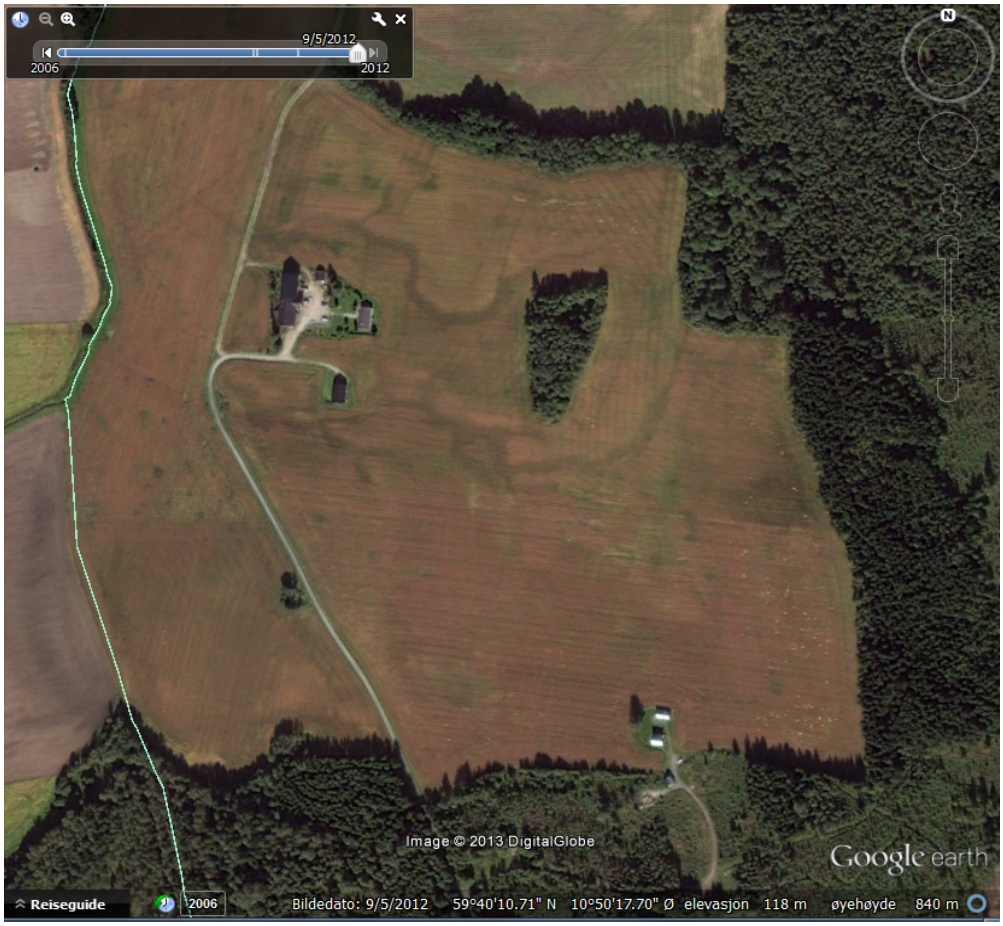

Figure 8.4 Google earth image showing the Gryteland catchment from the 05 September 2012. The stubbles are visible, together with some marks in the catchment which coincide with the depression in the landscape.

Appendix III Chain-pinboard conversion

TLS, stereophotos, Xtion and pinboard all yields elevation data directly, whereas the chain method data has to be converted to be compared with the other data. To convert the chain data, first the pinboard and chain data were related to each other. The profile length of the pinboard was calculated as the sum of straight length between two consecutively pins using Pythagoras sentence. The horizontal distance (x) between two pins is two cm, and consequently the distance between two pin-tips will be 2 cm or larger, whereas the straight length between two consecutively joints on the chain is 0.6 cm. Thus it is not a perfect approximation to construct the profile length from the pinboards to compare with the chain. Based on the calculated profile length and the known straight length of the pinboard (1 meter) it was possible to calculate the Cr-index as reported by Saleh (1993) and relate it to the Cr-index calculated from the chain. Figure 8.5 shows the correlation between Cr from chain and pinboard. A linear regression line shows that it is not a perfect 1:1 relation, with measurements from the pinboard giving a higher roughness value than from chain.

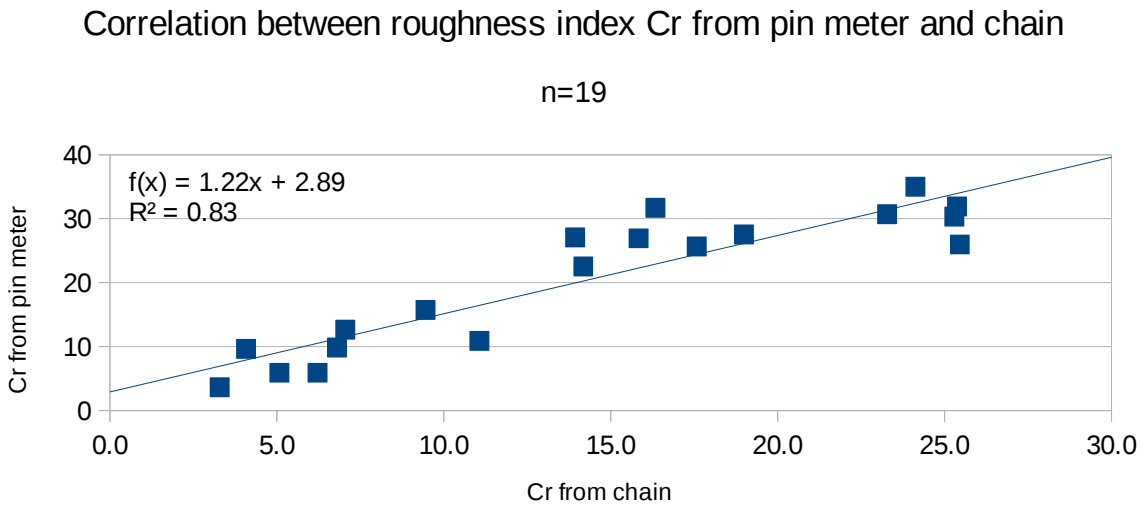

Figure 8.5: Scatter plot showing the relation between the Cr index calculated from chain and pinboard measurements respectively

Since the R^2 value was sufficiently high, although not as high as reported by Jester & Klik (2005), a regression to relate Cr from chain to random roughness (RR) as calculated from the pinboard was made, see figure . To get an acceptable fit 3 data points were excluded from the regression, which improved the R^2 from 0.55 to 0.82. The excluded data points were two measurements from ploughed areas and one from forest. With this conversion formula, (regression equation indicated on figure) RR-values from chain measurement were obtained. For the 3 outliers excluded from the regression, the RR value from pinboard replaced their value.

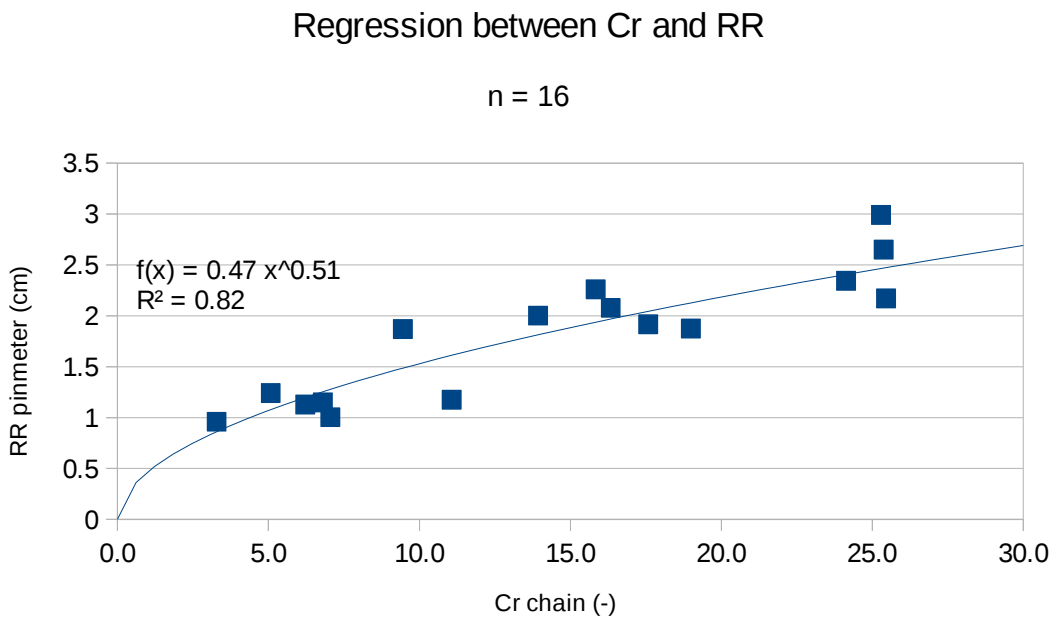

Figure 8.6: Regression between profile index Cr from chain measurement and random roughness (stdev of elevations) from pinboard measurements

the less than perfect 1:1 relation between the calculated Cr-index from pinboard and chain, figure 8.6 shows that the profile length calculated from pinboard data are longer than the profile. This is in accordance with findings from Jester & Klik (2005). They suggested that the difference is due to the fact that the pinboard manages to capture small gaps between soil aggregates which the chain cannot capture. This is confirmed by observations in the field. It was indeed difficult to make the chain fit each single soil aggregate, partly because the chain joints became a bit inflexible – especially after some days of fieldwork, where dust settled in the joints, partly because the soil was loose or moist, making it impossible to make the chain fit the aggregates accurately without destroying the soil surface. This also seems to be reflected in the regression between RR and Cr. Jester & Klik (2005) found a higher correlation coefficient, R^2=0.956, n=16, which is better than what our data yielded, even after removing outliers, figure 8.6. One important difference is that they only used two surfaces ('rough' and 'smooth') and compared before and after rain, whereas we in this study looked at 4 difference land uses and did not incorporate temporal changes, thus the spread in our data is probably higher. Jester & Klik (2005) further concluded that the smoother the surface the better is the pinboard-chain relation. Thus, an explanation might be that the regression between pinboard and chain is dependent on land use type and limited to smooth surfaces, while the discrepancies between the methods becomes to high when the surface is rough.

Based on the literature review executed for the background chapter in this thesis, it seems like there are very few studies that use the chain to obtain random roughness data with. Further, it is questionable how used the method is in general, especially recalling the critics the index received because of the lack of capabilities to captured differences between small and big tillage ridges (Skidmore, 1994). Based on our fieldwork observations it is suggested that the chain method is best suited for relatively smooth, but crusted surfaces which not easily is penetrated when the chain is laid out on the surface. The chain method is included in the subsequent statistical test, but not used further on in the model runs, because it basically is a function of the pinboard method.

Appendix IV All random roughness data

Point-cloud: 0.8mx0.8m region

	number of points	rr (cm)	Mean rr per LU	stdev
ls				
harrow	2134146	0.81	0.81	-
forest	2193589	1.05	1.05	-
xtion				
harrow Gryt	69945	0.75	1.18	0.33
Harrow 1	78069	1.29		
Harrow 2	74615	1.32		
Harrow 3	68958	0.79		
Harrow 5	81951	1.36		
Harrow 6	83057	1.58		
Forest 1	59551	1.30	1.65	0.59
Forest 2	57570	2.33		
Forest 3	59260	1.32		
Plough_Gryt1	71391	2.23	2.84	0.86
Plough_Gryt2	94710	2.47		
Plough_Gryt3	73981	3.83		
Stubble1	60636	2.16	2.04	0.57
Stubble2	74078	2.54		
Stubble3	68239	1.42		
stereo				
Harrow Gryt	105109	0.68	1.52	0.70
Harrow 1	7598	2.59		
Harrow 2	52705	1.09		
Harrow 3	26410	1.11		
Harrow 4	11275	2.33		
Harrow 5	41560	1.23		
Harrow 6	22725	1.60		
Forest 1	41340	1.13	0.94	0.24
Forest 2	53080	1.01		
Forest 3	168204	0.67		
Plough_Leir1	32776	2.39	2.70	0.55
Plough_Leir2	63235	2.06		
Plough_Leir3	39510	2.89		
Plough_Gryt1	36261	2.64		
Plough_Gryt2	11918	3.51		
Stubble1	35676	0.60	0.63	0.03
Stubble2	60598	0.64		
Stubble3	172761	0.66		

transects with 50 elevation recordings

pinboard	rr (cm)	Mean rr (cm)	Mean rr per LU	stdev
along				
harrow Gryt 1	0.94	0.84	1.43	0.59
harrow Gryt 2	0.99			
harrow Gryt 3	0.56			
harrow Gryt 4	0.86			
along				
Harrow1	1.87	1.82		
Harrow2	1.72			
Harrow3	1.53			
Harrow4	1.71			
Harrow5	1.55			
Harrow6	2.55			
across				
harrow Gryt 1	1.55	1.51	*1.86*	*0.38*
harrow Gryt 2	1.50		*(not used)*	
harrow Gryt 3	1.24			
harrow Gryt 4	1.77			
across				
Harrow1	2.33	2.09		
Harrow2	2.10			
Harrow3	2.32			
Harrow4	1.60			
Harrow5	2.08			
Harrow6	2.14			
forest				
forest1	1.89	1.38	1.38	0.53
forest1	1.97			
forest2	0.81			
forest2	1.67			
forest3	1.02			
forest3	0.89			
plough *no direction*				
leirsund1	2.49	2.54	2.54	0.39
leirsund2	2.80			
leirsund3	2.18			
leirsund4	2.11			
leirsund5	2.21			
leirsund6	2.91			
leirsund7	3.07			
Plough along				
gryt1	1.90	2.94	2.94	1.71
gryt2	1.62			
gryt3	2.08			
gryt4	3.34			
gryt5	5.76			
Plough across				
gryt1	2.77	4.09	*4.09*	*1.21*
gryt2	2.77		*not used*	
gryt3	4.84			
gryt4	5.02			
gryt5	5.07			
stubble				
stubble1	0.58	1.10	1.10	0.37
stubble2	1.68			
stubble3	1.14			
stubble4	0.87			
stubble5	1.07			
stubble6	1.24			

chain length=100.5 cm
chain measured length (cm)

f(x)=0.066x + 0.802
R^2= 0.62

along	1	2	3	4	average	Cr index	converted to rr (cm)	Mean rr per LU	stdev
harrow Gryt.	91				91	9.5	1.4	1.63	0.21
harrow Gryt.	94.5				94.5	6.0	1.2		
harrow Gryt.	91.5				91.5	9.0	1.4		
harrow Gryt.	94				94	6.5	1.2		
harrow	91	85	91.5		89.2	11.3	1.5		
harrow	85	80	93.5		86.2	14.3	1.7		
harrow	87	84	91.5		87.5	12.9	1.7		
harrow	85.5	80	79		81.5	18.9	2.0		
harrow	89.5	87.5	74.5		83.8	16.6	1.9		
harrow	85	81	73		79.7	20.7	2.2		
across									
harrow Gryt.	87	86.5	86	84.5	86	14.4	1.8	1.90	0.23
								not used	
harrow	86	86	87		86.3	14.1	1.7		
harrow	88	74	88.5		83.5	16.9	1.9		
harrow	82	88	94		88.0	12.4	1.6		
harrow	76	86	73		78.3	22.1	2.3		
harrow	85	83	85		84.3	16.1	1.9		
harrow	80.5	87	73		80.2	20.2	2.1		
forest									
forest1	95.5	97	96		96.2	4.3	1.1	1.07	0.03
forest2	96	95.5	97		96.2	4.3	1.1		
forest3	96	94	98		96.0	4.5	1.1		
forest4	96.5	94.5	98		96.3	4.1	1.1		
forest5	98	96	97		97.0	3.5	1.0		
forest6	95	98	98		97.0	3.5	1.0		
plough *no direction*									
leirsund1	85	67.5	80		77.5	22.9	2.3	2.23	0.34
leirsund2	79	75.5	76		76.8	23.5	2.4		
leirsund3	66	78.5	63.5		69.3	31.0	2.8		
leirsund4	79.5	74	72		75.2	25.2	2.5		
leirsund5	76.5	78	75		76.5	23.9	2.4		
leirsund6	73.5	76	84		77.8	22.6	2.3		
leirsund7	73				73.0	27.4	2.6		
leirsund8	67.5				67.5	12.8	1.6		
Plough along									
gryt1	83	83	65		77.0	10.6	1.5		
gryt2	83	79.5	76		79.5	16.4	1.9		
gryt3	*80*	*82*	*61*		*74.3*	*26.0*	*2.5*		
gryt4			*70*		*70.0*	*30.3*	*2.8*		
Plough across									
gryt1	84	93	86		87.7	12.8	1.6	1.59	0.18
gryt2	92.5	91	86		89.8	10.6	1.5	*not used*	
gryt3	85	89	78		84.0	16.4	1.9		
gryt4			90		90.0	10.4	1.5		
gryt5			91		91.0	9.5	1.4		
Stubble									
stubble1	94	94	94		94.0	6.5	1.2	1.24	0.10
stubble2	90	89	94.5		91.2	9.3	1.4		
stubble3	92.5	94	94		93.5	7.0	1.3		
stubble4	97	93.5	94		94.8	5.6	1.2		
stubble5	98	97	91.5		95.5	5.0	1.1		
stubble6	94	93	94		93.7	6.8	1.3		

Appendix V Results of statistical analysis

Comparison of methods. Analysis of variance.

One way Analysis of Variance test for difference between methods, analyzed separated for each land use type. First tests for normality and equal variance are executed, if it fails ANOVA on ranks are executed.

FOREST
Normality Test (Shapiro-Wilk) Passed (P = 0,411)

Equal Variance Test: Failed (P < 0,050)

Kruskal-Wallis One Way Analysis of Variance on Ranks

Forest Group	**N**	**Median**	**25%**	**75%**
Xtion	**3**	1,323	1,298	2,327
Stereo	**3**	1,010	0,668	1,130
Pinboard	**6**	1,345	0,870	1,910
Chain	**6**	1,081	1,032	1,089

H = 4,958 with 3 degrees of freedom. (P = 0,175)

The differences in the median values among the treatment groups are not great enough to exclude the possibility that the difference is due to random sampling variability; **there is not a statistically significant difference** (P = 0,175)

HARROW
Normality Test (Shapiro-Wilk) Passed (P = 0,262)

Equal Variance Test: Passed (P = 0,179)

Harrow Group	**N**	**Mean**	**Std Dev**	**SEM**
Xtion	**6**	1,182	0,333	0,136
Stereo	**7**	1,521	0,702	0,265
Pinboard	**10**	1,427	0,591	0,187
Chain	**10**	1,631	0,334	0,106

Source of Variation	**DF**	**SS**	**MS**	**F**	**P**
Between Groups	**3**	**0,791**	**0,264**	**0,999**	**0,407**
Residual	**29**	**7,658**	**0,264**		
Total	**32**	**8,449**			

The differences in the mean values among the treatment groups are not great enough to exclude the possibility that the difference is due to random sampling variability; **there is not a statistically significant differenc**e (P = 0,407).

Power of performed test with alpha = 0,050: 0,049

The power of the performed test (0,049) is below the desired power of 0,800.
Less than desired power indicates you are less likely to detect a difference when one actually exists. **Negative results**

should be interpreted cautiously.

PLOUGH
Normality Test (Shapiro-Wilk) Failed (P < 0,050)

Kruskal-Wallis One Way Analysis of Variance on Ranks

Plough				
Group	**N**	**Median**	**25%**	**75%**
Xtion	**3**	2,471	2,233	3,830
Stereo	**5**	2,639	2,222	3,200
Pinboard	**12**	2,351	2,086	3,027
Chain	**10**	2,334	1,825	2,501

H = 2,782 with 3 degrees of freedom. (P = 0,427)

The differences in the median values among the treatment groups are not great enough to exclude the possibility that the difference is due to random sampling variability; **there is not a statistically significant difference** (P = 0,427)

STUBBLE
Normality Test (Shapiro-Wilk) Passed (P = 0,071)

Equal Variance Test: Failed (P < 0,050)

Stubble				
Group	**N**	**Median**	**25%**	**75%**
Xtion	**3**	2,156	1,417	2,541
Stereo	**3**	0,640	0,596	0,657
Pinboard	**6**	1,105	0,796	1,346
Chain	**6**	1,240	1,163	1,300

H = 10,813 with 3 degrees of freedom. (P = 0,013)

The differences in the median values among the treatment groups are greater than would be expected by chance; **there is a statistically significant difference** (P = 0,013)

To isolate the group or groups that differ from the others use a multiple comparison procedure.

All Pairwise Multiple Comparison Procedures (Dunn's Method) :

Comparison	**Diff of Ranks**	**Q**	**P < 0.05**
xtion-s vs stereo-s	13,667	3,135	Yes
xtion-s vs pinboard-s	8,833	2,340	No
xtion-s vs chain-s	5,833	1,545	Do Not Test
chain-s vs stereo-s	7,833	2,075	No
chain-s vs pinboard-s	3,000	0,973	Do Not Test
pinboard-s vs stereo-s	4,833	1,280	Do Not Test

Note: The multiple comparisons on ranks do not include an adjustment for ties.

1. Comparison of land uses. Analysis of variance.

XTION
Normality Test (Shapiro-Wilk) Passed (P = 0,243)
Equal Variance Test: Passed (P = 0,454)

Xtion

Group	**N**	**Mean**	**Std Dev**	**SEM**
Forest	**3**	1,650	0,589	0,340
Harrow	**6**	1,182	0,335	0,137
Plough	**3**	2,843	0,863	0,498
Stubble	**3**	2,040	0,570	0,329

Source of Variation	**DF**	**SS**	**MS**	**F**	**P**
Between Groups	**3**	5,794	1,931	6,261	0,010
Residual	**11**	3,393	0,308		
Total	**14**	9,186			

The differences in the mean values among the treatment groups are greater than would be expected by chance; **there is a statistically significant difference** (P = 0,010).

Power of performed test with alpha = 0,050: 0,808

All Pairwise Multiple Comparison Procedures (Holm-Sidak method):
Overall significance level = 0,05

Comparison	**Diff of Means**	**t**	**Unadjusted P**	**Critical Level**	**Significant**
plough-x vs. harrow-x	1,662	4,231	0,001	0,009	Yes
plough-x vs. forest-x	1,193	2,632	0,023	0,010	No
stubble-x vs. harrow-x	0,858	2,186	0,051	0,013	No
plough-x vs. stubble-x	0,803	1,772	0,104	0,017	No
forest-x vs. harrow-x	0,468	1,193	0,258	0,025	No
stubble-x vs. forest-x	0,390	0,860	0,408	0,050	No

STEREO
Normality Test (Shapiro-Wilk) Passed (P = 0,263)

Equal Variance Test: Passed (P = 0,347)

Stereo

Group	**N**	**Mean**	**Std Dev**	**SEM**
Forest	**3**	0,937	0,239	0,138
Harrow	**7**	1,519	0,701	0,265
Plough	**5**	2,698	0,548	0,245
Stubble	**3**	0,633	0,0306	0,0176

Source of Variation	**DF**	**SS**	**MS**	**F**	**P**
Between Groups	**3**	10,198	3,399	11,152	<0,001
Residual	**14**	4,267	0,305		
Total	**17**	14,465			

The differences in the mean values among the treatment groups are greater than would be expected by chance**; there is a statistically significant difference** (P = <0,001).

Power of performed test with alpha = 0,050: 0,990

All Pairwise Multiple Comparison Procedures (Holm-Sidak method):
Overall significance level = 0,05

Comparison	**Diff of Means**	**t**	**Unadjusted P**	**Critical Level**	**Significant**
plough-s vs. stubble-s	2,065	5,121	<0,001	0,009	Yes
plough-s vs. forest-s	1,761	4,368	<0,001	0,010	Yes
plough-s vs. harrow-s	1,179	3,648	0,003	0,013	Yes
harrow-s vs. stubble-s	0,885	2,324	0,036	0,017	No
harrow-s vs. forest-s	0,582	1,527	0,149	0,025	No
forest-s vs. stubble-s	0,303	0,673	0,512	0,050	No

PINBOARD
Normality Test (Shapiro-Wilk) Failed (P < 0,050)

Kruskal-Wallis One Way Analysis of Variance on Ranks

Pinboard				
Group	**N**	**Median**	**25%**	**75%**
Forest	**6**	1,345	0,870	1,910
Harrow	**10**	1,540	0,920	1,757
Plough	**12**	2,350	2,087	3,030
Stubble	**6**	1,105	0,797	1,350

H = 18,380 with 3 degrees of freedom. (P = <0,001)

The differences in the median values among the treatment groups are greater than would be expected by chance**; there is a statistically significant difference** (P = <0,001)

To isolate the group or groups that differ from the others use a multiple comparison procedure.

All Pairwise Multiple Comparison Procedures (Dunn's Method) :

Comparison	**Diff of Ranks**	**Q**	**P < 0.05**
plough-p vs stubble-p	17,750	3,565	Yes
plough-p vs forest-p	14,250	2,862	Yes
plough-p vs harrow-p	13,950	3,272	Yes
harrow-p vs stubble-p	3,800	0,739	No
harrow-p vs forest-p	0,300	0,0583	Do Not Test
forest-p vs stubble-p	3,500	0,609	Do Not Test

Note: The multiple comparisons on ranks do not include an adjustment for ties.

CHAIN

Normality Test (Shapiro-Wilk) Passed (P = 0,324)

Equal Variance Test: Failed (P < 0,050)

Kruskal-Wallis One Way Analysis of Variance on Ranks

Chain Group	**N**	**Median**	**25%**	**75%**
Forest	**6**	1,085	1,030	1,093
Harrow	**10**	1,605	1,350	1,937
Plough	**10**	2,335	1,828	2,505
Stubble	**6**	1,240	1,160	1,298

H = 24,407 with 3 degrees of freedom. (P = <0,001)

The differences in the median values among the treatment groups are greater than would be expected by chance; **there is a statistically significant difference** (P = <0,001)

To isolate the group or groups that differ from the others use a multiple comparison procedure.

All Pairwise Multiple Comparison Procedures (Dunn's Method) :

Comparison	**Diff of Ranks**	**Q**	**P < 0.05**
plough-c vs forest-c	22,600	4,665	Yes
plough-c vs stubble-c	15,183	3,134	Yes
plough-c vs harrow-c	8,050	1,919	No
harrow-c vs forest-c	14,550	3,004	Yes
harrow-c vs stubble-c	7,133	1,473	No
stubble-c vs forest-c	7,417	1,369	No

Note: The multiple comparisons on ranks do not include an adjustment for ties.

Appendix VI Model version differences

Initially the rain event 04.09.2009 was calibrated using LISEMv2.54. Ksat was multiplied with 3, and the Manning's N for cultivated fields set to 0.45. See figure 8.7.

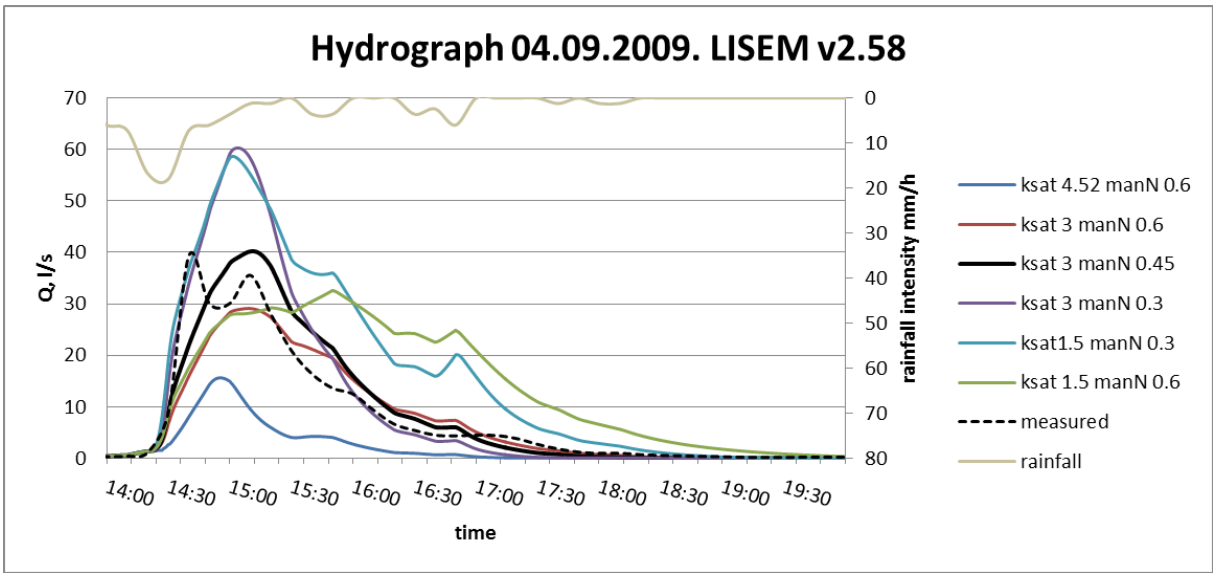

Figure 8.7: Calibration of rain event 04.09.2009. The various hydrographs indicate model runs with different Ksat multiplication factors and the chosen Manning's N. The thicker black line, indicates the model that fit the measured hydrograph best

With the chosen calibration factors the same rain event was modelled using openLISEM v1.34. A sensitivity analysis of the RR input data was executed. The model was run with the measured RR input values (obtained with a Terrestrial Laser Scanner (TLS)), afterwards RR input was increased and decreased 20 and 40%. As figure 8.8 shows this version of LISEM does not respond in the same way to the rain event as the former model version. All the hydrographs are following the same shape that is why only the blue line is visible. Figure 8.9 shows some other model runs trying to adjust Ksat and Manning's N to make the simulated data fit the measured.

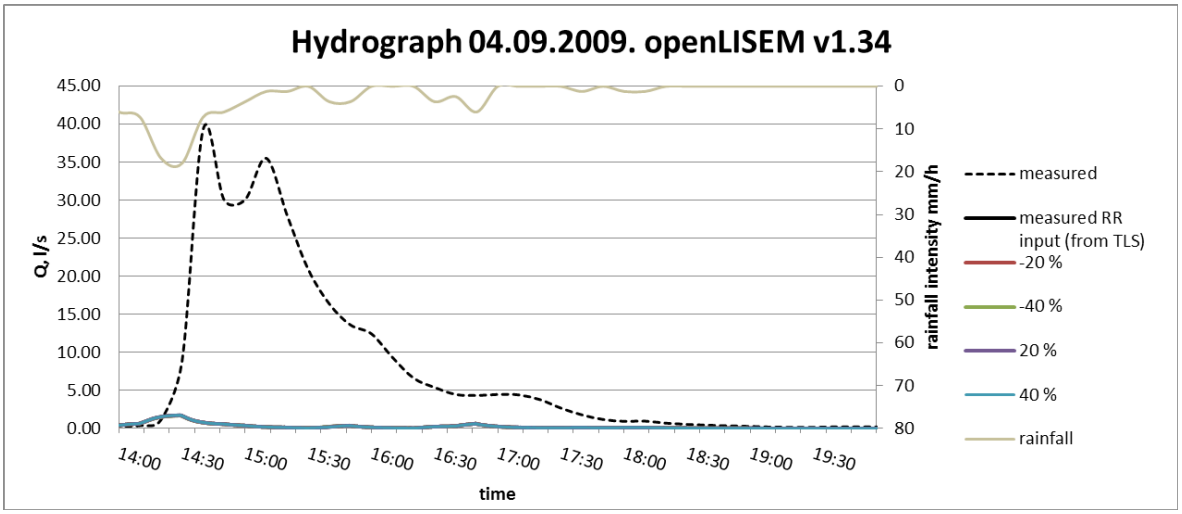

Figure 8.8: Model run using the openLISEM v1.34 and the same calibration factors as mentioned in the text above

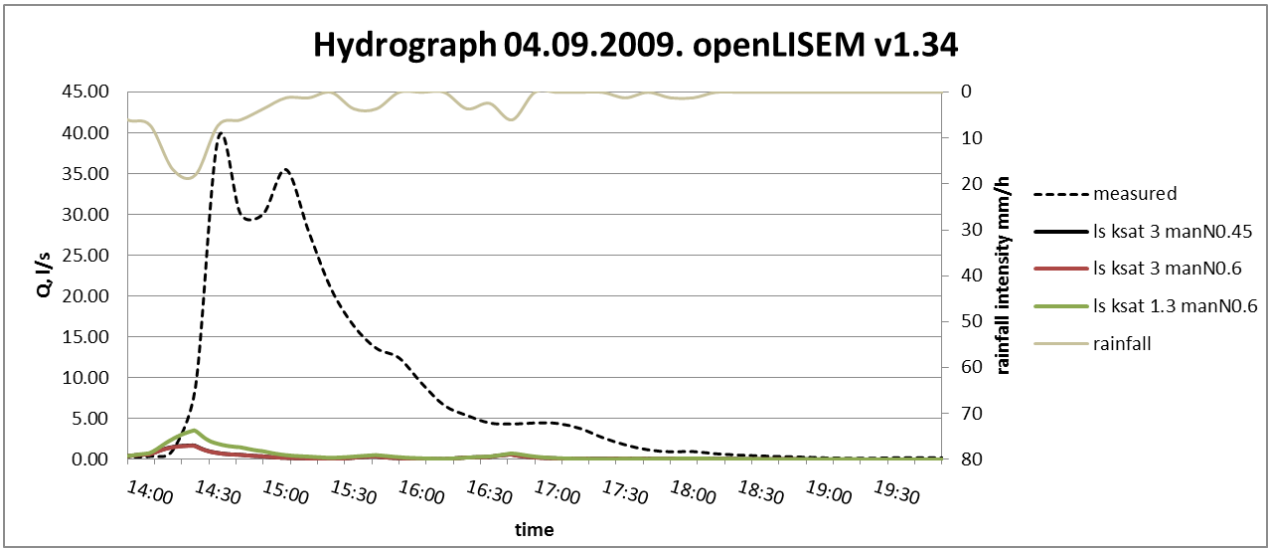

Figure 8.9: Model runs using openLISEM v1.34 and readjusting Ksat and Manning's N